`

VASCULAR BIOLOGY OF MARFAN SYNDROME: ANGIOTENSIN II RECEPTORS, LOSARTAN, AND NITRIC OXIDE

by

Stephanie Leigh Sellers

BSc., The University of Northern British Columbia, 2008

MSc., The University of Northern British Columbia, 2011

A THESIS SUBMITTED IN PARTIAL FULFILLMENT OF

THE REQUIREMENTS FOR THE DEGREE OF

DOCTOR OF PHILOSOPHY

in

THE FACULTY OF GRADUATE AND POSTDOCTORAL STUDIES

(PHARMACOLOGY & THERAPEUTICS)

THE UNIVERSITY OF BRITISH COLUMBIA

(Vancouver)

July 2017

Abstract

Marfan syndrome (MFS), a connective tissue disorder triggered by mutations in Fibrillin-1, causes life-threatening pathology including aortic aneurysm. Recently, controversy has arisen regarding the use of anti-hypertensive angiotensin-II (AngII) receptor type 1 (ATR1) blocker losartan in MFS as, despite success in animal models, losartan has failed to show superiority over standard β-adrenergic receptor blocker atenolol in preventing or slowing expansion of aortic root aneurysm in MFS patients. Overall, we hypothesized that we could provide new insight into this controversy via development of a novel MFS murine model lacking functional ATR1 signaling. Herein, using this novel model, we demonstrate that MFS aortic, pulmonary and skeletal pathology as well as the therapeutic benefit of losartan in MFS aneurysm prevention are ATR1-independent. Instead, we reveal the primary therapeutic pathway of losartan in MFS to be nitric oxide synthase (NOS)-dependent, as treatment of MFS aneurysm *in vivo* has no benefit upon inhibition of NOS. Furthermore, losartan is shown to mediate increased NO release in endothelial cells in the absence of AngII and correct NO levels in the plasma of MFS mice. In addition, declining plasma nitric oxide (NO) levels in mice were found to correlate to increasing aortic aneurysm size and sub-analysis of patients treated with losartan shows indices of improved endothelial function to correlate to regression of aortic aneurysm. Finally, we demonstrate the clinical potential of targeting endothelial dysfunction in MFS as murine models of endothelial nitric oxide synthase (eNOS) over-expression and hyper-activation as well as pharmacological activation of endogenous eNOS all result in prevention of MFS aneurysm. Overall, this study is the first to identify key aspects of MFS pathology and treatment including the ATR1-independent nature of MFS aortic, lung, and skeletal pathology and therapeutic benefit of losartan. Moreover, these studies are the first to show a NOS-dependent mechanism of losartan

and therapeutic benefit of increasing NO bioavailability and improving endothelial function in MFS. As such, they collectively provide a basis for guiding the evolution of managing and treating MFS as well as future pharmaceutical development.

Lay Summary

Marfan syndrome (MFS) is life-threatening as it can lead to premature and/or sudden death associated with dilation and dissection of the aorta, the large blood vessel carrying blood from the heart to the body. Herein, we investigated losartan, a drug being trialed in MFS patients to determine if it can prevent dilation of the aorta and improve patient outcomes. In doing so, we provide evidence that losartan works differently than previously thought and the receptor losartan is designed to block, ATR1, does not play a role in many aspects of MFS including aortic disease. Building on this, we identify nitric oxide, gas produced in blood vessels, and health of the inner lining of blood vessels as key components in MFS. Thus, overall this work provides new insight into MFS including a new understanding of the function of losartan and identification of potential targets for treating MFS patients in the future.

Preface

Stephanie L. Sellers (SLS) carried out the majority of the experiments and experimental planning with guidance from her supervisory committee. SLS also wrote the manuscripts resulting from this work and contributed to grant applications regarding future work. During the course of the presented work SLS mentored co-operative education students and undergraduate students as well as collaborated with graduate students and post-doctoral fellows. Notably, Rayleigh Chan assisted SLS with nitric oxide release studies and harvesting of animal tissue. Michael Mielnik, Una Jermilova, and Nadia Milad helped SLS with animal breeding and harvesting of tissue. Dr. Jeremy Hirota provided initial guidance on lung harvest and functional lung measurements. Dr. Michael A. Seidman (cardiac pathologist at St. Paul's Hospital) helped with design of histological approaches and in scoring histology as well as consulted on confirming echocardiogram findings. Dr. Jonathon Leipsic (St. Paul's Hospital, Department of Radiology) provided access to radiological imaging. Dr. Paul Huang (Harvard University), Dr. Rini de Crom (Erasmus University) and Dr. Hal Dietz (Johns Hopkins University) aided animal model development by providing mouse strains utilized in this work that were not commercially available. Dr. George Sandor (Vancouver Children's Hospital) provided patient data described in in Appendix C.

Currently, use of apolipoprotein E and endothelial nitric oxide deficient mice ($ApoE^{-/-}$ $eNOS^{-/-}$) to determine specificity of CavNOxin as discussed in Chapter 6 is published as:

Sharma, A, **S.L. Sellers**, N. Stefanovic, C. Leung, S.M. Tan, O. Huet, D. Granville, M. Cooper, J. de Haan, and P.N. Bernatchez. 2015. Direct Endothelial Nitric Oxide Synthase Activation Provides Atheroprotection in Diabetes-Accelerated Atherosclerosis. *Diabetes.* 64(11):3937-50.

For this work SLS was responsible for generation, treatment, tissue harvest and partial evaluation

of the ApoE$^{-/-}$ eNOS$^{-/-}$ mouse line. However, these data are not directly presented in this thesis Additionally, the majority of the contents of Chapter 4, Chapter 5 and Chapter 6 are currently detailed in a manuscript that is under review at a peer reviewed journal.

All experiments using animal models were conducted under approvals from the UBC Animal Care Committee under protocol numbers A12-0136, A12-0281, A14-0070, A14-0072, and A12-0152.

Table of Contents

List of Tables

List of Figures

List of Acronyms and Abbreviations

A: Alanine

AA: Aortic Aneurysm

AAA: Abdominal aortic aneurysm

ACE: Angiotensin converting enzyme

ACEi: Angiotensin converting enzyme inhibitor

AKT: Protein kinase B

Ala: Alanine

AngII : Angiotensin II

ApoE: Apolipoprotein E

ARB: Angiotensin receptor blocker

Asp: Aspartate

ATR1: Angiotensin II receptor type 1

ATR2: Angiotensin II receptor type 2

β-Blocker:

BAEC: Bovine aortic endothelial cell

BAL: Bronchoaveolar levage

bp: base pairs

C: Cysteine

COPD: Chronic obstructive pulmonary disease

CT: Computed tomography

CTGF: Connective tissue growth factor

D: Aspartate

DMSO: Dimethyl sulfoxide

DNA: Deoxyribonucleic acid

EC: Endothelial cell

ECG: Electrocardiogram

ECM: Extracellular matrix

EDTA: Ethylenediaminetetraacetic acid

EGF: Epidermal growth factor

EL: Ectopic lentis

EDTA: Ethylenediaminetetraacetic acid

eNOS: Endothelial nitric oxide synthase

ERK: Extracellular signal-regulated kinase

FMD: Flow mediated dilation

FBN1: Fibrillin-1

G: Glycine

GEM: Genetically engineered models

GFP: Green fluorescent protein

HCL: Hydrochloric acid

HRP: Horseradish peroxidase

HNE: Hydroxynonenal

ICAM-1: Intercellular adhesion molecule one

i.p.: intra-peritoneal

JAX: The Jackson Laboratory

JNK1: c-Jun N-terminal kinase one

L-NAME: L-N^G-Nitroarginine methyl ester

LAP: Latency associated peptide

LLC: Large latency complex

Lm: Mean linear intercept

LTBP: Latent transforming growth factor beta binding protein

M: Molar

MAP: Mean arterial pressure

MAPK: Mitogen-activated protein kinase

MFS: Marfan Syndrome

mg: milligram

MHz: Megahertz

ml: milliliter

mM: millimolar

MMP: Matrix metalloproteinase

MRI: Magnetic resonance imaging

MVD: Mitral valve disease

NADPH: Nicotinamide adenine dinucleotide phosphate

NaOH: Sodium hydroxide

NO: Nitric oxide

NOS: Nitric oxide synthase

NSAID: Non-steroidal anti-inflammatory drugs

NT: Nitrotyrosine

PCR: Polymerase chain reaction

Phe: Phenylalanine

PKC: Protein kinase C

PPAR-γ: Peroxisome proliferator-activated receptor gamma

ROS: Reactive oxygen species

S: Serine

Ser: Serine

sGC: soluble guanylate cyclase

SMC: Smooth muscle cell

SPH: St. Paul's Hospital

SU5416: Sugen

TAE: Tris, acetic acid, ethylenediaminetetraacetic acid buffer

Tg: Trangenic

TGF-β: Transforming growth factor beta

TGFβR1: Transforming growth factor beta receptor type 1

TGFβR2: Transforming growth factor beta receptor type 2

Thr: Threonine

TSP-1: Thrombospondin one

TIMP-1: Tissue inhibitor of matrix metalloproteinases one

UV: Ultra-violet

VCAM-1: Vascular cell adhesion molecule one

VEGF: Vascular endothelial growth factor

VEGFR2: Vascular endothelial growth factor receptor type 2

VSMC: Vascular smooth muscle cell

WT: Wild type

W/V: Weight per volume

Acknowledgements

I would like to acknowledge members of my supervisory committee (Dr. Pascal Bernatchez, Dr. Geoffrey Payne, Dr. David Granville and Dr. Ed Conway) for their advice, guidance, and thoughtful discussion. Furthermore, the many contributions and support of members of St. Paul's Hospital and the Centre for Heart Lung Innovation were central to the success of this work including the help of Rayleigh Chan, Una Jermilova, Nadia Milad, Dr. Arpeeta Sharma, Dr. Cleo Leung, Dr. Andy Trane, Amrit Samra, Juvena Burns, Dr. Jonathon Leipsic, Dr. Jeremy Hirota, Claire Smits, Dr. Stephanie Warner, Dr. Mark Kearns, Dr. Lisa Ang, and Dr. Kristin Bowden. In particular, much gratitude and thanks goes to Michael Mielnik, who brightened difficult days with his humor, to Dr. Dmitri Pavlov for sharing his amazing technical expertise, stories, and always going the extra mile and to Lubos Bohunek and Tatjana Bozin for their friendship and sharing their coffee and passion for doing great work. Finally, many thanks go to Dr. James Hogg and Dr. Michael Seidman for their invaluable mentorship and advice.

To my friends and family – thank you for seeing me through the highs and lows, your understanding, and always encouraging and supporting me. Additionally, my gratitude to Ali McLean, an extraordinary physiotherapist, who got me back in the lab and helps me do my best work.

This work was supported by the Canadian Institutes of Health Research (CIHR) grant to Casey Van Breemen, Mitra Esfrandiarei, and Pascal N. Bernatchez (PNB) and funding from the Heart & Stroke Foundation of BC & Yukon, CIHR, Jain Foundation, and Canadian Foundation for Innovation to PNB. Throughout my work I was is a recipient of studentship funding from CIHR, the CIHR Michael Smith Foreign Study Fund, and the University of British Columbia and

received funds in support of this work as the recipient the Jean Francois Bowden Cardiovascular Research Award, American Society of Pharmacology and Experimental Therapeutics (ASPET) travel awards, and UBC Department of Anesthesiology, Pharmacology & Therapeutics Research Day Awards.

Dedication

To Steve & Cindy - for all their support.

Chapter 1: Introduction

1.1 Marfan Syndrome

Marfan syndrome (MFS) is a life-threatening connective tissue disorder that was first described by French physician Antoine Marfan in 1896 [1, 2]. Generally, MFS patients present with systemic disease manifestations that include pathology in the cardiovascular, pulmonary, muscular, skeletal, and ocular systems. Of these, the most life threatening pathology is aneurysm of the aorta, which pre-disposes to aortic dissection (a tear in the wall of the aorta) including the possibility of acute rupture leading to sudden death. Commonly characterized as being caused by autosomal dominant mutations in Fibrillin-1 (*FBN1*), MFS is estimated to affect approximately 1 in every 5000 individuals without a gender or ethnic bias [3, 4]. Although this incidence makes MFS relatively rare, this is thought to be an under-estimate due to under diagnoses owing to the large range of associated severities and manifestations seen in MFS as is reflected in inter- and intra-familial variability of clinical manifestations [5]. Overall, MFS generally incurs a significantly shortened life expectancy, complex medical care, and diminished quality of life for patients. While advances in surgical interventions and pharmacotherapy are notable steps forward in the treatment and management of MFS patients, much room for improvement remains. Furthermore, as discussed in more detail below, recent clinical trials to compare the effectiveness of a variety of pharmaceutical-based approaches to prevent progression of aortic aneurysm in MFS patients have generated much controversy regarding the definitive pathology and best treatment options. However, herein, the data presented helps to shed light on some of these controversies and in doing so helps guide future work for the identification of new therapeutic targets in MFS and development of superior treatment options.

1.1.1 Fibrillin-1 Mutations in Marfan Syndrome

The *FBN1* gene on chromosome fifteen encodes for expression of fibrillin-1, a 320kD glycoprotein first identified in 1986 by Sakai *et al.*. Fibrillin-1 was found to be 2.2nm long and 148nm in width and is the primary component of 10-20nm microfibrils. In association with elastin, microfibrils also make up a component of elastic fibers, with both microfibrils and elastic fibers found in connective tissue throughout the body [6, 7]. Microfibrils are formed from a fibrillin core to give an ultrastructure bead-on-a-string appearance, which associates with many matrix proteins including fibulins and microfibril-associated glycoproteins that bind microfibrils to the surrounding extracellular matrix (ECM), cells, and elastin to form elastic fibers found throughout the body. Within the aorta, elastic fibers are found concentrically in the tunica media between layers of vascular smooth muscle cells (VSMCs) that make up much of the wall of the aorta. Additionally microfibrils are found between these concentrically arranged elastic fibers as well as in the basement membrane that runs beneath the endothelium which lines the lumen of the aorta and have been shown to regulate some aspects of endothelial cell function and signaling [8-12].

Reduced production of fibrillin-1 or manufacturing of dysfunctional fibrillin-1 is hypothesized to be the causative factor of MFS; initial studies in MFS patients showed a reduction in staining for fibrillin-1 in skin samples and fibroblast culture as well as a reduction in fibrillin-1 production and integration into the ECM [13-15]. While these studies suggested fibrillin-1 to be the causative pathogenic factor in MFS at the protein level, identification on the genetic level came later; MFS was first linked to chromosome 15 in 1990 by Kainulainen and colleagues in a Finnish family [16]. Dietz and colleagues and Tsipouras and colleagues, in American and British families respectively, subsequently confirmed this finding of the link to

chromosome 15 [17, 18]. Finally, the identification of mutations in *FBN1* as a causative factor in MFS was first reported in 1991 in *Nature* by Dietz and colleagues [19]. Interestingly, mutations within *FBN1* affect the synthesis of fibrillin-1 molecules and *FBN1* has two splice variants. Although it is unknown if these variants result in functional protein, it is hypothesized that they do not. As such, these findings suggest that therapeutics targeted at increasing generation of functional fibrillin-1 may mitigate MFS pathology [20, 21]. Beyond splice variants of fibrillin-1, other types of fibrillin have been identified: fibrillin-2 and fibrillin-3. Notably, fibrillin-2 plays a role in aortic development and microfibril formation. However, to date, mutations in fibrillin-2 have not been reported to cause MFS like phenotypes [22, 23].

Fibrillin-1 contains 47 epidermal growth factor-like (EGF-like) domains. Each of these domains has six conserved cysteine residues that form three disulfide bonds. The most common types of *FBN1* mutation seen in MFS are those that result in a disruption of one of these bonds [21]. The critical aspect in these types of mutations is that they disrupt the EGF-like domains, which are thought to be the main site of TGF-β sequestration in the extracellular matrix (ECM). As discussed in more detailed below, TGF-β is thought to be one of the main pathogenic drivers of MFS pathology and mutations in *FBN-1* are thought to contribute excessive activation of TGF-β as normal fibrillin-1 (no mutation) acts to limit TGF-β activation. This is achieved via fibrillin-1 binding and sequestration of the large latent complex (LLC) that is made up of TGF-β, its latency associated peptide [24], and latent TGF-β binding proteins (LTBPs). Mutations in fibrillin-1 result in a lack of latent TGF-β sequestration and are ultimately thought to lead to the aberrant increase in TGF-β observed in MFS [19, 25-27].

1.1.2 Diagnosis and the Ghent Criteria

Diagnosis of MFS, like many diseases and syndromes, is challenging; the large spectrum of MFS manifestations, the ever growing number of MFS-causing *FBN-1* mutations identified, the heterogeneity of disease severity, and the drastically different rate of progression have hindered development of a clear diagnostic criteria. However, continued progress towards understanding MFS pathology has brought about a refinement of diagnostic criteria and many online calculators for disease diagnostics are now available [28]. These stem from the first diagnostic criteria established for MFS in 1988 with publication of the Berlin Nosology [29]. The Ghent Nosology or Criteria replaced the Berlin Nosology in 2006 [30]. Finally, the Revised Ghent Nosology was published in 2010 in the *Journal of Medical Genetics* [31]. Generally, this new nosology states that diagnosis of MFS is made through a combination of factors associated with the MFS phenotype and aims to more accurately diagnose MFS patients. The nosology allows for the diagnosis of MFS when a combination of major or minor criteria identified in MFS patients (Table 1) and puts emphasis on the presence of aortic root (Ao) aneurysm and ectopia lentis (EL, dislocation of the lens of the eye). Aortic root pathology is assessed by Z-score (Z) at the Sinus of Valsalva which represents a measure of the standard deviation of aortic root size relative to the population based on height, weight, and age [32-34]. Systemic features are subsequently scored on a points system including the presence of facial features, deformities of the skeletal system, and pulmonary or dermal findings. Beyond the criteria and features presented in Table 1, the revised Ghent Nosology speaks to identification of *FBN-1* mutations, guides patient management, and outlines features of pathologies that make up the differential diagnosis of MFS and have overlapping findings. Although complex, the revised Ghent Nosology is aimed at identifying MFS patients so that they can receive proper care and

monitoring as well as avoiding inaccurately diagnosing patients. On one hand it is obvious why the diagnosis of patients is critical to providing appropriate care. However, on the other hand, inaccurately diagnosing MFS in a patient also has potentially severe yet less obvious consequences such as the restriction of life style and career as well as psychosocial effects [31].

Overall Criteria

A. Conditions for MFS Diagnosis (with no family history)

1. Ao (Z ≥2) and EL
2. Ao (Z ≥2) and FBN1 Mutation
3. Ao (Z ≥2) and Systemic Manifestations (≥7 points)*
4. EL and FBN1 Mutation with known Ao

B. Conditions for MFS Diagnosis (with family history)

1. EL and family history of MFS
2. Systemic Manifestations (≥7 points) and family history of MFS*
3. Ao (Z ≥2 in patients over 20 years of age or Z ≥3 in those below 20) and family history*

Scoring of Systemic Features

Systemic Feature	Score	Systemic Feature	Score
Wrist and thumb sign • Wrist or thumb sign	3 1	Facial features (3/5 of dolichocephaly, enophthalmos, downslanting palpebral fissures, malar hypoplasia, retrognathia)	1
Hindfoot deformity	2	Reduced elbow extension	1
Hindfoot deformity • plain pes planus	2 1	Myopia (>3 diopters)	1
Pneumothorax	2	Skin striae	1
Dural ectasia	2	Mitral valve prolapse	1
Protrusio acetabuli	2	Scoliosis or thoracolumbar kyphosis	1
Reduced upper segment/lower segment ratio and increased arm/height AND no severe scoliosis	1	Pectus carinatum deformity • pectus excavatum or chest asymmetry	2 1

Table 1: The revised Ghent Nosology for diagnosis of MFS.
The revised Ghen Nosology was established in 2010 [31] and establishes criteria for the diagnosis of MFS with and without familial history. *Denotes the caveat that MFS is diagnosed in these situations when discriminating features of differential diagnoses are not found.

1.1.3 Aortic Aneurysm

Aortic aneurysm is a central component to the diagnosis of MFS and is a major MFS phenotype. While aortic root aneurysms are the most common in MFS, patients also exhibit ascending aortic aneurysm and aneurysm of the descending aorta [35]. Many case reports also detail aneurysm throughout the vascular system including the iliac, carotid, and subclavian arteries [35-40]. However, development of aortic root aneurysm constitutes the most life-threatening aspect of MFS pathology and is the focus on the vast majority of MFS research. Aneurysm is generally defined as dilation of a blood vessel over 1.5 times is normal diameter and is monitored in MFS patients through use of imaging modalities including computed tomography (CT), magnetic resonance imaging (MRI) and echocardiography [31, 41, 42]. Notably, although not yet in clinical use, use of such imaging techniques continues to evolve and are being customized towards MFS specific pathology, such as the use of MRI contrast to analyze elastin content in the aortic wall [43]. Overall, monitoring of aneurysm in MFS patients using imaging modalities is aimed at determining both the overall aortic root diameter and rate of aneurysm progression, which are currently used to guide surgical intervention [31].

Histological analysis of the aortic wall in MFS reveals vascular smooth muscle cell (VSMC) apoptosis, fibrosis, and diffuse elastic fiber fragmentation [27, 44-46]. Elastic fiber fragmentation is associated with increased activity and expression of matrix metalloproteinsases (MMPs), which are zinc-containing endopeptidases, thought to mediate fragmentation of elastic fibers as is observed in MFS. Levels of MMPs have been reported to be elevated in the aortas of MFS patients along with altered expression of tissue inhibitors of MMPs (TIMPs) [47, 48]. Specifically, MMP-2 and MMP-9 have been shown to be particularly important. MMP-2 and MMP-9 were also shown to be elevated in the aortic wall of murine models of MFS.

Furthermore, these levels of MMP-2 and MMP-9 in murine models of MFS were shown to be reduced with doxycycline treatment and result in reduction in aortic wall pathology and extended life span [49, 50]. MMP levels have also been shown to be reduced by treatment of MFS mice with angiotensin receptor blocker (ARB) losartan or nonsteroidal anti-inflammatory (NSAID) indomethacin and result in reduction of aortic pathology [51, 52]. Moreover, knockout of MMP-2 in mice was shown to reduce aneurysm size, extend the life-span, prevent elastic fiber fragmentation, reduce pathogenic TGF-β signaling and extend life span in a murine model of MFS [53]. Notably, while loss of elastic fiber integrity and disorganization in the aorta is most commonly studied using staining of aortic sections, it has recently been shown that multi-photon microscopy analysis can be used to appreciate these aspects of MFS pathology. Furthermore, pathology of aortic sections was shown to correlate to similar loss of integrity and disorganization in the skin, thereby supporting the possibility of a skin biopsy for analysis and monitoring of MFS aortic pathology [54].

Reports have also identified infiltration of inflammatory cells in the media and adventitia of the ascending aorta or MFS patients including an increase in $CD4^+$ and $CD8^+$ T-cells as well as $CD20^+$ B-cells and $CD68^+$ macrophages. This increase in inflammatory cell accumulation in the ascending aorta of MFS patients was accompanied by increased expression of intracellular adhesion molecule-1 (ICAM-1) and vascular cell adhesion molecule-1 (VCAM-1) in the vasa vasorum [55] thereby indicating a inflammatory component to MFS aortic pathology. Moreover, such an inflammatory response may also contribute to activation of MMPs as inflammatory cytokine interleukin-6 has been shown to promote activation of MMP-9 and elastic fiber fragmentation in a murine model of MFS [56].

1.1.4 Mitral Valve Dysfunction

Aneurysm, particularly of the aortic root, is the main cardiovascular concern in MFS. However, MFS is associated with other manifestations in the cardiovascular system of which one of most common is mitral valve disease (MVD). MVD is the leading cause of death in children with MFS [57]. MVD in MFS leads to valve dysfunction associated with factors such as leaflet prolapse or annulus dilation thereby causing regurgitation [58-60]. Mitral valves from murine models of MFS show increased levels of active TGF-β signaling associated with myxomatous changes characterized by increased cell proliferation and decreased apoptosis along with morphological changes including leaflet thickening and increased length. Notably, leaflet thickening and increasing length was inhibited by use of neutralizing TGF-β antibody [57]. Moreover, similar signaling was found to be a feature of human myxomatous mitral valve degeneration [60].

1.2 Non-Cardiovascular Pathology of MFS

As reflected in the Ghent Criteria (reviewed above), the systemic MFS pathology outside of aneurysm development is diverse and has a wide range of phenotypic findings throughout MFS patients. Briefly outlined below are some of the systemic features of MFS found in the ocular, skeletal, and pulmonary systems.

1.2.1 Ocular Involvement

Pathology of the ocular system is a notable manifestation of MFS. In particular, ectopia lentis (EL) is a cardinal feature of MFS and is best described as a dislocation of the lens of the eye. EL results is proposed to result from altered microfibril arrangement that makes the

connective tissue which holds the lens of the eye too loose and thereby gives rise to dislocation of the lens [61]. The inclusion of EL as a major criterion in MFS diagnosis is reflective of its high incidence in the patient population. In fact, EL is estimated to be a definitive feature for diagnosis or exclusion of MFS in 86% of patients evaluated for MFS and occurs in 50-80% of individuals with MFS. Other features of MFS ocular pathology include myopia, retinal detachment, glaucoma, and abnormal eye alignment [62, 63].

1.2.2 Pulmonary Pathology

Reports of pulmonary pathology in MFS are relatively rare compared to the predominant focus on MFS aortic pathology. However, reports of pulmonary complications associated with MFS-like phenotypes date to before the identification of the role of *FBN-1* mutations [64, 65]. In MFS patients, descriptions of pulmonary pathology include findings of emphysema, interstitial lung disease, atelectasis, bullae formation, and spontaneous pneumothorax [65]. Spontaneous pneumothorax, the presence of air in the pleural space potentially causing the lung to collapse, likely from the rupture of blebs, occurs at a much high frequency in MFS patients, with an estimated 5-12% of patients affected based on initial case studies. Recent studies using radiological computed tomography analysis reveals the presence of blebs or bullae to correlate to a high rate of spontaneous pneumothorax in MFS patients [66-70]

Emphysema and lung fibrosis have also been reported in MFS patients [66, 67, 70-72]. The presence of emphysema-like air space enlargement is also reported in MFS animal models and is found as early as postnatal day one in some models suggesting lung pathology *in utero*. Such air space enlargement was found to be progressive as measured by increasing values of mean linear intercept (Lm) over time. Although no change in lung to body weight ratio was found,

histological analysis showed a distinct lack of aveolar septation associated with increased levels of TGF-β, increased levels of apoptosis of lung epithelial cells and increased activity of MMPs. Moreover, airspace enlargement was prevented in a dose-dependent manner with neutralizing TGF-β antibody [27].

Determining how histological changes relate to lung function is a natural extension of the obvious pathology seen in the MFS lung. However, reports of pulmonary function testing in MFS patients are limited. Some small early case studies have suggested that lung function may be normal [73-75]. Yet recent studies have shown markedly abnormal aspects of lung function in MFS patients relative to normal controls [76-78]. Moreover, case reports looking at histological changes in MFS lung pathology report an association with shortness of breath, chest pain and chronic obstructive pulmonary disease (COPD) [79]. In terms of animal models, until recently only histological reports were available for the analysis of MFS lung in murine models; in 2016 Lee *et al.* showed a distinct change in the mechanical properties of isolated lung tissue of MFS mice [80]. In addition, in 2015 da Palma *et al.* provided data suggesting an increased propensity towards pulmonary collapse in MFS mice, which corresponds to similar findings and an increased incidence of sleep apena in MFS patients [81, 82].

1.2.3 Skeletal System Involvement

Skeletal system abnormalities manifest in a number of ways in MFS. These include long bone overgrowth such as arachnodactyly (“spider fingers”), scoliosis, and changes in bone density and skeletal muscle content [31, 83]. As mircrofibrils are found in bone matrix, and given the central role of fibrillin-1 in microfibrils, it is not surprising the MFS exhibits a skeletal phenotype [84]. Recently however, how *FBN-1* mutations cause such skeletal manifestations has

begun to be answered from a molecular signaling perspective. In fact, akin to how fibrillin-1 contributes to the binding of TGF-β in the ECM, bone morphogenetic protein (BMP) complexes are also bound in the ECM. Mutations in *FBN-1* have been shown to regulate both TGF-β and BMP signaling which contribute to changes observed in MFS bone [85].

Beyond development of kyphoscoliosis and other bone deformations, MFS patients are also at risk of having reduced bone density (osteopenia). However, the finding of osteopenia is inconsistent and controversial likely due to complications incurred by sex and the relatively young age of MFS patients relative to the older patients who typically exhibit decreased bone density. In particular, in pediatric MFS patients osteopenia is difficult to diagnosis given poor reference data for the pediatric population on which to compare bone density [86-89]. Practically however, osteopenia presents a potential problem to MFS patients as reduction in bone density increases the risk of bone fracture [90]. Therefore, determining a potential mechanism of bone density changes in MFS is important and was recently addressed in a murine model of MFS. Therein, the authors found that excess bone resportion by osteoclasts caused decreased bone density and was treatable by use of alendronate that acts to reduce osteoclast driven bone resportion [91].

Associated with skeletal pathology, MFS patients often also exhibit skeletal muscle pathology including decreased muscle mass, hypertonia, and an inability to build muscle despite following appropriate exercise regimens [92, 93]. Reduced muscle mass is also thought to contribute to reduced bone mineral density in MFS [94]. MFS murine models exhibit decreased skeletal muscle mass associated with reduce myofiber size and number. Such changes in MFS skeletal muscle pathology is thought to be related to high levels of TGF-β that may inhibit myogenesis based on studies in murine models of MFS. In fact, in a mouse model of MFS

inability to repair skeletal muscle was improved by treatment with neutralizing TGF-β antibody or ARB losartan [93].

1.3 TGF-β, Angiotensin Receptors, and MFS Pathology

Many of the cardiovascular and systemic pathologies of MFS, as discussed above are associated with aberrant TGF-β signaling. TGF-β is produced as a pre-propolypetide, which undergoes cleavage in the Golgi apparatus prior to secretion as a propeptide that is sequestered in the ECM. Such sequestration functions to regulate its activity levels as well as direct sites of concentration of latent TGF-β. Mutations in *FBN-1* are proposed to give rise to aberrant TGF-β signaling as a result of lack of sequestration of TGF-β in the ECM; large latent binding protein (LTBPs) which make up the latent TGF-β complex have been found to bind to EGF-like domains in fibrillin-1. Mutations in *FBN-1,* which drive MFS are often found to affect such EGF-like domains and thus give rise to a larger non-sequestered pool of TGF-β [25, 95]. However, even in the instance that TGF-β is improperly sequestered in the ECM, it is important to note that as a propeptide, TGF-β is produced bound to a latency-associated peptide [24] [24, 95]. Hence, activation of TGF-β requires not only release from the ECM by also cleavage of the LAP. Notably, a number of means have been shown for this activation including the actions of proteases, reactive oxygen species (ROS), thrombospondins, and changes in pH [95-98]. For example, MMP-2 and MMP-9, which show strong association with MFS pathology, may contribute to this process as cleavage of LAP has been shown to occur by both proteases [99]. Interestingly, MMP-2 and MMP-9 are also strongly implicated in the pathology of abdominal aortic aneurysm (AAA), thereby indicating the central role in pathologies associated with degradation and damage of the elastic aortic wall [100]. However in contrast to MFS, in AAA

TGF-β has been shown to be protective in some studies; use of neutralizing TGF-β antibody in a murine model of AngII induced AAA was shown to exacerbate aneurysm development. Moreover, over-expression of TGF-β was shown to stabilize AAAs in rats [101, 102], which is in stark contrast to MFS murine models and human studies in which high levels of TGF-β are pathogenic and neutralizing TGF-β antibody minimizes many of the syndrome's manifestations.

The initial proposal of TGF-β as the main pathogenic driver of MFS pathology was by Neptune *et al.* in which the use of TGF-β neutralizing antibody was effective at preventing MFS pathology in the lung of murine models in a dose dependent manner [27]. Circulating plasma TGF-β levels were also shown to correlate to disease severity in MFS mice and patients [103]. This subsequently gave rise to a myriad of studies looking at TGF-β in MFS pathology including initial studies showing the ability of losartan to reduce canonical and non-canonical TGF-β signaling in murine models of MFS [45, 104]. A number of signaling pathways are associated with TGF-β. Those most closely associated with MFS pathology are those involve Smad, ERK and MAPK mediated signaling as outlined in Figure 1.

Canonical TGF-β signaling involves binding free, active TGF-β to the heterodimer made up of TGF-β receptors 1 and 2 (TGFβR1/2). Activation of the receptor stimulates phosphorylation of Smad2 and formation of a Smad2/3/4 complex, which translocates to the nucleus and stimulates transcription of genes including those leading to increased expression of MMPs, connective tissue growth factor (CTGF), and monocyte chemoattractant protein 1 (MCP-1) [105]. MMPs, as previously discussed have been shown to increase activation of TGF-β and break down of elastic fibers [49, 50, 99] while increased expression of CTGF is proposed to contribute to fibrosis and increased collagen deposition associated with MFS models [104, 106]. Furthermore, increased expression of inflammatory mediators such as MCP-1 and IL-6 are

associated with MFS pathology [107]. Non-canonical TGF-β signaling through p38, JNK1, and ERK mediates activation of mitogen activated protein kinase (MAPK) and drives increased expression of factors such as TGF-β, MMPs, CTGF, and thrombospondin-1 (TSP-1) which has been shown to contribute to activation of TGF-β [108].

Interaction of the angiotensin II (AngII) and angiotensin II receptor type 1 (ATR1) and angiotensin receptor type II (ATR2) with the TGF-β pathway has become a large focus of research in recent years. In particular, focus has been on blockade of ATR1, which was first cloned in the 1990s. It is largely considered that humans only express the alpha isoform of ATR1. However, Konish *et al.* report cloning of the beta isoform in a human placental cDNA library with identification of expression of the beta isoform by Northern blot in human tissue [109]. In murine models alpha and beta isoforms of ATR1 have been extensively studied [110-112]. In general, angiotensin receptors (ATRs) are a family of trans-membrane proteins that bind AngII and mediate intercellular signaling. Both ATR1 and ATR2 are seven pass transmembrane G-protein coupled receptors [113-115]. In the context of MFS, the main focus of study in regard to ATR1 signaling, beyond the classical study of reduction of blood pressure with receptor blockade, has been on determining how it contributes to canonical and non-canonical TGF-β signaling, expression of TGF-β, and activation of TGF-β receptors. Furthermore, as ATR1 is proposed to contribute significantly to development and progression of aortic aneurysm in MFS, the study of ATR1 blockade via angiotensin receptor blockers (ARBs) being a major current direction of investigation. Furthermore, the potential protective effects of ATR2 signaling has also been studied recently and proposed to counter pathological TGF-β signaling through the inhibition of ERK and JNK1 non-canonical TGF-β pathways [44, 104, 105, 116-119]. The utility

of ARBs for treating MFS, with a particular focus on losartan, is a point of continued study and controversy in the field of MFS research and is discussed further below.

Notably, AngII and ATR1 signaling may influence the development of aortic aneurysm by mechanisms other than TGF-β. AngII/ATR1 signaling has been shown to activate NADPH oxidase as well as contribute to the formation of superoxide, hydrogen peroxide, peroxynitrite [120-123]. In addition, use of ARBs to prevent activation of AngII/ATR1 signaling has been shown to reduce oxidative stress markers including production of hydrogen peroxide [124-126]. Importantly, oxidative stress markers have been shown to be elevated in MFS patients and murine models. Oxidative stress is also a component of endothelial dysfunction, which has also been reported in MFS patients and murine models in regard to pathology of the aorta and aortic stiffness [127-130].

AngII is also known to increase monocyte recruitment and macrophage activation, which may impact MFS as inflammatory markers and recruitment of inflammatory cells is reported to play a role in aortic aneurysm in MFS [107, 131]. Interestingly, AngII is also known to increase the incidence of abdominal aortic aneurysm as well as atherosclerotic lesions in the aorta without a change in blood pressure, lipoproteins or cholesterol concentrations [132]. Although an increased predisposition or severity of atherosclerosis has not been reported in the human MFS population, this may change as patients live longer. Notably, a murine model of MFS associated atherosclerosis exists in the form of $C1039G^{+/-}$ mice with apolipoprotein E (ApoE) deficiency ($C1039G^{+/-}$ $ApoE^{-/-}$ mice). These mice were found to have increased arterial stiffness and an increased burden of atherosclerotic plaque characterized by more adverse plaque features including increased inflammation and necrotic cores size [133].

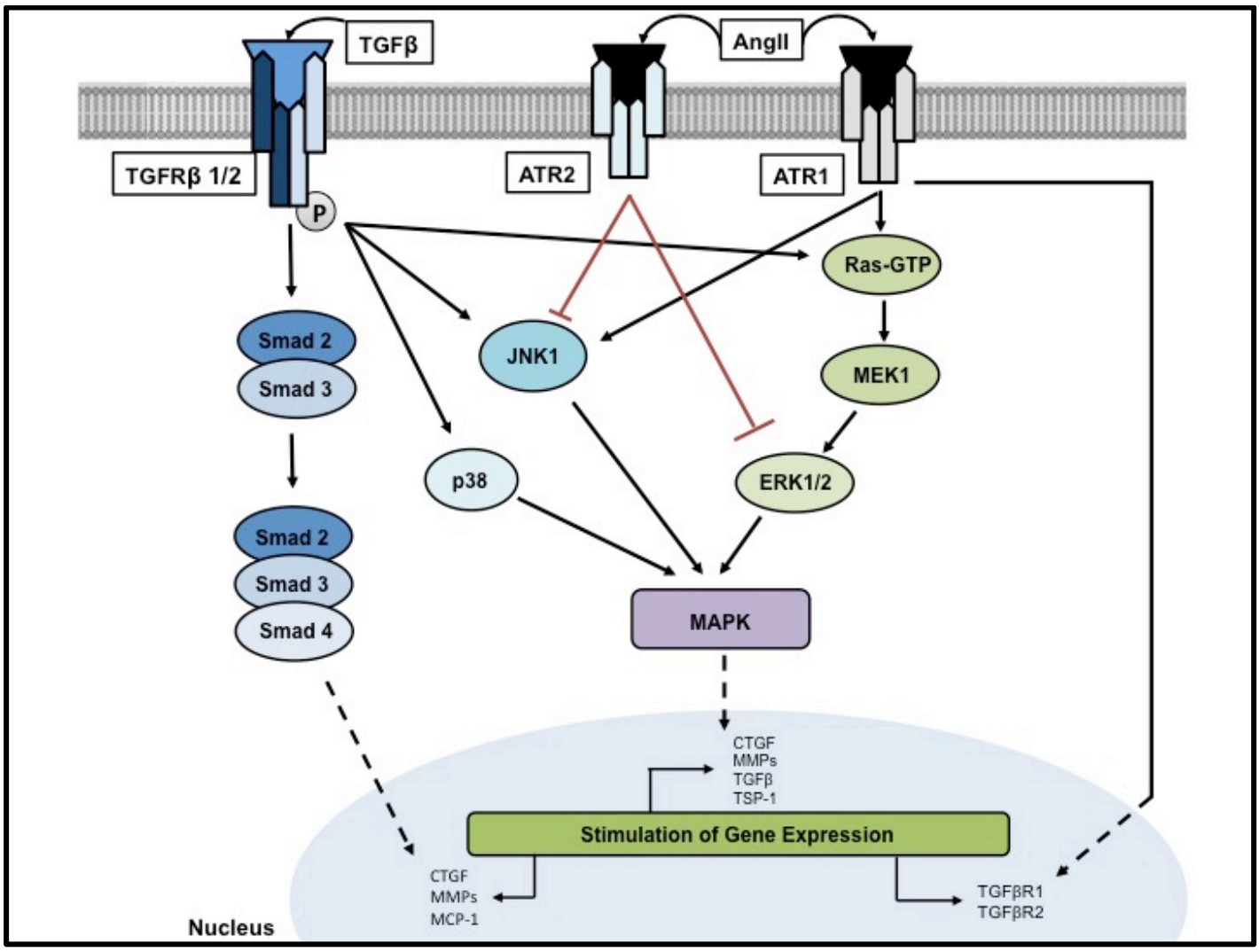

Figure 1: TGF-β signaling in MFS.
TGF-β signaling is thought to contribute to the pathology of MFS including life-threatening development of aortic aneurysm via both canonical TGF-β signaling via the Smad pathway or non-canonical signaling from the TGF-β receptors (TGFRβ) through p38, JNK or ERK1/2 mediated activation of MAPK. Interaction between pathological TGF-β and the AngII / ATR1 pathway is mediated through the stimulation of non-canonical TGF-β signaling or contribution to increased production of TGF-β and TGFRβ. Conversely, ATR2 signaling is proposed to be protective in MFS via its reported inhibition of components of non-canonical TGF-β signaling including reduction in JNK and ERK1/2 mediated signaling.

1.4 Management of MFS Aortic Aneurysm

The clinical approach to MFS is multi-factorial and complicated by the broad range of the systemic pathological manifestations of MFS as well as the wide spectrum of ages and severity and disease seen in the MFS population. Furthermore, pharmacological approaches to preventing life-threatening manifestations of MFS are still sub-optimal. As such, management of MFS aortic aneurysm in patients represents a balance between monitoring of disease progression, pharmacotherapy, and surgical intervention.

1.4.1 Surgical Intervention for Aortic Aneurysm

Surgical intervention in MFS is continuing to evolve and is extending the life expectancy and quality of life of MFS patients. Currently, surgical intervention is considered in adults with an aortic root diameter of greater or equal to 4.5cm or in those in whom rapid aneurysm progression of greater or equal to 0.5cm/year is observed [31]. These recommendations are based on rates of complication including aneurysm rupture, dissection, or sudden death [134-136]. Surgical options for MFS aortic aneurysm include replacement of the aorta with a synthetic graft. This may or may not include replacement of the aortic valve as well. The first reported complete replacement of the ascending aorta was in 1968 by Bentall [137]. This procedure, now commonly referred to as a "Bentall Procedure" involves replacement of the aortic valve, aortic root, and ascending aorta. A natural progression of this was the "David Procedure" which spares the aortic valve and thus reduces need for anti-coagulation. Currently, both approaches are still used, with recent meta-analyses revealing an increased incidence of need for re-intervention with a David Procedure, but an increased incidence of thromboembolic events with a Bentall procedure [138-141]. Beyond these two approaches, surgical management of MFS has continued

to evolve. This includes the use of a personalized external aortic root support, which is an external support tailored to the specific patient anatomy that has been shown to reduce aortic root dimensions, slow rate of aneurysm growth, and may improve aortic wall pathology [142-144]. Beyond the aortic root, a number of case reports detail treatment of non-aortic root aneurysm, such as those of the iliac and subclavian arteries that have been approached using both open and endovascular approaches with success [36, 37, 145].

1.4.2 Pharmacotherapy in MFS

Despite our continuously improving surgical management of MFS patients, thoracic surgery constitutes a major risk. One analysis of thoracic surgery on the ascending aorta and aortic arch for all-comers shows a 2.5% risk of death and an 8.3% chance of stroke along with other post-surgical complications [146]. Furthermore, in MFS patients, risk of dissection remains following aortic surgery and progressive aneurysm past the graft site is reported [147, 148]. Overall this highlights the need to improve pharmacological treatment of MFS in the hopes of halting pathology progression and limiting the need for surgery. This is particularly true for preventing or slowing the progression of aortic aneurysm and is represented by the number of pharmacological strategies have been investigated in this effort. Figure 2 shows four predominant pharmacological approaches used for treatment of MFS: angiotensin converting enzyme [149] inhibitors, angiotensin receptor blockers (ARBs), beta-adrenergic receptor blockers (β-Blockers), and MMP inhibitors. ACE inhibitors prevent the conversion of angiotensin I to angiotensin II thereby preventing activation of angiotensin receptors. Focus on ACE inhibitors has waned in favour of ARBs and β-Blockers. This is due to many recent findings of non-beneficial reduction aneurysm progression in MFS on ACE inhibitors [150, 151].

Furthermore, as depicted in Figure 1, ACE inhibitors also block the proposed protective effects of ATR2 signaling [44]. Fortunately, unlike ACE inhibitors, which block both ATR1 and ATR2 receptors, ARBs selectively block ATR1 and have been found to be more effective than ACE inhibitors in MFS [152]. Selective blockade of ATR1 results in reduction of pathological TGF-β signaling as pictured in Figure 1. The benefit of ARBs versus β-Blockers remains controversial and is discussed further below in considering recent and on-going clinical trials in MFS. While, both ARBs and β-blockers lower blood pressure, β-blockers inhibit beta-adrenergic receptors. Atenolol represents the predominant β-blocker used in MFS and acts to block β1-adrenergic receptors giving rise to both a significant chronotropic and inotropic effect through inhibition of catecholamine binding and has been shown to reduce rates of aortic aneurysm progression as well as pathological processes in the aortic wall leading to factors such as elastic fiber fragmentation and fibrosis. Finally, tetracyclines have been shown to inhibit MMPs [153] and have been found to reduce rate of aneurysm progression and aortic wall pathology in MFS murine models [49-51, 53, 154]. However, doxycycline has not been directly tested in MFS patients to date.

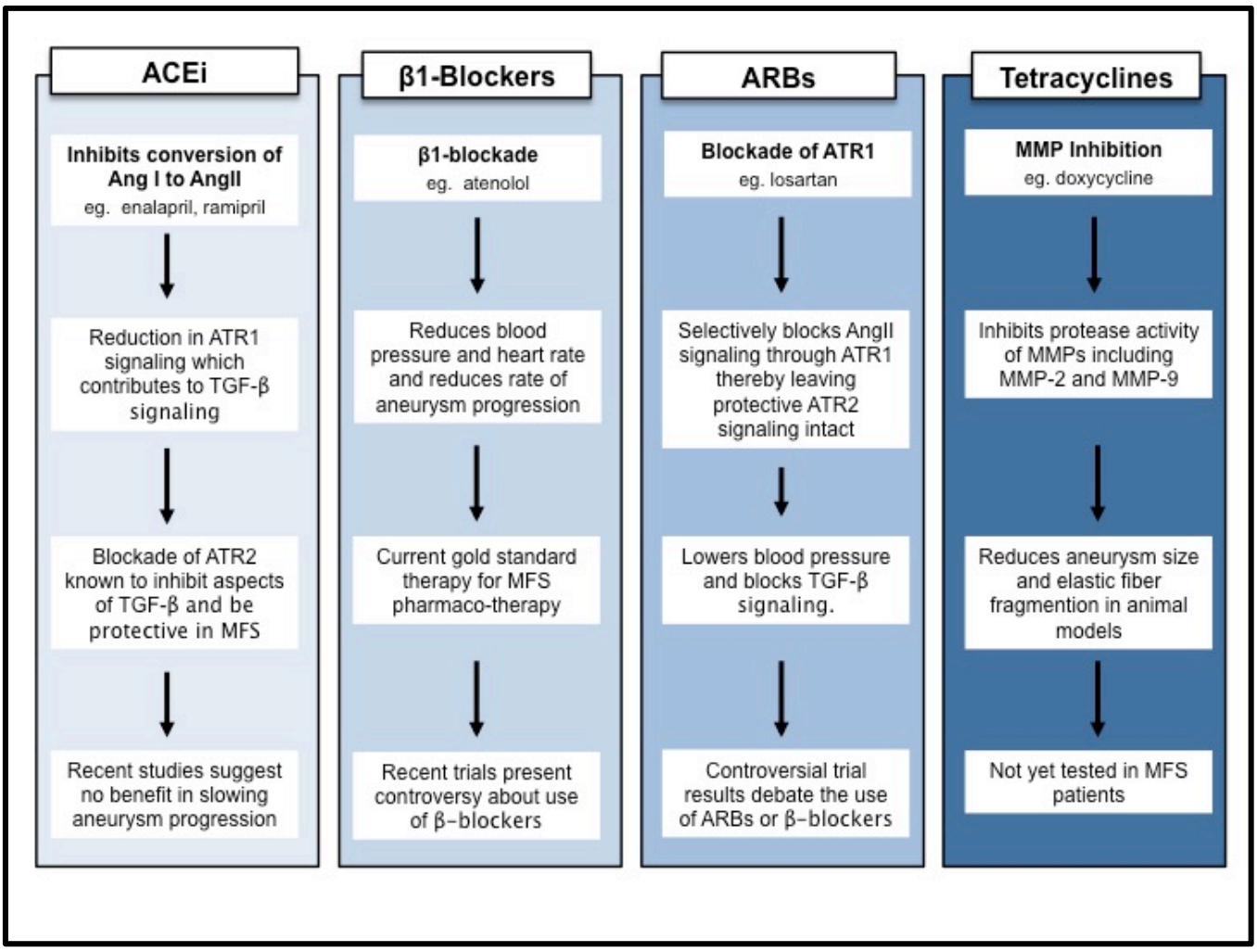

Figure 2: Pharmaceutical approaches to treating MFS.
The main pharmaceutical treatment approaches in MFS utilize ACE inhibitors (ACEi), angiotensin receptor blockers (ARBs), and β1-adrenergic receptor blockers (β1-blockers). In addition, the use of tetracyclines to inhibit MMPs has shown promise in murine models. These approaches all have different therapeutic targets aimed at reducing aneurysm formation and progression in MFS. Notably, while ACE inhibitors are used less frequently recently, much controversy remains around the use of β1-blockers versus ARBs.

1.4.3 ARBs and Losartan

The potential benefit of the use of ARBs for the treatment of MFS was first proposed in the laboratory of Hal Dietz in *Science* in 2006 from results of animal studies [104]. This study demonstrated the ability of losartan to slow aortic root aneurysm in a murine model of MFS

significantly compared to untreated controls or use of β-blocker propranolol. The reduction in aneurysm growth was associated with reduction in elastic fiber fragmentation in the aortic wall as well as a reduction in activation of the smad2 mediated TGF-β signaling pathway. The success of this study led to an initial trial of losartan in a small subset of pediatric MFS patients. This study, by Brooke *et al.* published in the New England Journal of Medicine (NEJM), showed losartan to significantly reduce aortic root dilation compared to previous medical therapy [155]. The success of this trial, further supported by subsequent study in murine models showing the pathogenic effect of TGF-β and the unique ability of ARBs to block ATR1 while maintaining ATR2 signaling [44], gave rise to a number of additional clinical trials including analysis of additional pediatric populations which showed beneficial response to losartan [156], as well as an adult population which showed losartan to be effective at reducing rate aortic root aneurysm expansion as well as aneurysm of the ascending aorta following aortic root replacement [157]. Interestingly, the authors of this study concluded that their trial supports the use of losartan in MFS aneurysm and have also published an analysis correlating TGF-β levels to aortic root size in MFS patients [158]. However, in sub-analysis from this study looking at TGF-β levels following 3 years of losartan treatment, patients with decreased TGF-β levels had significantly higher rate of aortic root aneurysm progression compared with those with increased TGF-β levels [159]. This suggests that losartan treatment may reduce the rate of aortic root dilation independently of a decrease in TGF-β and TGF-β levels may better serve as a marker of aortic damage and not one of MFS mechanism. Moreover, a subsequent study suggests that losartan may be more effective in some patients depending on their *FBN-1* mutation type [160].

1.4.4 Recent and On-going Clinical Trials for the Treatment of MFS

Based on the success of clinical trials of losartan, this led to questions of whether ARBs, particularly losartan, should be used instead of β-blockers. Unfortunately, the answer to this question has stirred controversy and remains openly debated. This diagreement stems from a number of recently published large clinical trials that have evaluated the use of losartan versus atenolol. In 2014, Lacro *et al.* published an analysis of atenolol versus losartan use in the NEJM, which showed reduction in aortic root growth with either treatment but no significant difference between treatment groups over three years [118]. However, this study was criticized for an unequal reduction in blood pressure between treatment groups and presented the argument that evaluation of losartan versus atenolol should be completed at doses that equally reduce blood pressure. Subsequently, Forteza *et al.* also demonstrated no superiority for atenolol or losartan in reducing aortic aneurysm progression in 2016 in the European Heart Journal using a combined pediatric and adult population [117].

Given the lack of superiority of losartan over atenolol, studies are now evaluating the use of β-blockers in combination with losartan. However, early results are also controversial. Chiu *et al.* reported a pilot study in a pediatric patient cohort demonstrating an added benefit of losartan when given in combination with β-blockers [161]. However, in 2015 Milleron *et al.* published a trial of addition of losartan to β-blocker therapy in an adult population and found no additional benefit versus β-blocker alone [162].

1.5 Management of Non-Marfan Aneurysm

Although the management of MFS-associated aortic aneurysm, it is important to consider what can be learned from other forms of aneurysm as aneurysms can form throughout the length

of the aorta in other disease processes. In fact, those of the abdominal aorta, which is anatomically defined as the length of aorta below the diaphragm, are the most prevalent form of aneurysm and account for an estimated 80% of all aortic aneurysms (AAs). In opposition to this, aneurysms of the thoracic aorta, above the level of the diaphragm, constitute the remaining forms of aortic aneurysms. In both cases, similar to MFS aortic root aneurysms in many ways, such thoracic and abdominal aneurysms demonstrate diverse pathogenesis but are generally characterized by factors that induce injury to the vessel wall such as increased production of inflammatory cytokines and infiltration of inflammatory cells, vascular smooth muscle cell apoptosis within the medial aortic layer, increased levels of oxidative stress, formation of atherosclerotic plaque, and high levels of protease activity as well as accelerated rates of extracellular matrix degradation and elastic fiber fragmentation [163-165].

Despite our knowledge of the complex pathogenesis of non-MFS aneurysms, it is estimated that up to 30,000 deaths a year can be contributed to AAA alone in just the USA. This is largely due to the complete lack of markers by which to detect such aneurysms at early stages of development, as they are often asymptomatic and diagnosed by chance during imaging for other diagnostic purposes. Furthermore, once diagnosed patients and doctors alike are faced with the reality that there are no current therapeutic interventions consistently shown to prevent or slow progression of non-MFS thoracic and abdominal aneurysms. Current standards of care recommend use of blood pressure lower medications similar to those used in MFS treatment including β-blockers, ACE inhibitors, and ARBs in an attempt to decrease stress and pressure placed on the weakened aortic wall within an aneurysm. Additionally, protease inhibitors and anti-inflammatory medications are also being trialed. Unfortunately, meta-analysis of the therapeutic utility of any of these interventions is inconclusive or suggests no significant

treatment benefit in the context of AAAs [166-168]. This leaves open or endovascular repair as the only option for treatment prior to life-threatening acute rupture. However, new treatment options on the horizon for AAAs that help to shed light on the pathology of MFS aneurysm as while the pathogenesis of such aortic aneurysms is complex, a role for TGF- β is highly supported similar to MFS pathology. However, in respect to MFS this is somewhat of a conundrum that requires further investigation. In AAA, use of neutralizing TGF- β antibody in an angiotensin II (AngII) induced murine model was shown to exacerbate AAA development. Furthermore, adenoviral mediated overexpression and induction of endogenous TGF-β has been shown to stabilize AAAs in rats models [101, 102]. Collectively, these studies support TGF-β as being protective against aneurysm, however in the case of MFS aneurysm TGF-β is thought to be the main pathogenic driver of aneurysm formation. Thus, development of new models of MFS and future studies of MFS aortic aneurysm may benefit from the juxtaposition of findings in AAAs.

1.6 Models of Marfan Syndrome

A large component to understanding the pathology of MFS and design of new therapeutic approaches has been dependent on murine models. Such is the case of the work presented herein. A number of MFS models of MFS exist and are briefly detailed in Table 2. The most frequently utilized of these MFS murine models are the C1039G, MgR, and MgΔ strains. However, other less commonly used models also exist including the MgN, GT8, and HΔ1 murine strains. All of these models express mutations in *Fbn-1* and include a single residue substitution in the C1039G strain, disruption in exons 18-19 in the MgR strain, and deletion of exons 19-24 in the MgΔ strain. Accordingly, a range of phenotypes are observed with these strains (Table 2).

Model	Genetic Mutation	Notable Phenotype Components
C1039G	Cysteine to glycine missense mutation at Fbn-1 residue 1037	• Homozygotes die at 4-10 days of age. Heterozygotes live a normal life span [26] • Aortic root and ascending aorta aneurysm [26] with fibrosis and elastic fiber fragmentation • Airspace enlargement [104], mitral valve dysfunction [57], and kyphosis [26] • Muscle myopathy and reduced muscle repair [93]
MgR	Neomycin disruption cassette in exons 18 and 19.	• Homozygotes die from aortic dissection at ~ 4 months of age [169] • Aneurysm, aortic fibrosis and elastic fiber pathology, kyphosis, osteopenia [169] [91]
Mg Δ	Deletion of exons 19-24	• Homozygotes lethal at 3 weeks of age due to cardiovascular collapse. Heterozygotes are normal [170]. • Airspace enlargement / lack of aveolar septation [27]
MgN	Null Fbn-1 allele	• Homozygotes die within 2 weeks due to cardiovascular and pulmonary collapse associated with skeletal and muscle pathology. Heterozygotes live normal lifespans [23]. • Airspace enlargement / lack of aveolar septation [27].
GT-8	Truncated Fbn-1 tagged with GFP	• Homozygotes show early post-natal lethality. Heterozygotes show elastic fiber fragmentation in the aortic wall consistent with a MFS phenotype [171].
H1Δ	Deletion of exon 7	• No reported MFS phenotype [171].

Table 2. Comparison of MFS murine models.
A number of murine models of MFS have been developed. These models differ in genetic abnormality as well as phenotype. Notably, the $C1039G^{+/-}$ strain is the model that best recapitulates the human phenotype of MFS.

The C1039G murine strain is utilized throughout this thesis. This strain encodes a cysteine to glycine mutation in *Fbn-1*. Although the strain name suggests this substitution occurs at residue 1039 of the *Fbn-1*, it actually occurs at residue 1037. The use of 1039 was a naming error in the original strain that is maintained by convention. The C1039G mutation is similar to one known to cause MFS in humans – C1039T – that encodes a missense mutation through substitution of cysteine for tyrosine. As discussed in section 1.1.1, a cysteine to glycine missense mutation constitutes the most common type of mutation seen in MFS in that it is a cysteine substitution that occurs in a predicted EGF-like [21, 172]. EGF domains are thought to be responsible for sequestration of the latent TGF-β complex in the extracellular matrix with mutations in these domains thought to result in a reduction in sequestration of latent TGF-β and thereby resulting in aberrant increased levels of non-sequestered TGF-β thought to drive MFS pathology [26, 27]. The importance of such substitutions is perhaps reflected in the lethality of the C1039G strain in its homozygous form ($C1039G^{-/-}$) that die at four to ten days of age [26]. Therefore, the C1039G strain is utilized in its heterozygous form ($C1039G^{+/-}$) and manifests many human MFS phenotypes; $C1039G^{+/-}$ mice exhibit the predominant clinical MFS features including development of aortic root aneurysm, emphysema-like lung destruction, kyphoscoliosis, and muscle and skin abnormalities [26, 93, 104]. Similar to human MFS, aneurysm development in $C1039G^{+/-}$ animals is progressive. Furthermore, emphysema-like lung destruction can be observed at early stages of disease and is also progressive [64]. $C1039G^{+/-}$ animals also exhibit mitral valve dysfunction as a result of aberrant TGF-β signaling with valves exhibiting more compliance to stretch associated with a decline in elastin within the valve leaflets and is a notable feature of the $C1039G^{+/-}$ model as mitral valve dysfunction is a common reason surgery in young MFS patients and a cause of morality in such patients [57] [173].

Chapter 2: Rationale, Aims, and Hypotheses

2.1 Rationale

The use of losartan to treat development and progression of MFS aortic root aneurysm has recently generated a number of high impact publications. Collectively, these publications present data supporting the use of losartan for its selective ATR1 blockade, which results in a reduction of canonical and non-canonical TGF-β signaling thought to drive MFS aneurysm pathology [26, 45, 104]. These findings led to initial clinical trials demonstrating the utility of losartan to reduce the rate of aortic root aneurysm in small groups of patient and subsequently led to the start of large multi-center trials comparing the use of losartan to that of current gold standard treatment, β1-adrenergic receptor blocker atenolol [130, 156, 157, 162, 174]. However, despite this important work and the continuation of clinical trials, the specificity of losartan remains unconfirmed in MFS. Beyond the specificity of losartan, the larger over-arching question of the penetrance of ATR1 signaling in MFS pathology is also unknown. Restated, this is simply the question of what aspects of MFS aortic pathology, if any, would remain in the case of the development of a perfect ATR1 blocker? In answering this question and determining the specificity of losartan, the field can begin to address if in fact treatment of MFS aortic aneurysm is multi-factorial and potentially best achieved by drug cocktails to target a number of pathogenic pathways or if focus should be on the development of superior forms of losartan with higher ATR1 specificity and potency.

Related to determining the penetrance of ATR1 signaling in MFS, the systemic pathology of MFS must be considered and evaluated. This is of importance when considering the improvement of quality of life for patients as the systemic manifestations of MFS, as discussed above, have a notable impact. Furthermore, from a clinical perspective, this is also of growing

importance; given the increasing life expectancy of MFS patients due to improved cardiac treatment, monitoring and surgical intervention for aortic aneurysm, systemic MFS features are more likely to adversely affect patients and complicate care in the future. Perhaps the most salient example of this is that of MFS lung pathology. From case reports of airspace destruction and spontaneous pneumothorax in patients to MFS animals model demonstrating significant and progressive emphysema-like lung destruction [67, 77, 79, 175], MFS presents a non-trivial lung component [27, 104]. Moreover, in the context of patients with significant cardiovascular disease, such as those with MFS, lung pathology is of particular concern; synergistic effects are often seen between lung and cardiovascular disease and compromised lung function places additional demands on the cardiovascular system. Despite this, little focus has been placed on characterizing MFS lung pathology and determining if drugs such as atenolol or losartan address pulmonary MFS complications or if other therapeutic means should be utilized.

2.2 Aims

In order to evaluate the penetrance of ATR1 signaling in MFS and determine the specificity of losartan in treating MFS aortic root aneurysm, the presented work aimed to:

- Generate a novel model of MFS lacking expression of ATR1.
- Evaluate the impact of lack of ATR1 expression on development of the pathological features of MFS.
- Determine if the therapeutic effects of Losartan in reducing the incidence and severity of aortic root aneurysm in MFS are ATR1 specific.

To enhance our understanding of the pathology and treatment of MFS lung pathology, the presented work aimed to use a murine model of MFS to:

- Characterize airspace enlargement.
- Establish the impact of MFS on lung function.
- Evaluate the pharmacological means of treating MFS lung pathology.

2.3 Hypotheses

From the established aims of the presented work, hypotheses were generated regarding the role of ATR1 in MFS, the specificity of losartan and the phenotype and treatment of MFS lung pathology. Specifically, as losartan, an ATR1 specific ARB, has been shown to be effective at treating MFS aortic root aneurysm and airspace enlargement, we hypothesized that a model of MFS lacking ATR1 expression would be protected from development of MFS aortic and lung pathology. Furthermore, we hypothesized that as a MFS model deficient in ATR1 lacks the proposed target of losartan, losartan would have no therapeutic benefit in preventing aortic root aneurysm. Finally, as MFS models show progressive airspace enlargement that is treatable with losartan, we hypothesized that MFS models would show significant changes in lung function that would be improved with losartan treatment.

Chapter 3: Materials and Methods

Materials and methods utilized throughout the presented work are described and discussed below. Specifically, animal models are addressed in section 3.1, treatment regimens utilized in animal models are detailed in section 3.2, methods of evaluating animal models are provided in section 3.3, histological methods are found in section 3.4, and detailed descriptions of *in vitro* studies are in section 3.5. N-values for experiments are indicated in subsequent chapters.

3.1 Animal Models

Murine models were used extensively throughout the presented work. Section 3.1 encompasses details of known strain phenotype, justification of strain selection, breeding strategies and genotyping approaches. All animals were housed in the Genetically Engineered Models [176] facility at the Centre for Heart Lung Innovation at St. Paul's Hospital (SPH). All strains were verified as pathogen free prior to use in establishing experimental lines. Animals were housed in groups in climate controlled, hepa-filtered cages on a standard 12-hr light/dark cycle and provided food and water *ad libitum*. Breeder pairs were fed a diet formulated to support successful breeding (PicoLab Mouse Diet 20, LabDiet, Catalog #5058; Appendix IA). All other animals were fed standard laboratory chow (Laboratory Rodent Diet, LabDiet, Catalog #5001; Appendix IB). Animals were weaned at 3-4 weeks of age and subsequently genotyped. The University of British Columbia Animal Care Committee, under protocol numbers A12-0136, A12-0281, A14-0070, A14-0072, and A12-0152, approved all animal use and procedures.

3.1.1 Marfan (*Fbn1* C1039G) Mice

The *Fbn1* C1039G mouse strain was used as a model of MFS throughout the presented work. Mice from this strain were originally supplied from the laboratory of Dr. H. Dietz (Johns Hopkins University) in 2011 and maintained on a C57 BL/6 background in the GEM facility at the Centre for Heart Lung Innovation at SPH. Notably, the C1039G strain (B6.129-Fbn1tm1Hcd/J, stock #012885) is now available through The Jackson Laboratory (JAX) [177]. However, mice used throughout this work were obtained from the laboratory of Dr. H. Dietz. The C1039G strain is a model of MFS that exhibits a cysteine to glycine missense mutation in *Fbn1* as a result of a single base pair alteration (thymine to guanine) [26]. Although the strain name suggests this mutation occurs at codon 1039 of the *Fbn1* gene, it actually occurs at codon 1037. The use of 1039 was a naming error in the original strain that is maintained by convention. The C1039G mutation is similar to a mutation known to cause MFS in humans – C1039Y – which encodes a missense mutation through substitution of cysteine for tyrosine [21]. Notably, mice homozygous for the C1039G mutation ($C1039G^{-/-}$) die at ten to fourteen days of age [26]. However, heterozygous mice exhibit pathology of MFS akin to many of the phenotypes observed in human MFS (Table 2, Chapter 1) in which aortic root aneurysm, lung airspace enlargement, kyphosis, and myopathy are noted [26, 57, 93, 104]. Therefore, studies presented throughout utilize the C1039 strain in heterozygous form ($C1039G^{+/-}$).

Generation of $C1039G^{+/-}$ mice for experimental purposes (eg. comparison of lung function in $C1039G^{+/+}$ vs $C1039^{+/-}$ animals) was completed by crossing $C1039G^{+/-}$ mice to wild-type C57 BL/6 mice (JAX, stock #000664) [178] (Figure 3). However, in all cases where mice with multiple genetic variations were generated (ie. C1039G strain with a subsequent gene knockout), a breeding strategy (described in subsequent sections) was utilized that would allow for the

possibility to generate C1039G$^{-/-}$ animals that could result if any intervention utilized was capable of preventing early post-natal lethality of C1039G$^{-/-}$ animals.

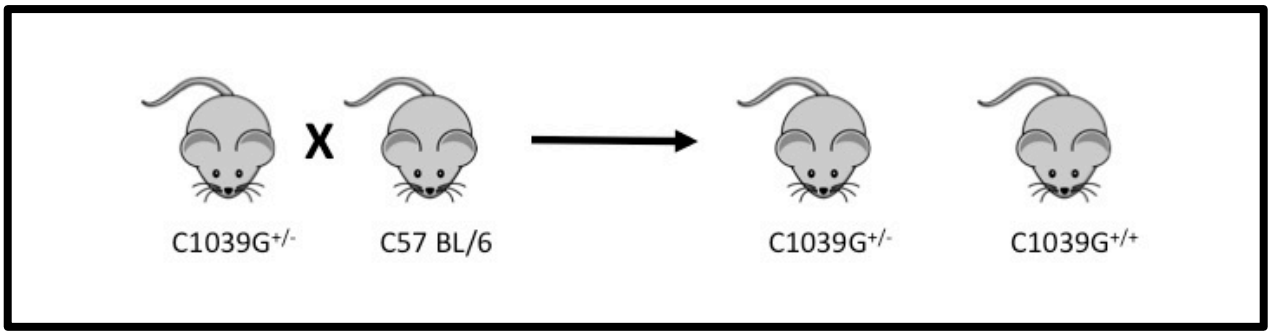

Figure 3: Breeding scheme for standard C1039G strain.
The *Fbn1* C1039G strain was maintained on a C57 BL/6 background via cross breading of C1039G$^{+/-}$ animals to C57 BL/6 mice to generate C1039G$^{+/-}$ mice, which exhibit the MFS phenotype and C1039G$^{+/+}$ wild-type controls.

A number of considerations led to the choice to use the C1039G model over other available MFS strains; from a logistical and ethical standpoint, the model C1039G is used throughout the collaborative MFS research groups in Vancouver. As such, choosing the C1039G model allowed us to provide samples to our collaborators, which were of the same model and similar genetic background, thereby reducing overall animal numbers and helping to fulfill the "Three Rs" (Reduction, Replacement, Refinement) requirement of UBC animal ethics. Furthermore, MgR and C1039G strains of MFS mice (Table 2, Chapter 1) are the most commonly used murine models of MFS [26, 169]. However, while MgR mice exhibit many phenotypes of human MFS including kyphosis, long bone over-growth, aortic aneurysm and elastic fiber fragmentation in the aortic wall, they are a more severe MFS model relative to the C1039G strain [169]; Homozygous MgR mice are reported to die at 3.8±3.4 months of age of vascular and potentially pulmonary causes and they exhibit cardiac phenotypes beyond those typically seen in human MFS including cardiomyopathy and elastic fiber fragmentation throughout the length of the aorta

[179, 180]. In addition, C1039G mice have a cysteine substitution in an EGF-like domain instead of the insertion of a neomycin disruption cassette insertion between two exons as is seen in MgR mice. Therefore, the C1039G strain presents itself as a model carrying a genetic mutation more representative of the human syndrome it is aimed to recapitulate [26, 169].

Genotyping for C1039G mice was completed throughout the presented work by two methods. The first method utilized primers that amplified the same region in both the WT and mutant gene. Subsequently, the PCR product was digested with KpnI as the C1039G mutation introduces a KpnI restriction site within the amplicon and $C1039G^{+/-}$ mice can thus be differentiated from $C1039G^{+/+}$ mice by electrophoretic separation of the digested PCR products [26]. As of 2012, a second method was used for genotyping that employed a primer system that gives rise to two distinct PCR products for WT and C1039G alleles [177]. Primer sequences and resulting DNA fragment size are given in Table 3.

3.1.2 ATR1-alpha Deficient Mice

Mice deficient for ATR1-alpha (denoted throughout as $ATR1^{-/-}$ subsequently for clarity) were purchased from the Jackson Laboratory (B6.129P2-Agtr1atm1Unc/J, stock #002682) [181] and maintained on a C57 BL/6 background in the GEM facility at Centre for Heart Lung Innovation. $ATR1^{-/-}$ mice represent a targeted disruption of ATR1-alpha and have been shown to lack pressor responses to infusion of AngII and have a significant reduction in blood pressure. Notably, this model has been used extensively to determine the contribution of ATR1 signaling to pathology including studies of AngII induced aortic aneurysm and development of atherosclerosis in the aortic root [182, 183].

Initially, $ATR1^{-/-}$ mice were crossed with $C1039G^{+/-}$ mice to generate $ATR1^{+/-}$ $C1039G^{+/-}$ mice (Figure 4A). Subsequently $ATR1^{+/-}$ $C1039G^{+/-}$ littermates were crossed to generate experimental MFS mice deficient in ATR1-alpha ($C1039G^{+/-}$ $ATR1^{-/-}$) and littermate control groups ($C1039G^{+/+}ATR1^{+/+}$, $C1039G^{+/-}ATR1^{+/+}$, and $C1039G^{+/+}ATR1^{-/-}$) as shown in Figure 4B. Mice heterozygous for ATR1 ($ATR1^{+/-}$) generated from crossing of $ATR1^{+/-}$ $C1039G^{+/-}$ littermates were not utilized and culled from the colony. Genotyping for ATR1 was completed using primer sequences provided by the Jackson Laboratory from which animals were purchased [181]. Primer sequences and expected sizes of PCR products are given in Table 3. Examples of genotyping of $C1039G^{+/-}$ $ATR1^{-/-}$ mice are given in Figure 5 below and demonstrate a clear ability to determine genotype of this novel strain prior to evaluation.

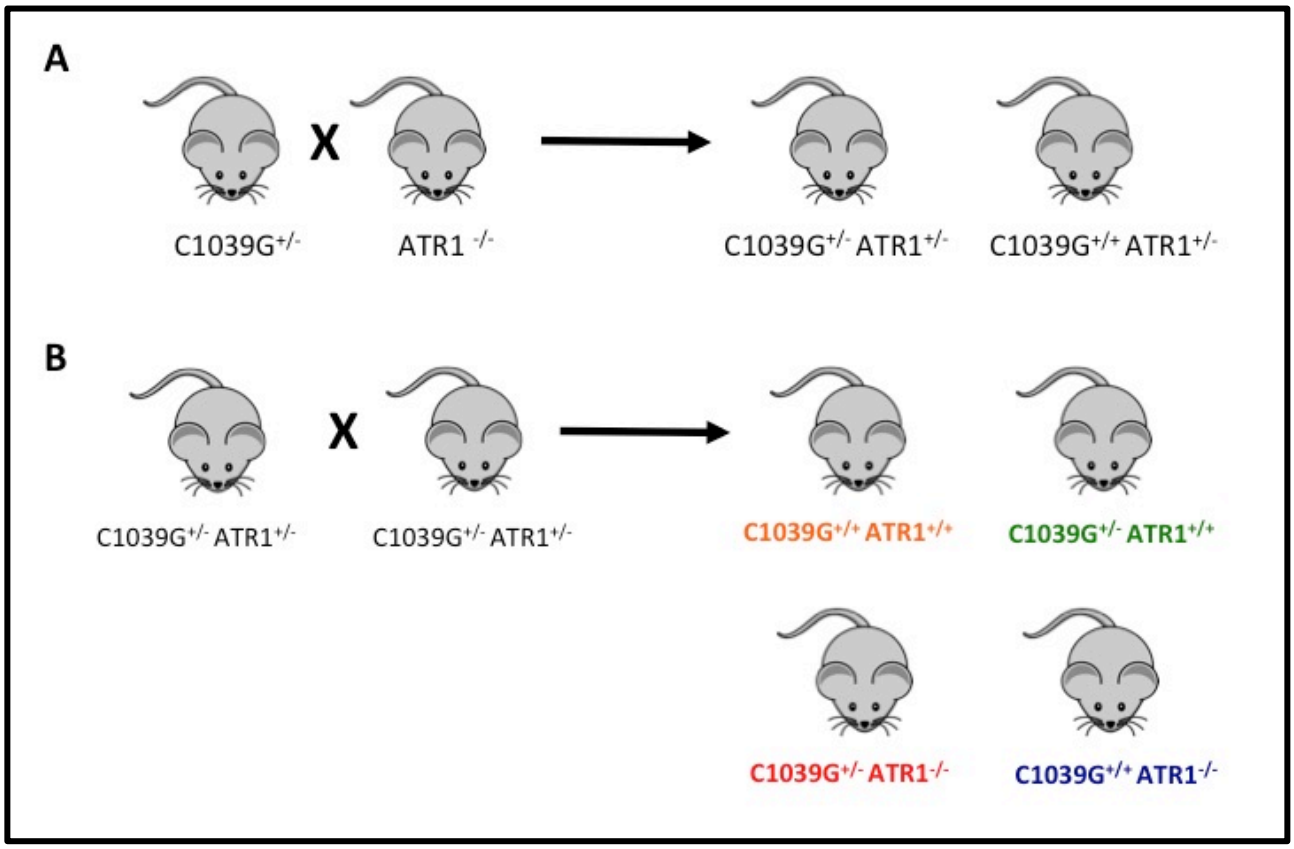

Figure 4: Breeding scheme for C1039G$^{+/-}$ ATR1 deficient model.
C1039G$^{+/-}$ mice lacking ATR1-alpha expression were generated by first crossing C1039G$^{+/-}$ mice to ATR1$^{-/-}$ mice (**A**). Subsequently, C1039G$^{+/-}$ ATR1$^{+/-}$ littermates were crossed (**B**) to generate experimental MFS mice lacking ATR1 expression (C1039G$^{+/-}$ ATR1$^{-/-)}$ and littermate controls (C1039G$^{+/-}$ ATR1$^{+/+}$, C1039G$^{+/+}$ ATR1$^{-/-}$, C1039G$^{+/+}$ ATR1$^{+/+}$).

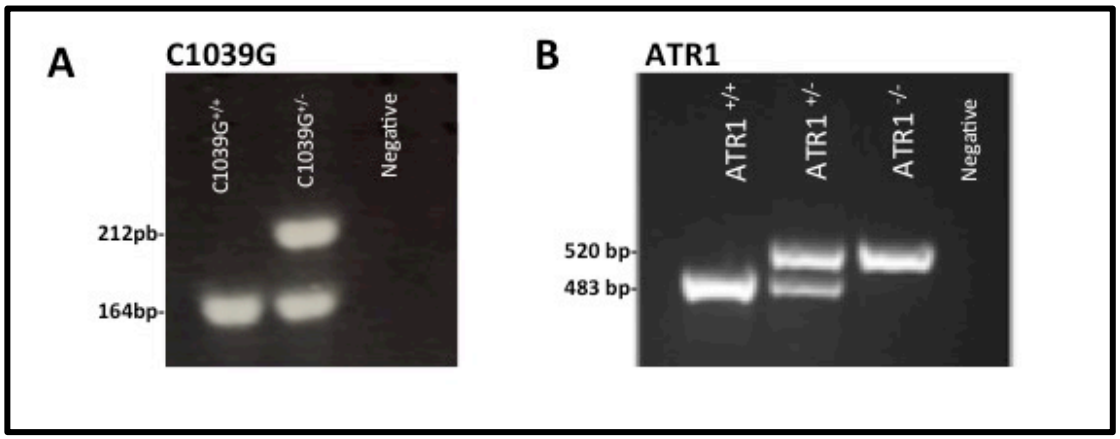

Figure 5: Genotyping of C1039G$^{+/-}$ ATR1$^{-/-}$ Mice.
Genotyping of C1039G$^{+/-}$ mice generated clearly differentiable PCR products for C1039G$^{+/+}$ (WT, 164bp) and C1039G$^{+/-}$ (MFS, 212bp) mice (**A**). Similarly, genotyping from ATR1 within this line of mice easily identifies ATR1$^{+/+}$ (WT, 483bp), ATR1$^{+/-}$ (483 + 520bp), and ATR1$^{-/-}$ (520bp) animals (**B**). A negative control (Negative), denotes PCR performed in the absence of added genomic DNA for both A and B.

3.1.3 ATR1-alpha / Beta Deficient Mice

Mice deficient in both alpha and beta isoforms of ATR1 (ATR1$\alpha^{-/-}\beta^{-/-}$) were obtained from the laboratory of Dr. Coffman (Duke University)[111]. Initial mice obtained from Dr. Coffman to establish a colony were crossed to C57 BL/6J mice. Pups resulting from this cross were harvested by caesarean section and fostered to pathogen-free CD-1 mice to eliminate pathogens present in the founder mice supplied by Dr. Coffman. Resulting pathogen free cousins were then crossed to regenerate ATR1$\alpha^{-/-}\beta^{-/-}$ animals. Notably, this strain is maintained on a mixed background of B6 and 129. Discussion with Dr. Coffman's group revealed that attempts to move this strain to a pure B6 background had previously resulted in infertility and that their group recommends maintaining the line on a mixed B6 / 129 background.

However, the use of a mixed B6 / 129 strain presented issues with generating MFS mice lacking both alpha and beta ATR1 isoforms with a consistent genetic background. Therefore, we

attempted to backcross ATR1$\alpha^{-/-}\beta^{-/-}$ to C57 BL/6 animals. Unfortunately, we observed similar issues as Dr. Coffman's group – mixed coat litters with declining litter frequency and pup numbers. Therefore, we concluded we were unable to generate MFS ATR1$\alpha^{-/-}\beta^{-/-}$ mice in a manner that would be comparable to our MFS ATR1-alpha deficient model.

3.1.4 eNOS Phospho-mutant Mice

Dr. Paul Haung (Harvard University) kindly provided mice that are considered to be "phospho-" mutants of eNOS. These mice contain a knock-in to the endogenous eNOS gene that introduces a mutation at one of the main phosphorylation sites of eNOS – serine 1176 (S1176). S1176 corresponds to Serine 1177 in human and Serine 1179 in bovine. The phosphorylation state of this serine has been shown to regulate the activity of eNOS and production of NO and play a role in vascular homeostasis and disease pathology. Reduced levels of NO are observed in the less-active un-phosphorylated state and increased NO levels are seen in the active phosphorylated state [184-190].

In order to investigate the effect of both decreased and increased levels of NO, Dr. Huang kindly provided both Ser-1176-Asp (S1176D) and Ser-1176-Ala (S1176A) knock-in phospho-mutant models which act as an eNOS phospho-mimetic (constitutively phosphorylated with increased NO levels) and phospho-dead (cannot be phosphorylated and have decreased NO levels) models respectively as described in more detail below. However, it is important to note that both of these strains had been backcrossed to a C57 BL/6 background. Furthermore, these mice are different than those previously described that harbor the same eNOS substitutions as a model developed using a trans-gene approach [191]. As the S1176D and S1176D models utilized here are knock-in models, the phospho-mutations are regulated by the endogenous eNOS

promoter, as opposed to the transgenic models that express endogenous eNOS in addition to a eNOS phospho-mutant transgene. Thus, the choice of a knock-in model avoids issues that may arise with a transgenic model such as determining copy number and impact of the site of transgene insertion. In line with this, both S1176A and S1176D knock-in phospho-mutant models have been shown to have similar localization and expression levels of total eNOS [188].

In all cases, eNOS phospho-mutant knock-in mice were re-derived from cryogenically preserved homozygous knock-in embryos at the Life Sciences Centre at UBC. Subsequently, mice were confirmed to be pathogen free and maintained on a C57 BL/6 background in the GEM facility at the Centre for Heart Lung Innovation. Genotyping for both phospho-mutant strains was completed using primers specific to the knock-in construct. Primer sequences and PCR product sizes are shown in Table 3. An example of agarose gel electrophoresis of the products of this PCR strategy is shown in Figure 6A.

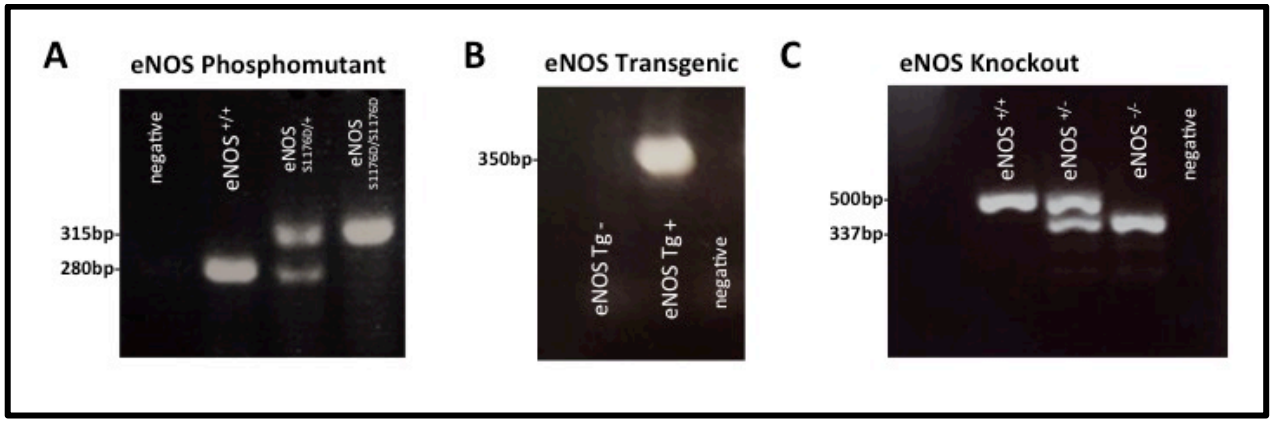

Figure 6: Genotyping of phospho-mutant, eNOS transgenic, and eNOS knockout animals. Genotyping of S1176D or S1176A mice show bands that are clearly able to identify homozygous (315bp), heterozygous (280bp + 315bp) or wild type animals (280bp) (**A**). Similarly, genotyping of eNOS transgenic animals shows clear identification of the transgene in Tg^{+} (350bp) animals with no bands present in Tg^{-} animals (**B**). Finally, genotyping of eNOS knockout animals showed distinctly different PCR products for $eNOS^{+/+}$(500bp), $eNOS^{+/-}$(500+337bp), and $eNOS^{-/-}$ (337bp) animals (**C**).

3.1.4.1 eNOS Phospho-mimetic eNOS Ser-1176-Asp (S1176D) Mice

eNOS phospho-mutant S1176D knock-in mice are considered an eNOS phospho-mimetic model as they mimic a constitutively phosphorylated state of S1176. Prior to the development of animal models, this substitution in eNOS was studied in cell culture; the creation of eNOS phospho-mimetic transgenic and knock-in strains is based on previous work in ECs showing that substitution of an aspartate group, to mimic the negative charge of a phosphate group, gives rise to increase levels of NO [184, 185] attributable to preventing dissociation of calmodulin and enhanced enzymatic activity of eNOS [192]. This is consistent with S1176D knock-in mice that have increased basal levels of NO and increased NO production upon treatment with calcium ionophore in isolated ECs. Furthermore, S1176D mice show increased acetylcholine stimulated cGMP levels in aortic rings [188, 189].

To generate a line of MFS mice with an eNOS phospho-mimetic knock-in, $C1039G^{+/-}$ mice were crossed with homozygous S1176D knock-in mice ($eNOS^{1176D/S1176D}$) (Figure 7A). The resulting $C1039G^{+/-}$ $eNOS^{S1176D/+}$ littermates were crossed to generate experimental $C1039G^{+/-}$ $eNOS^{S1176D/S1176D}$ animals with littermate controls ($C1039G^{+/+}$ $eNOS^{+/+}$, $C1039G^{+/-}$ $eNOS^{+/+}$, and $C1039G^{+/+}$ $eNOS^{S1176D/S1176D}$) as shown in Figure 7B.

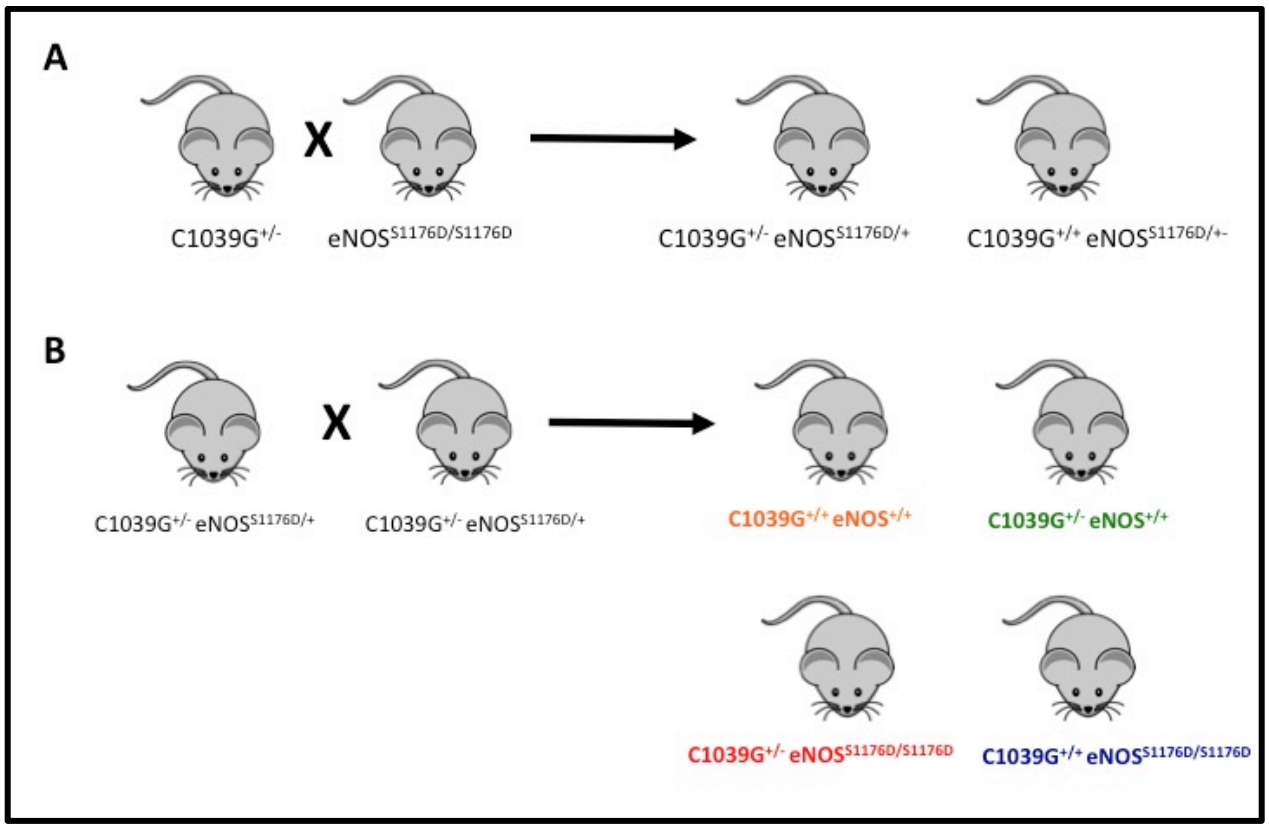

Figure 7: Breeding scheme for C1039G eNOS Ser1176 Asp (S1176D) model.
C1039G$^{+/-}$ with an eNOS gene knock-in introducing a serine to aspartate (S1176D) substitution at residue 1176 were generated by crossing MFS C1039G$^{+/-}$ mice to mice homozygous for S1176D knock-in (eNOS$^{S1176D/S1176D}$) to generate MFS C1039G$^{+/-}$ mice heterozygous for S1176D knock-in (eNOS$^{S1176D/+}$) (**A**). These mice (C1039G$^{+/-}$ eNOS$^{S1176D/+}$) were subsequently crossed (**B**) to generate experimental MFS animals homozygous for S1776D knock-in (C1039G$^{+/-}$ eNOS$^{S1176D/S1176D}$) and littermate controls (C1039G$^{+/+}$ eNOS$^{+/+}$, C1039G$^{+/-}$ eNOS$^{+/+}$, and C1039G$^{+/+}$ eNOS$^{S1176D/S1176D}$).

3.1.4.2 eNOS Phospho-dead eNOS Ser-1176-Ala (S1176A) Mice

eNOS "phospho-dead" knock-in mice that exhibit a serine (S) to alanine (A) substitution at eNOS residue 1176 (S1176A). The introduction of an alanine residue means no phosphorylation can take place and the mice are therefore "phospho-dead" and only a low level of NO is produced. Physiologically, this results in increased mean arterial pressure and blunted vascular relaxation to acetylcholine treatment [189]. Prior to the development of S1176A animals, the Ser-to-Ala substitution was investigated *in vitro* and showed that the Ser-to-Ala substitution in

cell culture did not change eNOS expression levels but did result in reduced NO production [184, 185].

In order to evaluate the impact of a S1176A substitution in MFS, we generated MFS mice homozygous for a S1176A knock-in ($eNOS^{S1176A/S1176A}$). To do so, $C1039G^{+/-}$ mice were crossed with homozygous S1176A knock-in mice ($eNOS^{S1176A/S1176A}$) to generate $C1039G^{+/-}$ $eNOS^{S1176A/+}$ littermates (Figure 8A). These littermates were crossed to produce experimental $C1039G^{+/-}$ $eNOS^{S1176A/S1176A}$ animals with littermate controls ($C1039G^{+/+}$ $eNOS^{+/+}$, $C1039G^{+/-}$ $eNOS^{+/+}$, and $C1039G^{+/+}$ $eNOS^{S1176A/S1176A}$) (Figure 8B).

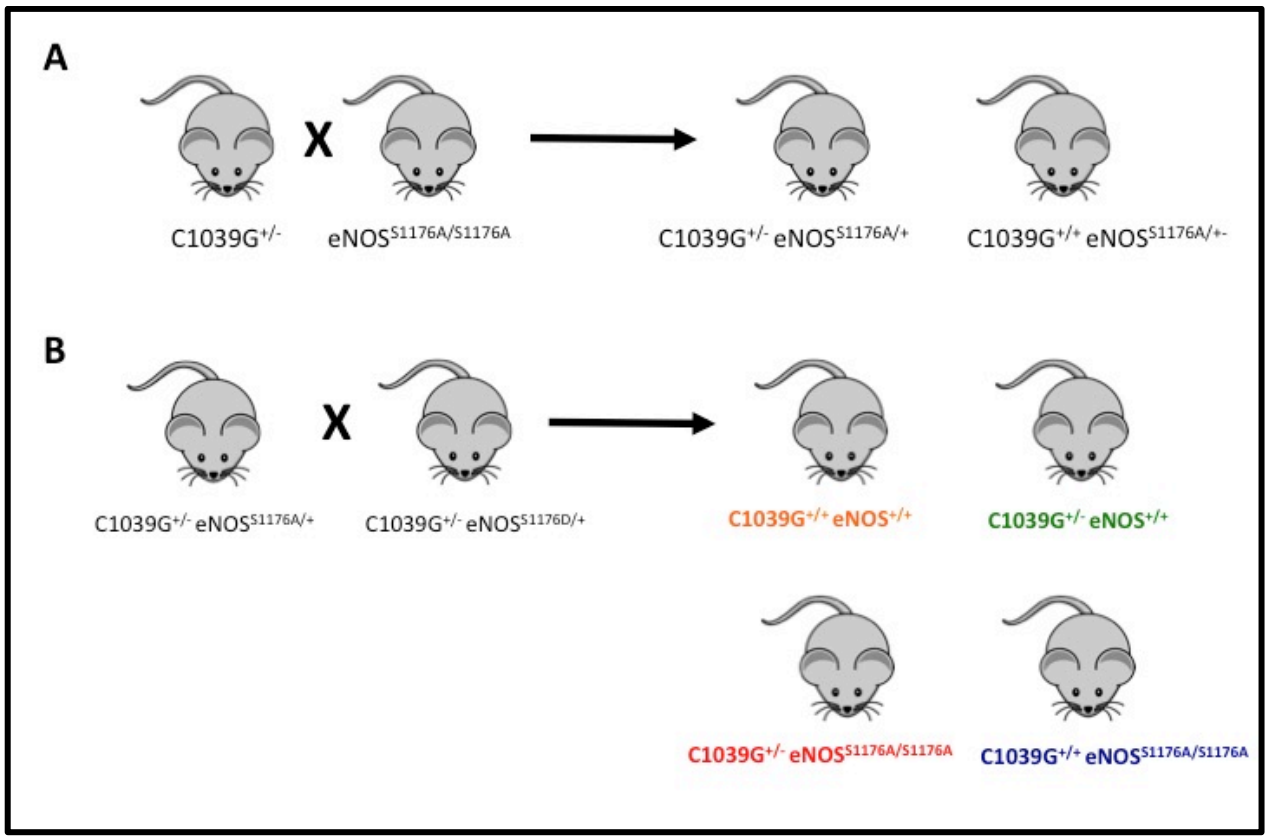

Figure 8: Breeding scheme for C1039G eNOS Ser 1176 Ala (S1176A) model. C1039G$^{+/-}$ encoding an eNOS gene knock-in introducing a serine to alanine (S1176A) substitution at residue 1176 were generated by crossing a MFS C1039G$^{+/-}$ mice to mice homozygous for S1176A knock-in (eNOS$^{S1176A/S1176A}$) to generate MFS C1039G$^{+/-}$ mice heterozygous for S1176A knock-in (eNOS$^{S1176A/+}$) (**A**). These mice (C1039G$^{+/-}$ eNOS$^{S1176A/+}$) were subsequently crossed (**B**) to generate experimental MFS animals homozygous for S1776A knock-in (C1039G$^{+/-}$ eNOS$^{S1176A/S1176A}$) and littermate controls (C1039G$^{+/-}$ eNOS$^{+/+}$, C1039G$^{+/+}$ eNOS$^{S1176A/S1176A}$, C1039G$^{+/+}$ eNOS$^{+/+}$).

3.1.5 eNOS Transgenic Mice

Dr. Rini de Crom (Erasmus University, Netherlands) kindly provided mice containing a green florescent protein (GFP) tagged transgene for eNOS that had been backcrossed to C57 BL/6 mice for greater than ten generations [193]. Initial mice received from Dr. de Crom were crossed to C57 BL/6J mice and the resulting pups were collected immediately upon birth and fostered to pathogen-free CD1 mice in order to eliminate pathogens present in initial animals received. Subsequently, eNOS Tg^{+} animals were maintained in the sterile barrier facility of the

GEM facility at the Centre for Heart Lung Innovation on a B6 background. Genotyping for the eNOS transgene was completed using the primers listed in Table 3 and yielded a distinct indication for the presence of the transgene as demonstrated in Figure 6B. Initial genotyping results were confirmed under UV-light examination of animal ears, which showed fluorescence in eNOS Tg^{+} mice and no fluorescence in eNOS Tg^{-} animals.

Hemizygous animals (eNOS Tg^{+}) have previously been shown to exhibit increased eNOS activity in aortic tissue of approximately 30-fold over Tg^{-} controls which resulted in increased NO levels in the aorta of approximately twice that seen in Tg^{-} controls. eNOS protein resulting from the transgene was observed in endothelial cells throughout the body. Further, within the ECs, eNOS-GFP was found to be mainly localized to the plasma membrane and Golgi complex [193]. Overall, these finding are indicative of a transgenic approach that resulted in appropriate localization of eNOS that increased production of NO in the vasculature. Therefore, we chose to use these mice to generate a line of MFS mice overexpressing eNOS. To do so, hemizygous eNOS transgenic mice (eNOS Tg^{+}) were bred to $C1039G^{+/-}$ animals. This single cross gave rise to experimental animals ($C1039G^{+/-}$ eNOS Tg^{+}) and littermate controls ($C1039G^{+/+}$ eNOS Tg^{-}, $C1039G^{+/-}$ eNOS Tg^{-}, $C1039G^{+/+}$ eNOS Tg^{+}) as detailed in Figure 9.

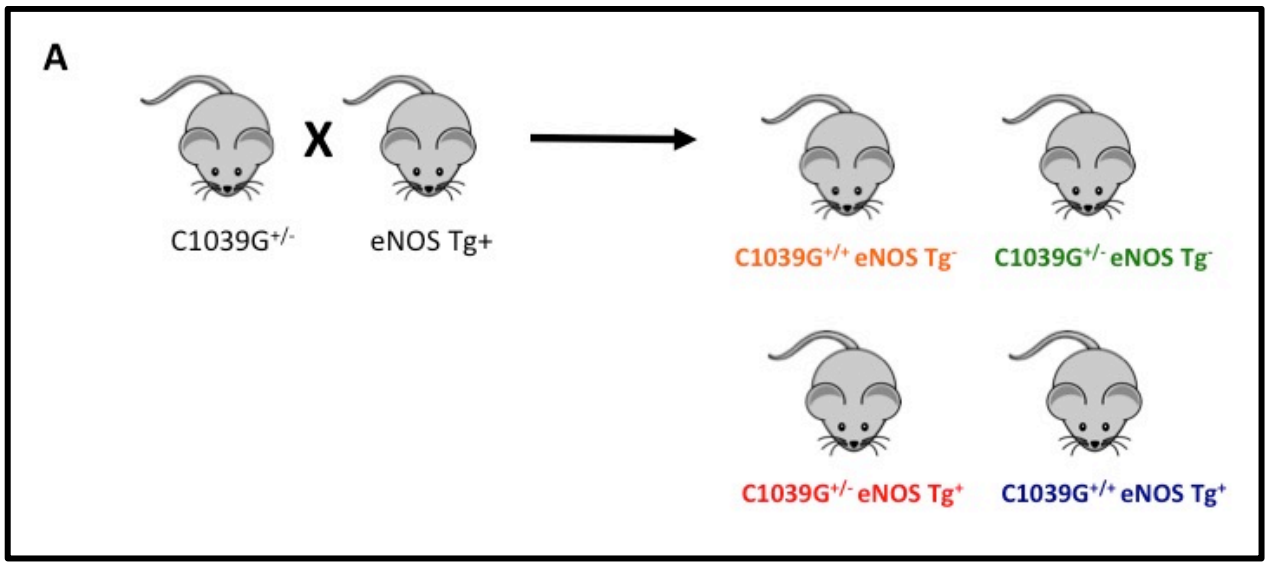

Figure 9: Breeding scheme for C1039G eNOS transgenic model.
C1039G$^{+/-}$ with hemizygous expression of an eNOS transgene (eNOS Tg^{+}) were generated by crossing C1039G$^{+/-}$ to hemizygous eNOS transgenic mice (eNOS Tg^{+}) to generate experimental C1039G$^{+/-}$ eNOS Tg^{+} mice and littermate controls (C1039G$^{+/+}$ eNOS Tg^{-}, C1039G$^{+/-}$ eNOS Tg^{-}, C1039G$^{+/+}$ eNOS Tg^{+}).

3.1.6 eNOS Knockout Mice

Mice deficient in eNOS (eNOS$^{-/-}$) mice were purchased from the Jackson Laboratory (stock #002684, B6.129P2-Nos3tm1Unc/J)[194, 195]. eNOS knockout mice have previously been shown to be deficient in eNOS, lack endothelial specific production of NO, and exhibit elevated blood pressure and decreased heart rate [195].

Initial mice received from the Jackson Laboratory were crossed to C57 BL/6J mice and resulting pups were collected immediately upon birth and fostered to pathogen-free CD-1 mice in order to eliminate pathogens present in initial animals. The genotyping of eNOS$^{-/-}$ mice was completed using the primers listed in Table 3 and allowed a clear distinction between eNOS$^{+/+}$, eNOS$^{+/-}$, and eNOS$^{-/-}$ animals (Figure 6C). eNOS$^{-/-}$ mice were crossed to C1039G$^{+/-}$ animals to generate C1039$^{+/-}$ eNOS$^{+/-}$ animals. Subsequently C1039$^{+/-}$eNOS$^{+/-}$ littermates were crossed to generate MFS mice lacking eNOS (C1039$^{+/-}$ eNOS$^{-/-}$) and littermate controls (Figure 10A, B).

However, generation of experimental animals was low owing to infrequent litters and small litter size. Furthermore, of the pups produced, the rate of generation of C1039$^{+/-}$ eNOS$^{-/-}$ was much lower than expected and did not adhere to expected Mendelian ratios, a factor that has been noted with use of the eNOS$^{-/-}$ strain previously [196]. Therefore, in an attempt to expedite generation of experimental animals C1039$^{+/-}$ eNOS$^{-/-}$ were crossed to eNOS$^{-/-}$ animals (Figure 10C). Despite this, the number of animals generated was still very low and this paucity of experimental animals is reflected in the analysis of C1039G$^{+/-}$ eNOS$^{-/-}$ mice in Chapter 6.

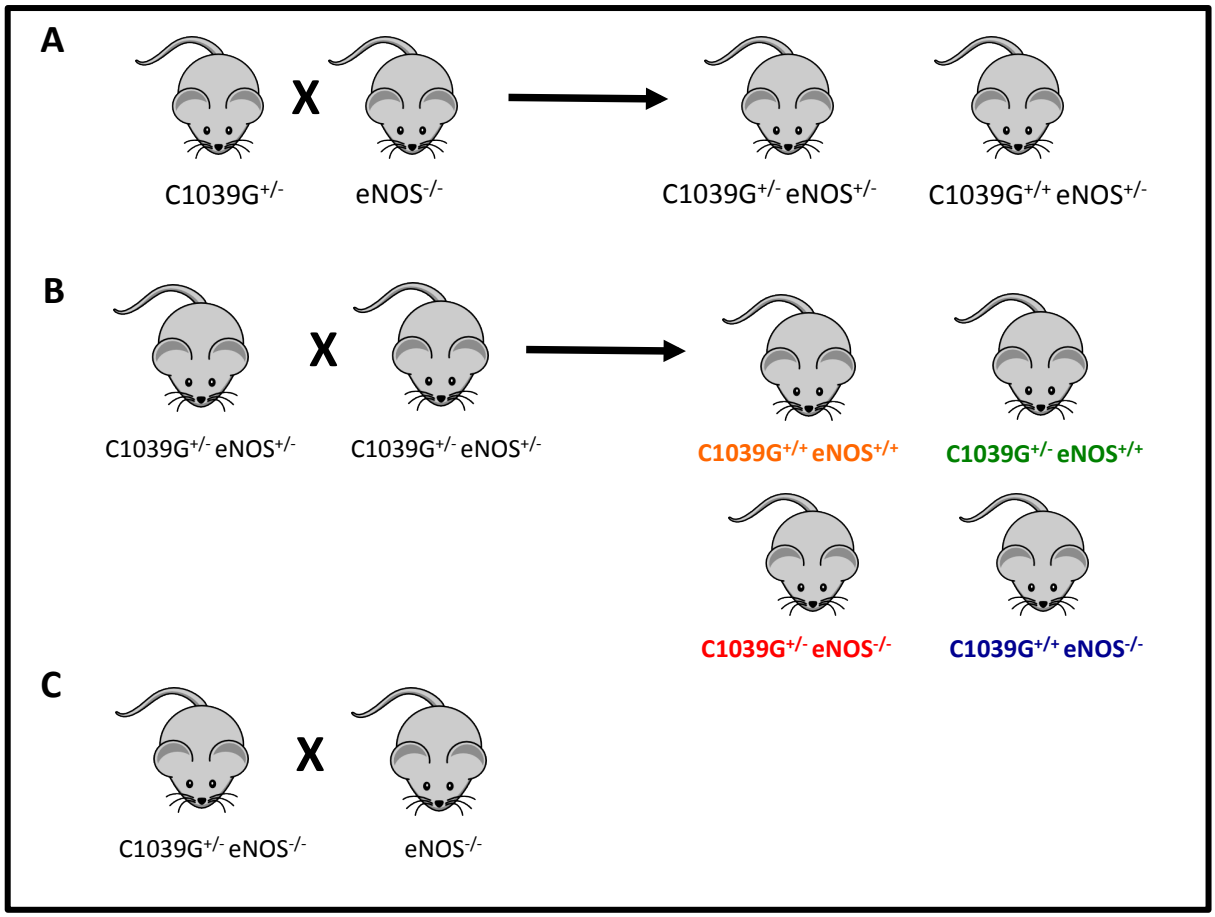

Figure 10: Breeding scheme for C1039G eNOS knockout mice.
C1039G$^{+/-}$ mice deficient in eNOS were generated by crossing by MFS C1039G$^{+/-}$ mice to eNOS knockout mice (eNOS$^{-/-}$) to generate C1039G$^{+/-}$ eNOS$^{+/-}$ (**A**). Subsequently C1039G$^{+/-}$ eNOS$^{+/-}$ mice were crossed to generate experimental C1039G$^{+/-}$ eNOS$^{-/-}$ and littermate controls (C1039G$^{+/+}$ eNOS$^{+/+}$, C1039G$^{+/-}$ eNOS$^{+/+}$, and C1039G$^{+/+}$ eNOS$^{-/-}$) (**B**). However, this yielded low numbers of experimental mice and an alternative method was used to generate experimental mice and littermate controls by crossing C1039G$^{+/-}$ eNOS$^{-/-}$ and eNOS$^{-/-}$ animals (**C**).

3.1.7 DNA Extraction, PCR Amplification and Gel Electrophoresis

For genotyping performed on all strains described above, DNA was extracted from tissue obtained from ear notching of animals. Tissue lysis was carried out by submersion of each clip in 100µl of 25mM NaOH, 0.2mM EDTA solution, which was subsequently heated to 95^{o}C for 1 hour. Samples were then neutralized by addition of 100µl of 40mM Tris-HCl (pH=5) and then stored at -20^{o}C until analysis using PCR. Alternatively, DNA was extracted using the manufacturer's instructions for the KAPA Mouse Genotyping Kit (Kit #KK7352, KAPABiosystems).

PCR reactions were carried out on a standard BioRad thermocycler. PCR reagents were utilized from Qiagen (TopTaq DNA Polymerase Kit, Catalog #200203 or the KAPA Mouse Genotyping Kit (Kit #KK7352, KAPABiosystems). A standard negative control (no addition of genomic DNA) containing all PCR reaction components was run for each set of the reactions. A list of all primer sequences utilized is given in Table 3.

Post-amplification, electrophoresis of the resulting PCR products was completed using standard agarose gel electrophoresis with gels (w/v) prepared using 1X TAE (40mM Tris, 20mM Acetic Acid, 1mM EDTA), containing 1x GelRed Nucleic Acid Stain (Biotium, Catalog #41002). Nucleic acid bands were visualized using a Stratagene Eagle Eye UV-trans-illumination system. Band sizes were determined relative to a standardized DNA ladder with 100bp gradations (ThermoFisher Scientific, Catalog #: 15628019).

Gene	Primer Sequences	PCR Product Size
Fibrillin-1 (C1039G)	5'-TTGTCCATGTGCTTTAAGTAGC-3' 5'-ACAGAGGTCAGGAGATATGC-3'	Post KpnI Digest: Wild-type: 515bp $C1039G^{+/-}$: 250bp + 515bp
Fibrillin-1 (C1039G)	5'-CTCATCATTTTTGGCCAGTTG-3' 5'-GCACTTGATGCACATTCACA-3'	Mutant ($C1039G^{-/-}$): 212bp Wild type: 164bp Heterzygote ($C1039G^{+/-}$): 212bp + 164bp
ATR1-alpha Knockout	5'-TGAGAACACCAATATCACTG-3' 5'-TTCGTAGACAGGCTTGAG-3' 5'-CCTTCTATCGCCTTCTTGACG-3'	Wild type: 483bp Mutant ($ATR1^{-/-}$): 520bp Heterozygous ($ATR1^{+/-}$): 483bp + 520bp
eNOS phospho-mutant (S1176D, S1176A)	5'-AGGTTCCTCCGGCTGTGGTAG-3' 5'-GGTGTCTGGGACTCACTGTCAAAG-3'	Wild type: 280bp Heterozygous: 280 + 315bp Homozygous: 315bp
eNOS GFP Transgenic	5'-AGCTGACCCTGAAGTTCATCG-3' 5'-GACGTTGTGGCTGTTGTAGTTG-3'	Tg Negative: No product Tg Positive: 350bp
eNOS Knockout	5'-AATTCGCCAATGACAAGACG-3' 5'-AGGGGAACAAGCCCAGTACT-3' 5'-CCTGTCCCCTAGGCACCTCT-3'	Wild type: 500bp Heterozygous: 500 + 337bp Knockout: 337bp

Table 3: PCR primer sequences.
Genotyping of noted mouse strains was completed using the described primer sequences. All primers were obtained from Sigma Aldrich lyophilized and desalted and subsequently re-suspended in sterile DNase/RNase free water and stored at -20^{o}C.

3.2 Therapeutic Interventions

A number of therapeutic interventions were utilized throughout the described work and are described below in terms of dose, administration route, and length of treatment. During therapeutic interventions mice were monitored daily. Notably, no toxicity or adverse events were observed in any of the interventions.

3.2.1 Losartan Treatment of Animals

Losartan was given in drinking water at a dose of 0.6g/L. Losartan tablets were supplied from the clinical pharmacy at St. Paul's Hospital and crushed and then finely ground using a mortar and pestle prior to suspension in drinking water. Fresh losartan was given to animals once per week and topped up once during the week. Losartan treatment was started at six weeks of age and continued until age of sacrifice and tissue harvest as described for each data set.

3.2.2 L-NAME Treatment of Animals

Nω – Nitro – L-arginine methyl ester hydrochloride (L-NAME) (Sigma-Aldrich, catalog #N5751) was given in drinking water (0.5mg/ml) starting at six weeks of age. L-NAME was also simultaneously administered via i.p. injection (10mg/kg suspended in sterile saline) bi-weekly [197]. In experiments where L-NAME and losartan were given in combination, both were added to drinking water.

3.2.3 CavNOxin Treatment of Animals

CavNOxin is a 4.7kDa cell permeable peptide that has been shown to increase NO production *in vivo* [198]. Notably, the concept of CavNOxin originated with the invention of

Cavtratin, a peptide mimetic of residues 82-101 of the scaffolding domain of caveolin-1. As binding of eNOS to the scaffolding domain of caveolin-1 decreases production of NO, by mimicking the binding site of eNOS by caveolin-1, Cavtratin was found to inhibit eNOS and decrease NO production [149]. Subsequently, three key residues in Cavtratin (Thr-90, Thr-91, Phe-92) were shown to be responsible for inhibition of eNOS [199]. Moreover, generation of a new peptide, CavNOxin, with alanine substitutions at Thr-90, Thr-91, and Phe-92 resulted in increased endogenous NO production [198]. A schematic diagram of the mechanism of action of CavNOxin is provided in Figure 11 [200].

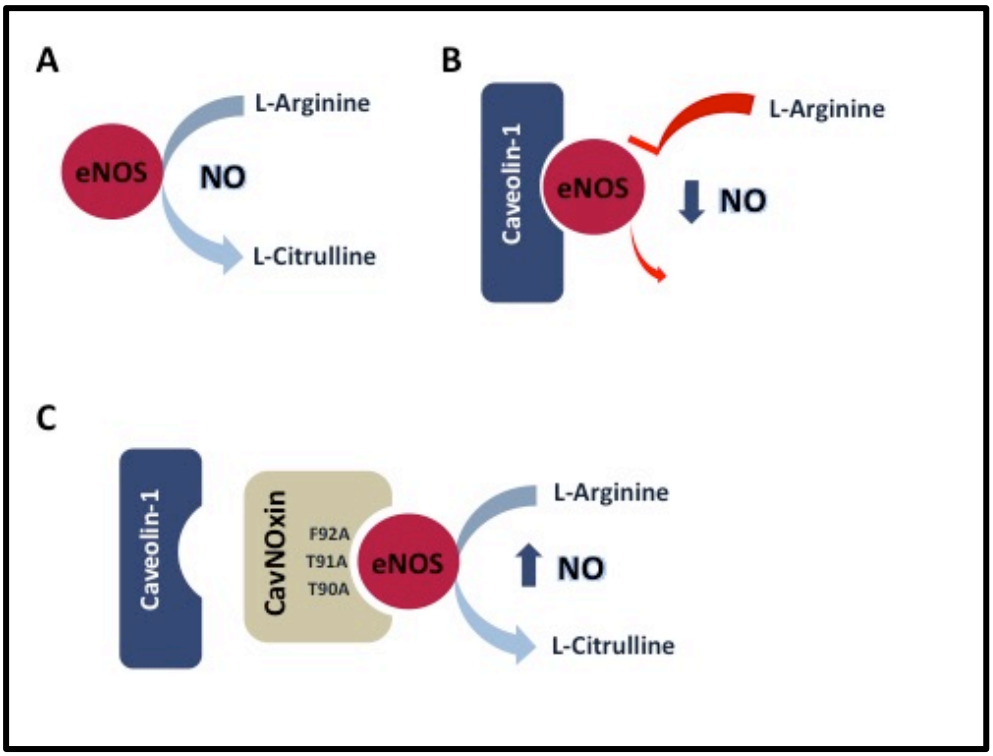

Figure 11: Schematic representation of CavNOxin function.
The conversion of L-arginine to L-citrulline by eNOS yields nitric oxide (NO) as a by-product (**A**). Typically, the scaffolding domain of caveolin-1 binds eNOS and prevents phosphorylation. Thus, due to an unphosphorylated less-active state of eNOS, NO production is decreased when eNOS is bound to caveolin-1 (**B**). However, CavNOxin competes with caveolin-1 to bind eNOS by mimicking the scaffolding domain of caveolin-1 (**C**) but results in an increase in endogenous NO as it contains three point mutations that allow increased eNOS activity.

To assess the ability of CavNOxin to prevent aortic root aneurysm in MFS, CavNOxin was used for treatment of C1039G$^{+/-}$ and C1039G$^{+/+}$ animals starting at four weeks of age for a duration of eight weeks. CavNOxin (0.1mM in 1% DMSO) was given via i.p. injections three times per week at a dose of 5µl per gram of body weight.

3.3 Animal Evaluation Methods

In order to characterize the development of MFS pathology in the animal models described above, a number of evaluation techniques were utilized and are described below. These evaluations were aimed at determining the extent of aortic aneurysm pathology as well as evaluating systemic manifestations of MFS including kyphosis and pulmonary pathology.

3.3.1 Echocardiograms

Echocardiograms were performed on mice anesthetized with isofluorane using a VisualSonics Vevo 2100 system with a MS-550D 40MHz probe. Body temperature was measured and maintained via a heated platform. Heart rate, breathing rate, and an electrocardiography (ECG) trace were acquired and monitored by sensors built into the Vevo 2100 imaging platform. All echocardiograms were performed and analyzed by a technician trained in murine echocardiography. The technician was blinded to both genotype and treatment groups. Furthermore, multiple clinicians with cardiac echo experience confirmed initial experiments and identification of appropriate landmarks for aortic root and pulmonary artery measurements.

Aortic root measurements were averaged from multiple measurements taken in both anatomical M- and B-mode at the level of the Sinus of Valsalva. Ascending aorta measurements

were averaged from B-mode images. Pulmonary artery measurements were taken at the level of the pulmonary valve and averaged from multiple measurements taken in B-mode. To control for the effect of blood flow on the distension of the pulmonary artery, all measurements were gated to the acquired ECG trace and taken in diastole. A four-chamber view echocardiogram method was utilized to determine ventricle size and volume as well as cardiac parameters of cardiac output, ejection fraction, stroke volume, and factional shortening.

3.3.2 Lung Function and Bronchoalveolar Lavage

Measurement of lung function was completed using the Scireq FlexiVent system using the FX1 module. To do so, mice were anesthetized with ketamine/xylzine (12.25mg ketamine, 1.5mg xylazine per ml given at a dose of 100ul per 10g of body weight) via i.p. injection. Subsequently, a tracheotomy was performed in which a blunted 18-gauge needle was inserted and secured into an incision made into the trachea. The FlexiVent system was then connected and the default ventilation pattern (150 breaths per minute) was initiated. Once baseline ventilation was established, pancuronium bromide (Sigma-Aldrich, Catalog #P1918, 2mg/ml given at a dose of 10µl per 10g of body weight) was administered via i.p. injection and allowed to circulate for 5 minutes. Following this equilibration, compliance, elastance, and hysteresis were measured as a function of the FlexiVent standard mouse perturbation script. Each script performs three complete cycles and each script was run three times. Therefore, data values for each animal represent the average of nine values. Notably, the FlexiVent system was calibrated for animal weight and tracheotomy tube used for each animal studied.

3.3.3 AngII Blood Pressure Response

Evaluation of changes in resting blood pressure due to ATR1 deficiency was evaluated using the Kent Scientific Corp CODA2 tail cuff system in $C1039G^{+/+}ATR1^{+/+}$, $C1039G^{+/-}ATR1^{+/+}$, $C1039G^{+/-}ATR1^{-/-}$ and $C1039G^{+/+}ATR1^{+/+}$ animals. Systolic and diastolic blood pressures were averaged over a five-day period in animals anesthetized with 1.5% isoflurane. Mean arterial pressure (MAP) was calculated using the equation:

$$MAP = \frac{[(2 \times \text{diastolic pressure}) + \text{systolic pressure}]}{3}$$

Loss of functional response to AngII in mice deficient in ATR1 was confirmed by blood pressure response to acute infusion of AngII. To do so, mice were injected i.p. with AngII at a dose of 0.2mg/kg (1mg/ml re-suspended sterile water, Sigma-Aldrich Catalog #A9525). Changes in blood pressure were measured over a ten minute period to determine peak response to AngII. Changes in blood pressure are expressed as change in systolic and diastolic pressures from baseline at peak response to AngII. Peak blood pressure values were averaged for each animal studied.

3.3.4 Aortic Root Histology, Lung Histology, and Bronchoaveolar Levage

All heart and lung samples were harvested from mice anesthetized with 2% isoflurane and sacrificed via cardiac puncture with subsequent cervical dislocation with hearts and lungs dissected *en bloc*. The right lung was tied off at the level of the main bronchus and collected for subsequent studies. The left lung was inflated with 0.5ml of 10% buffered formalin through a blunted needle secured in the upper trachea. Hearts and inflated lungs were fixed for at least 24hrs in 10% buffered formalin and then dissected for histology.

Bronchoaveolar lavage was performed on mice immediately post-sacrifice prior to lung inflation. Lungs were lavaged by washing lungs twice with 250µl of phosphate buffered saline (PBS) (Gibco Life Technologies, reference #14190-144) through a 1ml syringe attached to a tracheotomy performed using a blunted 18-gauge needle. Collected lavage fluid was centrifuged at 1500rpm for 10min. Supernatant was then removed and discarded and the cell pellet was re-suspended in 150µl of PBS. Cells number was then determined using manual counting via a standard hemocytometer and upright bright field microscope.

Hearts were bisected parallel to the atrioventricular plane and embedded in paraffin. Sections were analyzed every 50µm throughout the aortic root. Elastic fibers were assessed at the Sinus of Valsalva on slides stained with Movat's pentachrome by a blinded cardiac pathologist. Elastic fiber fragmentation was scored on a scale of 0 to 3 scale wherein 0= no fragmentation, 1= mild fragmentation (0-20%), 2= moderate fragmentation (20-40%), 3= extensive fragmentation (>40%). Observable webbing, defined as interlinking of elastic fibers between concentric layers, was also scored on a scale of 0 to 3 using the same parameters as fragmentation.

Analysis of histology of the left lung was performed post-inflation on formalin fixed samples embedded in paraffin. Processing, staining, and quantification of histology were performed in a manner blind to genotype and treatment group. Airspace enlargement was calculated as density of positive pixels or mean linear intercept on Masson's Trichrome stained sections of the distal airspaces as previously described [201].

3.3.5 AngII and p-ERK Immunohistochemistry

Assessment of AngII binding to aortic root sections was completed using biotin-conjugated AngII (ANA-SPEC, Catalog #AS-60276-5) with avidin-biotin HRP detection (Vector

Laboratories, Catalog #SK-4105). Staining was completed on 30μm frozen sections of aortic root and descending aorta in the presence and absence of losartan. Staining of myocardium was evaluated on standard sections of aortic root. However, aortic root sections were evaluated in slides in which myocardium was removed prior to staining. Prior to staining, slides were fixed in methanol and quenching of endogenous peroxidases was completed by treatment with hydrogen peroxidase (Fisher Scientific, catalog #: H325-500).

Staining of phospho-ERK was completed on 5μm paraffin sections that were consecutive sections from those previously stained with Movat's pentachrome and used for analysis of elastic fiber fragmentation. Briefly, samples were de-paraffinized in xylene and dehydrated in 100% ethanol prior to antigen retrieval using citrate buffer (Dako, pH=6, Catalog #S2369). Slides were incubated with primary p-ERK (1:1000, Cell Signaling, catalog #: 9101S) followed by secondary antibody (Biotin goat anti-rabbit, Vector Laboratories, 1:1000, Catalog #BA1000) and developed using the manufacturer's instructions for the VectaStain ABC Elite HRP Kit (Vector Laboratories, Catalog #PK-6100).

3.3.6 TGF-β Assays

TGF-β levels were analyzed in plasma. Plasma was obtained from experimental animals upon sacrifice via cardiac puncture. Blood was collected in syringes containing 30μl of heparin obtained from the St. Paul's Hospital pharmacy (Pharameutical Partners of Canada Inc., Reference #C504710) and then centrifuged immediately at 4000rpm for 10 minutes at 4^{o}C. Plasma was immediately separated and stored at -80^{o}C until assayed.

Analysis of plasma TGF-β was completed using the manufacturer's directions for the Legend Max Free Active TGF-β1 ELISA Kit (Biolegend, Catalog #437707) and the Quantikine TGF- β1 ELISA Kit (R&D Systems, Catalog #MB-100B).

3.3.7 *In-vivo* NO Levels

NO levels were assessed *in vivo* in plasma. Plasma was obtained from blood collected via the facial vein of animals fasted overnight for 12 hours. Blood was collected in lithium heparin coated tubes (Multivette, 600 LH, catalog #15.1673.100) and centrifuged immediately at 4000rpm for 10 minutes at 4^{o}C. Following centrifugation, plasma was immediately separated and stored at -80^{o}C until assayed. NO levels were measured according to the manufacturer's instructions for the Enzo Total Nitric Oxide Detection Kit (Enzo, catalog #: ADI-917-020) with samples assayed in duplicate.

3.4 NO Release *In Vitro*, Cell Culture and Western Blotting

The effect of losartan on NO release was determined by measuring soluble nitrite levels, a stable breakdown product of NO, in the supernatant of cultured bovine aortic ECs (BAECs) using a Sievers Nitric Oxide Analyzer. BAECs isolated from freshly harvested bovine aortas were cultured in Dulbecco's modified eagle medium (Gibco DMEM; Life Technologies, Catalog #1196-092) containing 5% fetal bovine serum (FBS; Hyclone Lab, catalog #SH30071.03 which was heat inactivated at 56^{o}C for 30min) and antibiotics (10units/ml of penicillin streptomycin, Sigma-Aldrich, Catalog #P4333). For all studies, confluent BAECs were starved in FBS-free DMEM for 24hrs prior to treatment with calcium ionophore (10mM stock dissolved in DMSO, Sigma-Aldrich, Catalog #A23187, diluted in DMEM to give a final concentration of 1μM) to

induce NO release. For acute studies, cells were treated with losartan (100mM stock stored at -20^{o}C dissolved in DMSO, Sigma-Aldrich, Catalog #D2438) diluted in DMEM to a final concentration of 10^{-8}M, 10^{-7}M or 10^{-6}M in combination with calcium ionophore. Supernatant was collected 15 minutes after treatment and analyzed. For chronic NO studies, cells were pre-treated with losartan for 72hrs or 48hrs followed by treatment with losartan in combination calcium ionophore. Values presented represent assays completed in triplicate.

For studies with VEGFR2 knockdown, BAECs were treated with VEGFR2 siRNA (Qiagen, target sequence: CAGAAGTGATTGGAAATGATA) for 48hrs prior to treatment with losartan and subsequent NO release studies were performed as detailed above. Knockdown of VEGFR2 was confirmed via western blot (VEGFR2/Flk-1, SantaCruz, 1:1000) and quantified relative to a HSP-90 loading control (HSP-90, BD Biosicences, 1:1000).

Chapter 4: Development and Evaluation of An ATR1 Deficient Marfan Model

4.1 Introduction

ATR1 signaling is thought to contribute to the manifestations of MFS as it is proposed to increase activation of the TGF-β signaling pathways associated with MFS pathology. As reviewed in Figure 1, signaling has been shown to occur between ATR1 and TGF-β signaling pathways. Moreover, as detailed in Chapter 1, the main evidence for a role of ATR1 in MFS is the effectiveness of ATR1 blocker losartan in reducing excessive TGF-β signaling similar to the use of TGF-β neutralizing antibody in previous murine studies [27, 104]. These studies were initially translated into human studies as well as, showing an ability to reduce the rate of aortic root aneurysm progression and thereby supporting the conclusion for a pathogenic role of ATR1 in MFS [155]. In addition to the findings of successful use of losartan to treat MFS, the use of AngII converting enzyme [149] inhibitors has also provided evidence for the role of ATR1 signaling as a pathogenic target in MFS. Specifically, the use of ACE inhibitors has been found in many studies to be unsuccessful in retarding progression of aortic aneurysm in MFS patients [150, 152]. The proposed explanation for this is that the selectivity of ARBs such as losartan for ATR1 allows ATR2 signaling to remain intact (Figure 10). This theory is based on the work of Habashi *et al*. wherein it was shown in the C1039G murine model of MFS that knockout of ATR2 increases the rate of aneurysm progression as well as increased rate of death from aortic dissection [44]. Moreover, the authors demonstrated that the full therapeutic benefit of losartan in C1039G MFS mice required intact ATR2 signaling. This finding was linked to the ability of selective ATR1 blockade to increase protective ATR2 signaling which antagonizes downstream canonical TGF-β signaling via ERK. In a separate study of rats, overexpression of ATR2 was

found to downregulate ATR1 expression [202]. Overall, this suggested that blockade of ATR1 may contribute to MFS pathology while ATR2 may be protective (Figure 12).

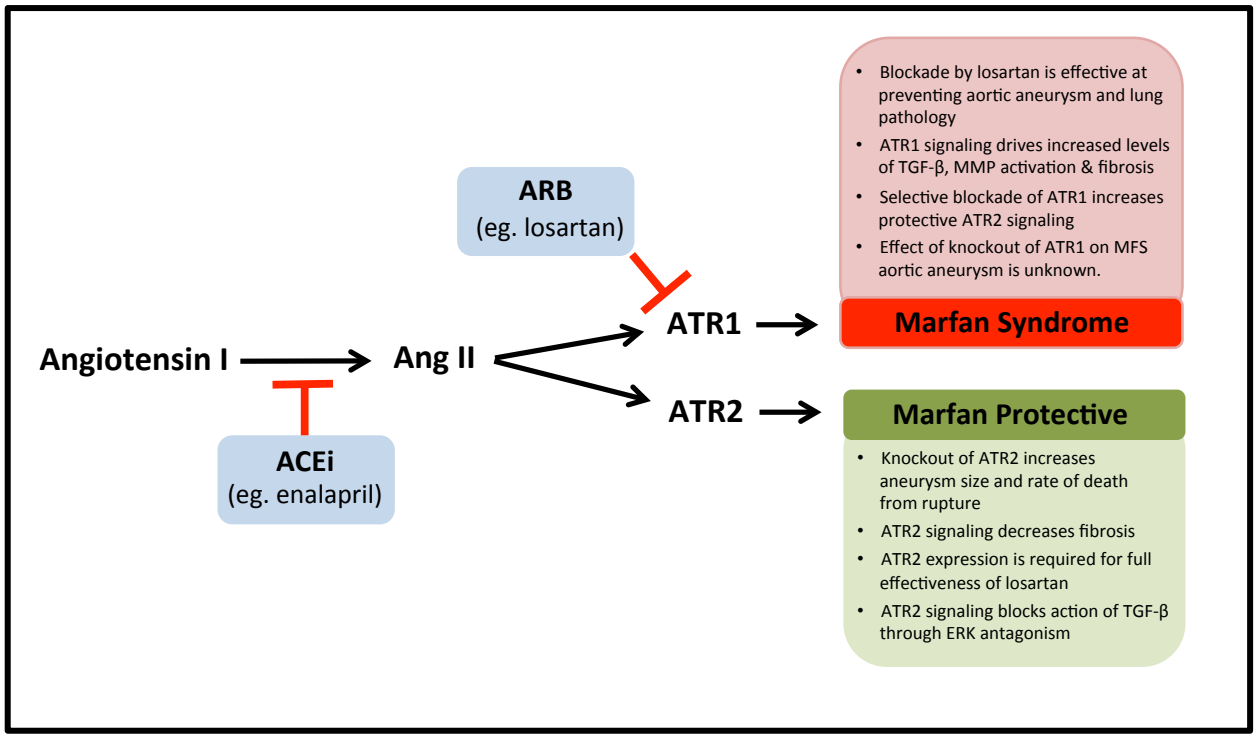

Figure 12: Signaling through and blockade of ATR1 and ATR2 in MFS.
Signaling through ATR1 is thought to contribute to the development of MFS pathology through increasing TGF-β signaling associated with factors such as increased activation of MMPs and fibrosis. ATR2 was shown to be protective in MFS wherein ATR2 signaling was required for the benefits of losartan and knockout of ATR2 was detrimental. However, the effect of knockout of ATR1 is unknown. The differential effects of ATR1 and ATR2 signaling is hypothesized to explain the findings of the effectiveness of ARB losartan in blocking pathological ATR1 signaling versus the use of ACE inhibitors (ACEi) such as enalapril which block both the pathological and protective signaling pathways.

Despite the reported success of targeting ATR1 with losartan in patients and murine models, as well as assessment of the consequence of ATR2 knockout on MFS pathology, the penetrance of ATR1 signaling in MFS pathology has never been explored. Re-stated, this is addressing the pathology that would be prevented in MFS if a method to completely silence ATR1 was achieved and determining what pathology would remain. From a pharmacological

perspective, answering such questions would also allow us to determine how best to treat MFS and guide future drug development. For example, in the case that MFS pathology is largely or entirely dependent upon ATR1 signaling, then focus should shift towards development of more potent and specific ARBs. Moreover, partial penetrance of ATR1 would suggest the need for more specific ARBs along with investigation of the use of drug cocktails to target pathologies not dependent on ATR1 (eg. doxycycline to target MMPs). Finally, in the event that ATR1 silencing does not provide protection, particularly for development of aortic aneurysm that predisposes to the life threatening consequence of aortic dissection, focus must move to re-evaluating the pathological mechanisms driving MFS and what pharmaceuticals may be re-purposed or designed for new targets.

4.2 Experimental Approach and Chapter Specific Aims

To address the unanswered question regarding the role and penetrance of ATR1 in MFS pathology we aimed to develop a novel mode of MFS lacking ATR1. To do so, as described in detail in Chapter 3, a model of MFS lacking ATR1 expression was generated through breeding of MFS mice ($C1039G^{+/-}$) and ATR1-alpha deficient mice ($ATR1^{-/-}$) to produce experimental $C1039G^{+/-}$ $ATR1^{-/-}$ mice along with littermate control (WT - $C1039G^{+/+}$, MFS - $C1039G^{+/-}$ $ATR1^{+/+}$, and ATR1 knockout - $C1039G^{+/+}$ $ATR1^{-/-}$). The effect of deletion of ATR1-alpha was assessed in the cardiovascular, pulmonary, and skeletal systems as they have been shown to develop human MFS-like pathology in the $C1039G^{+/-}$ model of MFS [26, 104].

4.3 Results

4.3.1 ATR1 Knockout Does Not Prevent Aortic Aneurysm in MFS Mice

As previously reported, aortic root aneurysm at the level of the sinus of Valsalva was observed in C1039G$^{+/-}$ at as early as three months of age with aneurysm clearly visible on echocardiograms performed in a manner blind to genotype and averaged from both anatomical M mode and B-mode images [104]. As they lack the assumed pathological ATR1 expression, we hypothesized that C1039G$^{+/-}$ ATR1$^{-/-}$ mice would be protected from aneurysm development. However, we unexpectedly observed that C1039G$^{+/-}$ ATR1$^{-/-}$ mice showed a nearly identical degree of aneurysm on echocardiogram as C1039G$^{+/-}$ mice (Figure 13A). Indeed, C1039G$^{+/-}$ and C1039G$^{+/-}$ ATR1$^{-/-}$ mice showed a highly similar and significant degree of aneurysm development with average aortic root diameters of 1.84±0.04mm in C1039G$^{+/-}$ and 1.88±0.04mm in C1039G$^{+/-}$ ATR1$^{-/-}$ compared to 1.45±0.04mm in wild type controls at three months of age (Figure 13C). Moreover, at six months of age, quantification of echocardiograms revealed both C1039G$^{+/-}$ and C1039$^{+/-}$ ATR1$^{-/-}$ mice to have similar progression of aneurysm size (Figure 13B, D) where the average aortic diameter in C1039G$^{+/-}$ and C1039G$^{+/-}$ ATR1$^{-/-}$ was found to be 2.04±0.09mm and 2.01±0.06mm respectively.

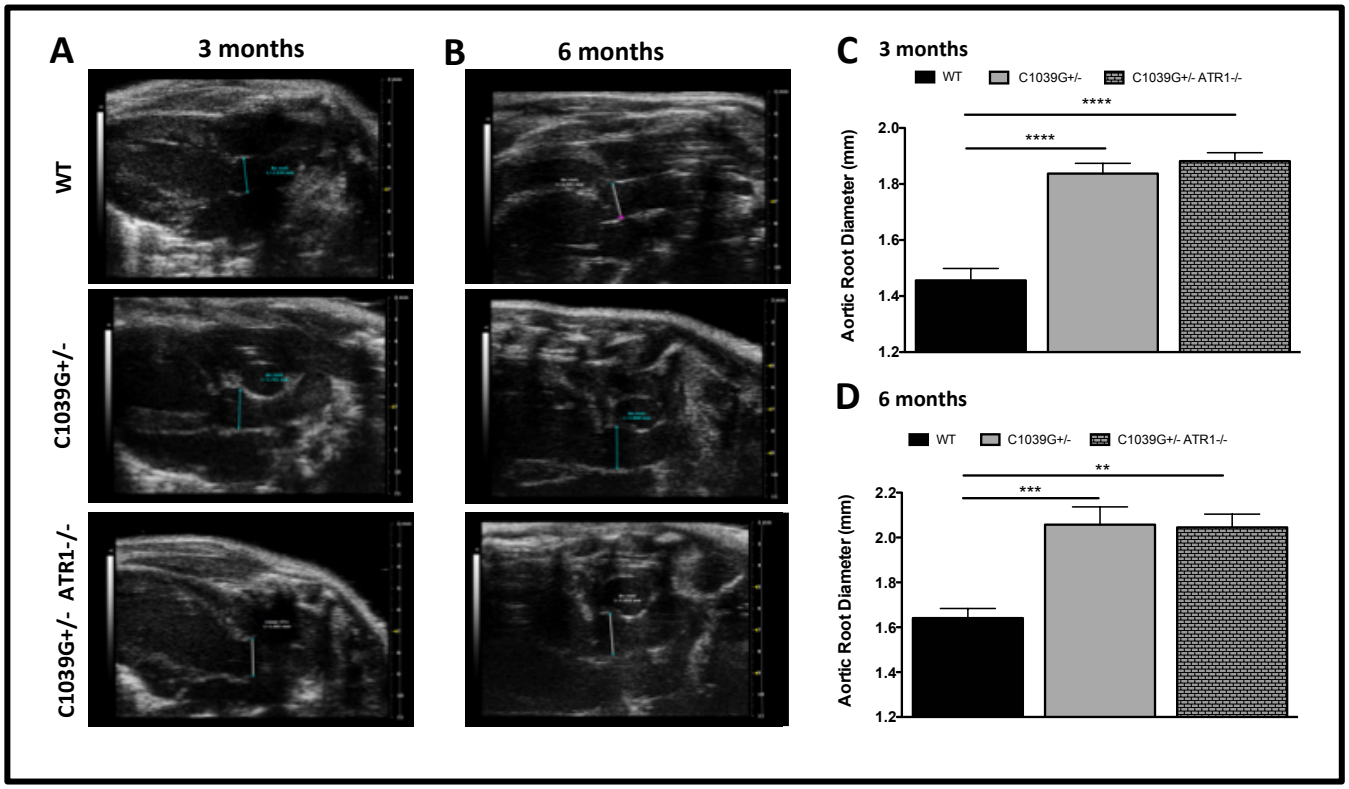

Figure 13: Knockout of ATR1 does not prevent aortic root aneurysm in MFS mice.
To determine development and progression of aortic root aneurysm echocardiograms of WT, C1039G$^{+/-}$, and C1039G$^{+/-}$ ATR1$^{-/-}$ mice at three months of age (**A**) and six months of age (**B**) were performed by a blinded technician. Quantification of aortic root diameter via echocardiograms (**C, D**) revealed significant aortic root enlargement in both C1039G$^{+/-}$and C1039G$^{+/-}$ ATR1$^{-/-}$ mice at three and six months. Values represent mean group aortic root diameter ±SEM wherein diameter from each animal studied was determined by averaging of multiple measurements taken in both M- and B-mode and show significant aneurysm in C1039G$^{+/-}$ and C1039G$^{+/-}$ATR1$^{-/-}$ groups. At three months WT n=11, C1039G$^{+/-}$ n=9, C1039G$^{+/-}$ ATR1$^{-/-}$ n=6 and at six months WT n=6, C1039G$^{+/-}$ n=7, C1039G$^{+/-}$ATR1$^{-/-}$ n=6. **p<0.01, ***p<0.001, ****p<0.0001.

As the finding of equal aneurysm size and rate of progression in C1039G$^{+/-}$ and C1039G$^{+/-}$ ATR1$^{-/-}$ mice was surprising, we sought to confirm that there was no confounding phenotype of the ATR1$^{-/-}$ strain. To do so we compared C1039G$^{+/+}$ ATR1$^{+/+}$ and C1039G$^{+/+}$ ATR1$^{-/-}$ littermates by echocardiogram and found no difference in aortic root size at either three or six months of age (Figure 14A-C).

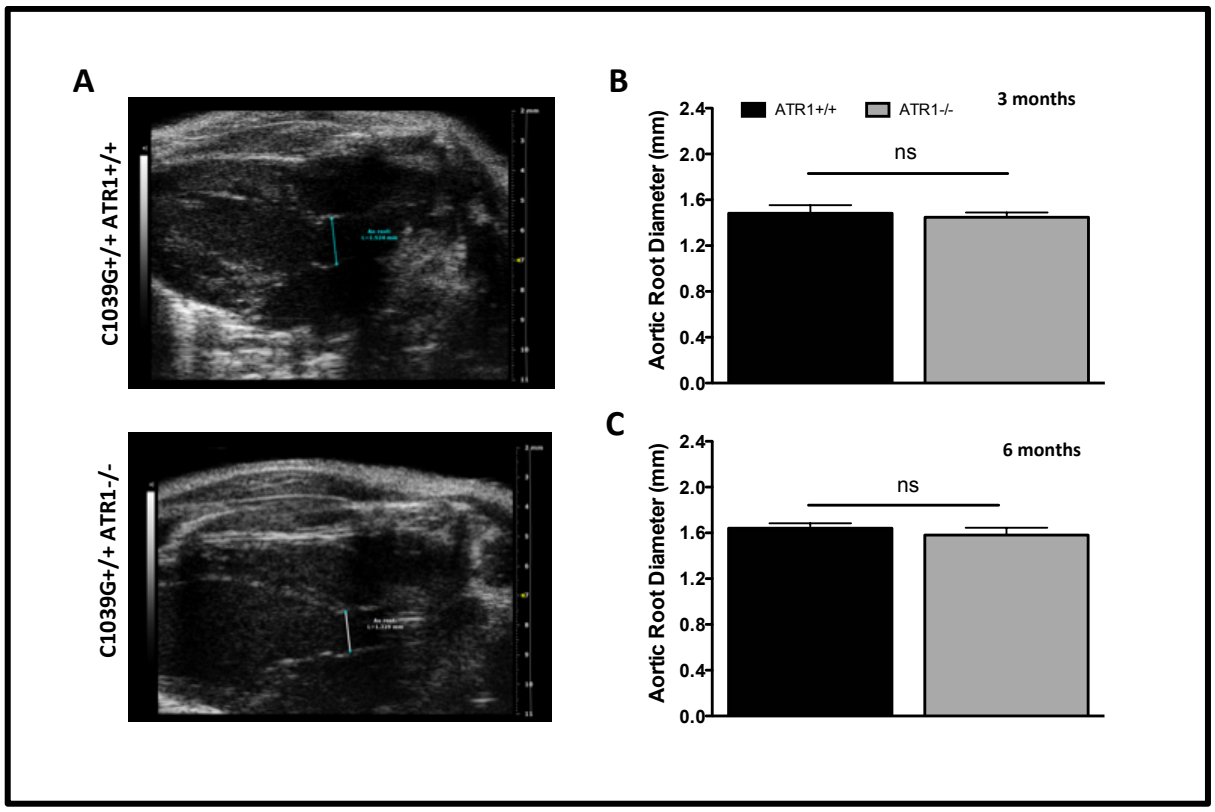

Figure 14: Mice lacking ATR1 expression do not exhibit changes in aortic root diameter relative to wild-type controls.
Representative images of B-mode echocardiograms of $ATR1^{+/+}$ and $ATR1^{-/-}$ mice at three months of age for determination of aortic root diameter in anesthetized mice by a blinded technician (**A**). Quantification of aortic root diameter via echocardiograms performed by blinded technicians show no difference between groups where values represent mean group aortic root diameter ±SEM at 3 months of age ($ATR1^{+/+}$ n=6, $ATR1^{-/-}$ n=6) (**B**) and at six month of age ($ATR1^{+/+}$ n=6, $ATR1^{-/-}$ n=5) (**C**) where ns denotes no significant difference.

To expand upon our findings at three and six months of age, a group of animals was also evaluated at nine months of age time point to confirm the observed lack of effect of ATR1 deficiency over disease progression. Echocardiogram analysis of the aortic root revealed aneurysm progression to be the same in both $C1039G^{+/-}$ and $C1039G^{+/-}$ $ATR1^{-/-}$ mice (Figure 15A, B). Furthermore, $C1039G^{+/+}$ $ATR1^{+/+}$ and $C1039^{+/+}$ $ATR1^{-/-}$ animals still showed no difference in aortic root diameter (Figure 15C).

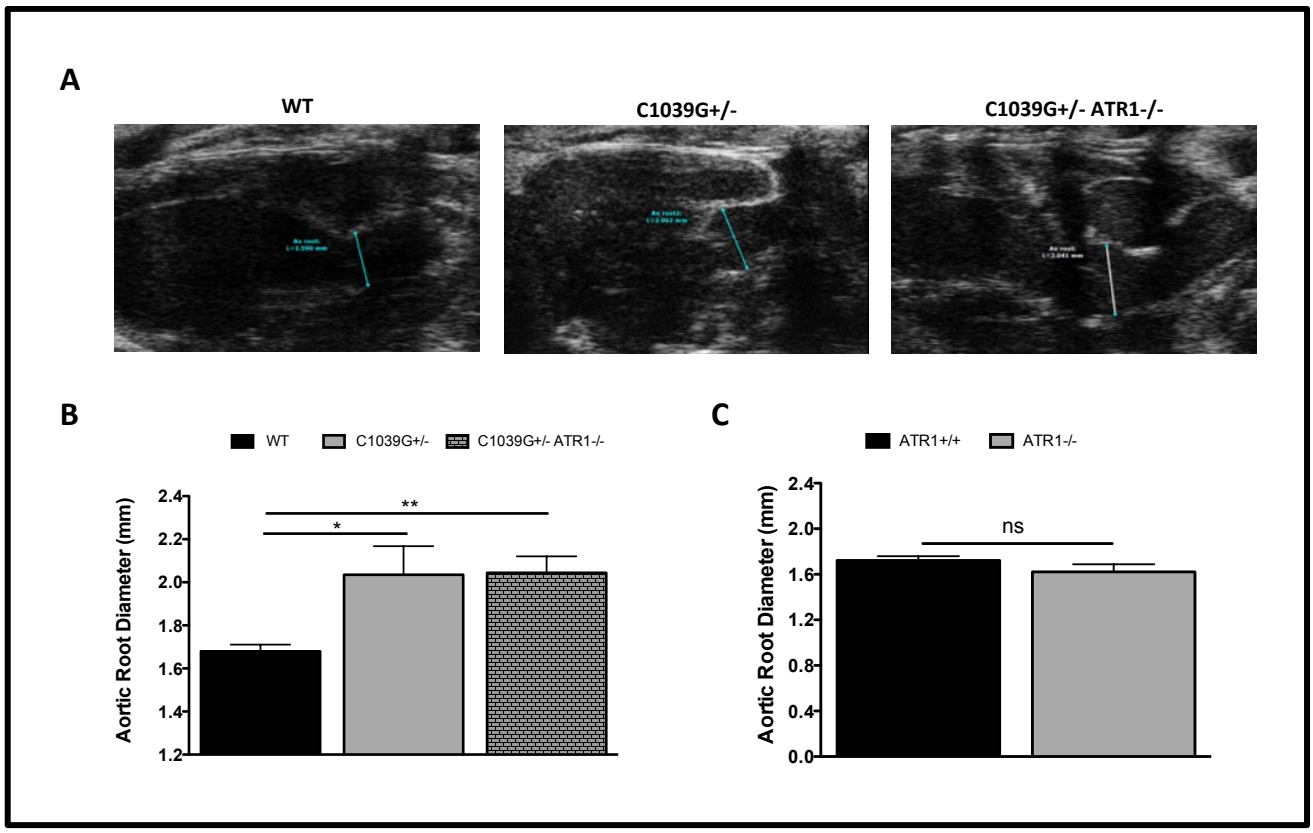

Figure 15: Loss of ATR1 expression does not prevent aneurysm at nine months of age. Representative images of B-mode echocardiograms of WT, C1039G$^{+/-}$, and C1039G$^{+/-}$ ATR1$^{-/-}$ mice at nine months of age for determination of aortic root diameter in anesthetized mice by a blinded technician (**A**). Quantification of echocardiograms in WT, C1039G$^{+/-}$, and C1039G$^{+/-}$ ATR1$^{-/-}$ mice (**B**) show significant differences in aortic root diameters of C1039G$^{+/-}$, and C1039G$^{+/-}$ ATR1$^{-/-}$ mice compared to WT wherein WT n=6, C1039G$^{+/-}$ n=8, and C1039G$^{+/-}$ ATR1$^{-/-}$ n=6. Comparison of echocardiogram derived aortic root diameter in WT (C1039G$^{+/+}$ ATR1$^{+/+}$) animals lacking to those lacking ATR1 (C1039G$^{+/+}$ ATR1$^{-/-}$) at nine months (**C**) where ATR1$^{+/+}$ n=6, ATR1$^{-/-}$ n=5. In all groups, values represent mean group aortic root diameter ±SEM. For each animal studied diameter represents the average of multiple measurements taken in both M- and B-mode *p<0.05, **p<0.01

4.3.2 ATR1 Deficiency in C1039G$^{+/-}$ ATR1$^{-/-}$ Confers Reduction of Blood Pressure and Lack of Functional Response to AngII

Although the ATR1$^{-/-}$ animals used to generate C1039G$^{+/-}$ ATR1$^{-/-}$ are commercially available [181], can clearly be genotyped within the C1039G$^{+/-}$ ATR1$^{-/-}$ strain (Figure 5, Chapter 3), and are well characterized to have no response to AngII [203], given the surprising lack of effect of ATR1 deficiency on C1039G$^{+/-}$ animals, we investigated blood pressure and response to

AngII in our ATR1 deficient MFS strain. Analysis of blood pressure using a tail-cuff system demonstrated that ATR1 deficiency ($ATR1^{-/-}$) reduced MAP in both $C1039G^{+/-}$ and $C1039G^{+/+}$ animals. However, no significant difference was seen in the blood pressure of $C1039G^{+/-}$ $ATR1^{-/-}$ and $C1039G^{+/+}$ $ATR1^{-/-}$ animals thereby confirming that resting blood pressure reduction mediated by loss of ATR1 expression occurs independently of MFS pathology (Figure 16A). Therefore, we next investigated changes in blood pressure in response to acute AngII infusion and found that both $C1039G^{+/-}$ and $C1039G^{+/+}$ with intact ATR1 expression ($ATR1^{+/+}$) showed a significant increase in blood pressure following infusion (Figure 16B). Conversely, both $C1039G^{+/-}$ and $C1039G^{+/+}$ mice lacking ATR1 expression ($ATR1^{-/-}$) showed an equally significantly blunted response to AngII, and thereby confirming that loss of functional ATR1 vasopressor responses in ATR1-deficient mice regardless of MFS status ($C1039G^{+/+}$ or $C1039G^{+/-}$).

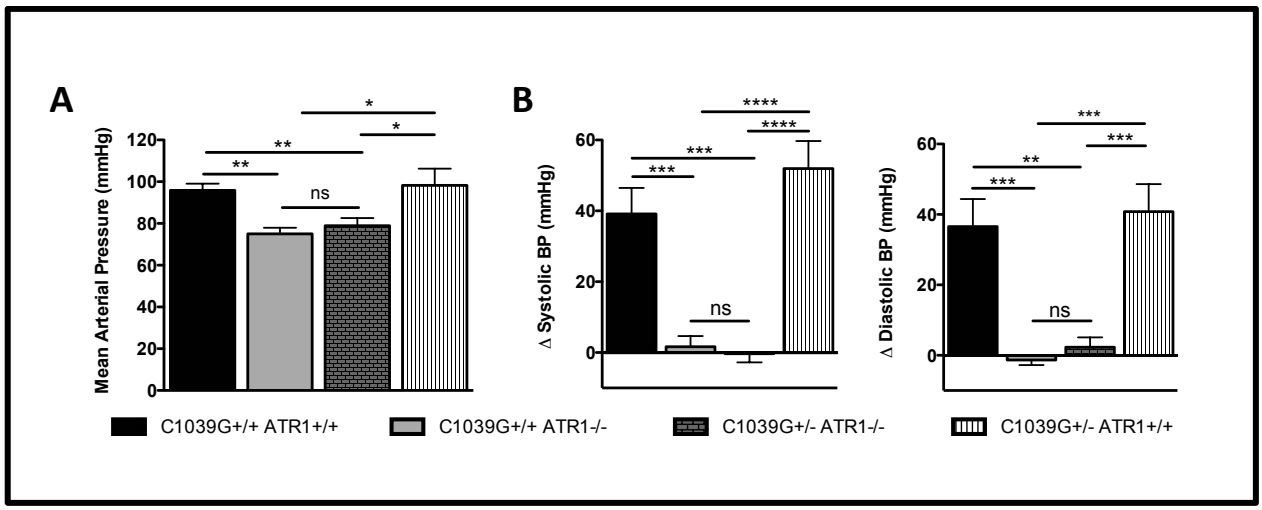

Figure 16: MFS aortic root aneurysm is independent of blood pressure reduction or loss of AngII vasopressor responses.
Evaluation of mean arterial pressure (MAP) was completed through analysis of baseline MAP in $C1039G^{+/+}$ and $C1039G^{+/-}$ mice with ($ATR1^{+/+}$) and without ATR1 ($ATR1^{-/-}$) expression as determined by repeated measurements using a tail cuff system (**A**) and showing a reduction in MAP in ATR1 deficient groups where $C1039G^{+/+}$ $ATR1^{+/+}$ n=8, $C1039G^{+/-}$ $ATR1^{-/-}$ n=7, $C1039G^{+/-}$ $ATR1^{+/+}$ n=5, and $C1039G^{+/-}$ $ATR1^{-/-}$ n=5. Lack of vasopressor responses was seen in ATR1 deficient groups following acute AngII injection (**B**) wherein change in systolic or diastolic blood pressure [204] represents differential in BP from established baseline to values following AngII infusion where $C1039G^{+/+}$ $ATR1^{+/+}$ n=7, $C1039G^{+/-}$ $ATR1^{-/-}$ n=6, $C1039G^{+/-}$ $ATR1^{+/+}$ n=6, and $C1039G^{+/-}$ $ATR1^{-/-}$ n=6. MAP, and change in BP values represent mean ±SEM where **p<0.01, ***p<0.001, ****p<0.0001.

4.3.3 Loss of ATR1 Expression Does Not Prevent Pathology Within the Aortic Wall of MFS Mice

Having observed no reduction in MFS aneurysm size in MFS lacking ATR1 expression, we aimed to support this provocative observation by determining if ATR1 inactivation blocks aortic wall remodeling that is associated with MFS. Aortic wall architecture analyses revealed clear increases in the degree of elastic fiber fragmentation at six months of age in $C1039G^{+/-}$ mice relative to WT control as has previously been reported (Figure 17A, B) [26, 104]. Markedly, similar elastic fiber fragmentation was seen in $C1039G^{+/-}$ $ATR1^{-/-}$ (Figure 17A, B). In addition to elastic fiber fragmentation, both $C1039G^{+/-}$ and $C1039G^{+/-}$ $ATR1^{-/-}$ groups demonstrated a trend towards increased webbing of elastic fibers (Figure 17C) and a significant

increase in aortic wall thickness (Figure 17D). Furthermore, this trend of increased elastic fiber fragmentation, elastic fiber webbing, and aortic wall thickening progressed with age in both C1039G$^{+/-}$ and C1039G$^{+/-}$ ATR1$^{-/-}$ groups (Figure 17A-D). Overall, these data suggest that loss of ATR1 does not attenuate MFS-associated loss of aortic wall integrity, which contributes to the pathology of aortic root aneurysm in MFS.

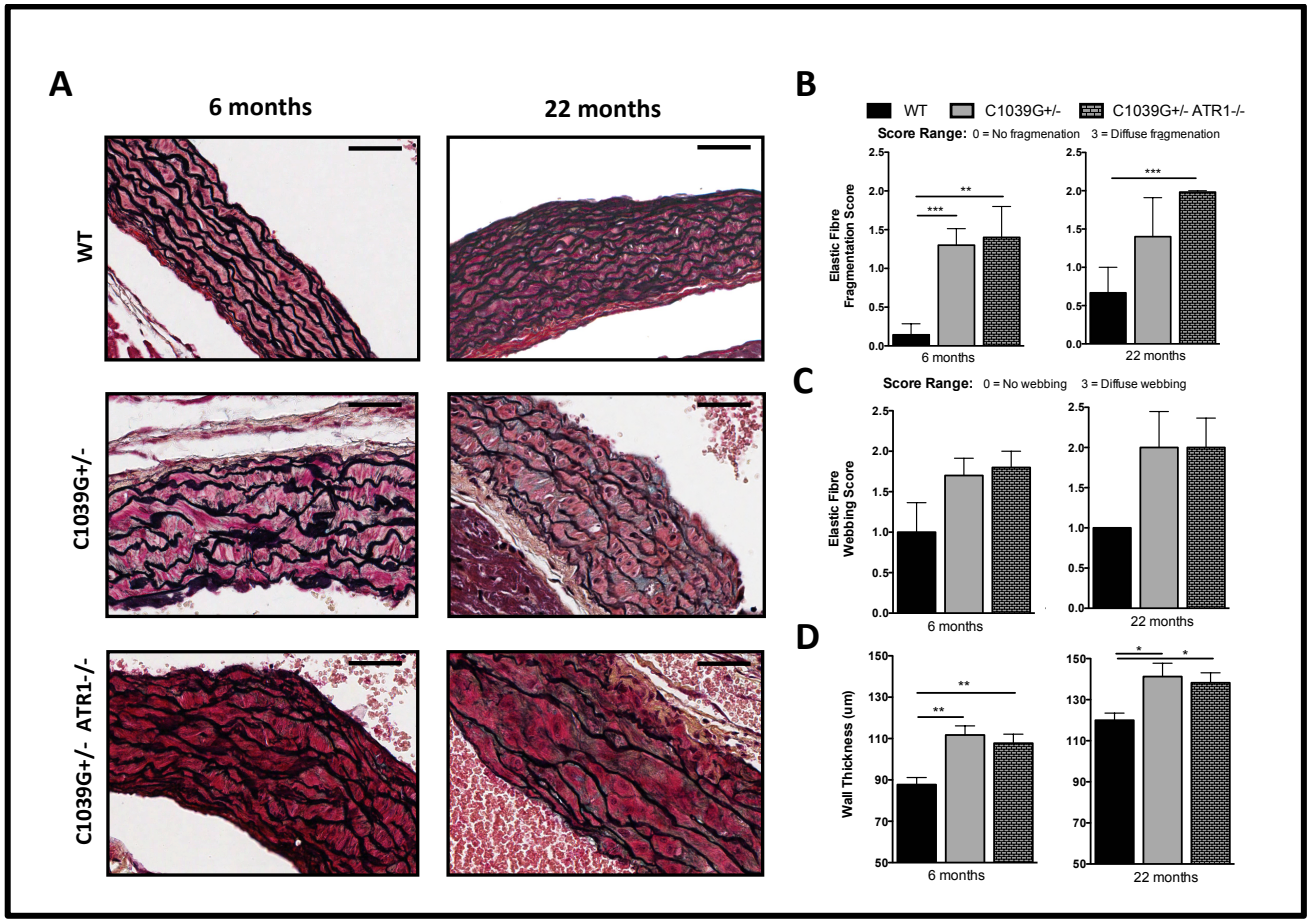

Figure 17: Knockout of ATR1 does not improve pathology within the aortic wall.
Further analysis of aortic root pathology was completed by histology (**A**) where aortic root sections at the level of the Sinus of Valsalva were stained with Movat's pentachrome at six and twenty-two months of age (scale bar =100μM). Histology was assessed to determine elastic fiber fragmentation (C1039G$^{+/+}$ n=7, C1039G$^{+/-}$ n=10, C1039G$^{+/-}$ATR1$^{-/-}$ n=5 at 6 months and C1039G$^{+/+}$ n=3, C1039G$^{+/-}$ n=5, C1039G$^{+/-}$ATR1$^{-/-}$ n=6 at 22 months) (**B**), elastic fiber webbing (**C**), and aortic wall thickness (**D**). *p<0.05, **p<0.01, ***p<0.001.

4.3.4 Loss of ATR1 Expression Does Not Prevent Skeletal or Pulmonary Pathology in MFS Mice

C1039G$^{+/-}$ mice have been shown to develop skeletal manifestations of MFS including kyphosis [26]. Standard lateral radiographs of anesthetized mice were used to evaluate kyphosis and showed readily appreciable kyphosis in C1039G$^{+/-}$ animals compared to WT controls as previously reported for the C1039G$^{+/-}$ strain [26]. However, subsequent analysis of our MFS ATR1 deficient strain revealed no improvement of kyphosis in C1039G$^{+/-}$ATR1$^{-/-}$ animals (Figure 18).

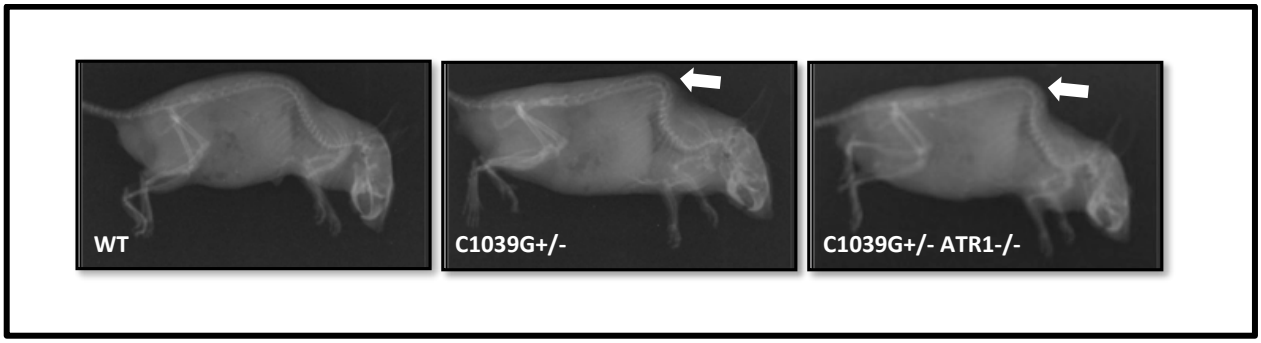

Figure 18: Loss of ATR1 expression does not prevent kyphosis in C1039G$^{+/-}$ mice.
Lateral radiographs of anesthetized animals show clear development of kyphosis (white arrows) in C1039G$^{+/-}$ animals compared to wild type (WT) control as previously reported [26]. Despite loss of ATR1 expression, C1039G$^{+/-}$ ATR1$^{-/-}$ mice show clear indication of kyphosis.

To further evaluate the impact of ATR1 knockout on systemic MFS pathology, emphysema-like airspace enlargement was analyzed using histology of harvested and inflated lungs (Figure 19). Significant airspace enlargement was observed in both C1039G$^{+/-}$ and C1039G$^{+/-}$ ATR1$^{-/-}$ mice at six months relative to control (Figure 19A, C) with progression seen at twenty-two months of age (Figure 19B, E). Notably, no inflammatory infiltrates were observed on histological sections. Additionally, the possibility of an inflammatory component was investigated by looking at cell numbers in bronchoalveolar lavage fluid (Figure 19D), which

revealed no significant change in cell numbers between WT, C1039G$^{+/-}$ and C1039G$^{+/-}$ ATR1$^{-/-}$ mice. Initially, lavage fluid was further analyzed by cytospin centrifugation to analyze cell types within the lavage fluid (data not shown). However, the overall low numbers of cells and lack of inflammatory response within the studied strains meant relatively few cells were observed with no obvious shift in cell type. Therefore, no further cytospin analysis was completed. Overall, these findings demonstrate that lack of ATR1 expression and associated hypotension does not prevent lung and skeletal MFS manifestations.

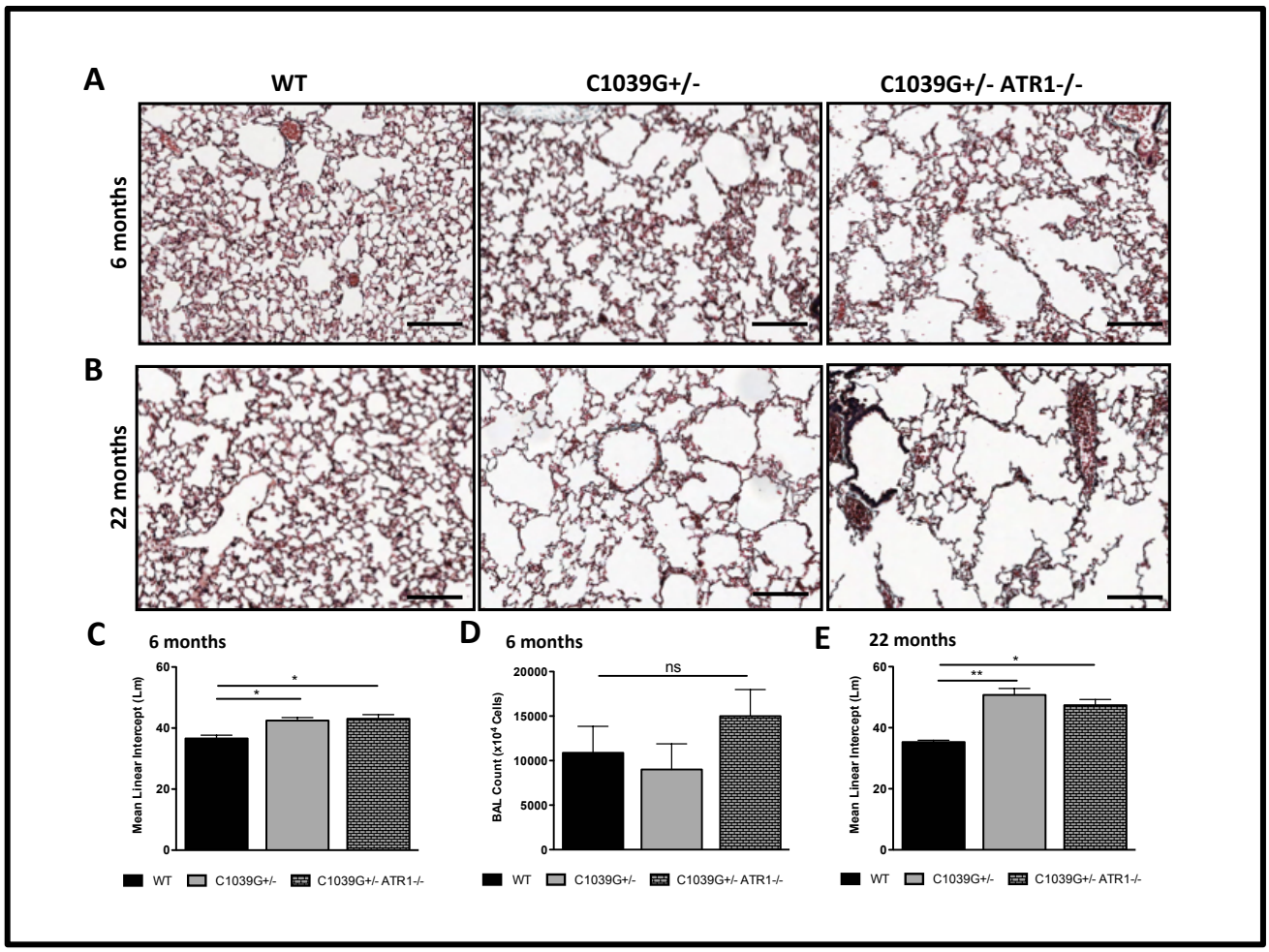

Figure 19: Loss of ATR1 does not prevent airspace enlargement in MFS C1039G$^{+/-}$ mice. Similar airspace enlargement was seen in C1039G$^{+/-}$ and C1039G$^{+/-}$ ATR1$^{-/-}$ mice on Mason's trichrome stained sections of inflated lungs relative to wild-type (WT) controls at six month of age (**A**) and quantified using measurement of mean linear intercept (**C**) show a increase in airspace enlargement in C1039G$^{+/-}$ and C1039G$^{+/-}$ ATR1$^{-/-}$ mice where WT n=5, C1039G$^{+/-}$ n=11, and C1039G$^{+/-}$ ATR1$^{-/-}$ n=4. No inflammation was seen on histology (**A, B**) or in bronchoalveolar lavage (BAL) fluid (**C**) where WT n=5, C1039G$^{+/-}$ n=8, C1039G$^{+/-}$ ATR1$^{-/-}$ n=6. However, airspace enlargement was found to be progressive in both C1039G$^{+/-}$ and C1039G$^{+/-}$ ATR1$^{-/-}$ mice at twenty two months of age (**B**, **E**) wherein WT n=3, C1039G$^{+/-}$ n=5, and C1039G$^{+/-}$ ATR1$^{-/-}$ n=6. Scale bar = 100μM and ns=no significant difference, *p<0.05, **p<0.01.

4.4 Discussion

Collectively, the findings presented above support the surprising conclusion that deletion of the AngII/ATR1 axis with resulting hypotension does not prevent MFS-associated aortic root,

lung or skeletal pathology in the C1039G MFS murine model. As such, our findings bring new light to a number of controversies in the MFS field. First, ATR1 is proposed to be a major therapeutic target in MFS, with selective blockade of ATR1 proposed to block downstream pathogenic TGF-β signaling while also inhibiting TGF-β by increasing 'protective' ATR2 signaling [44, 104]. However, our data suggest that ATR1 is in fact not a therapeutic target in MFS, as knockout of the receptor does not have a beneficial effect in the MFS murine model previously used to establish much of basis for pursuing ATR1 blockade to treat MFS.

Next, as a secondary outcome of ATR1 knockout in C1039G$^{+/-}$ mice, our study sheds new light on the controversy surrounding the benefit of blood pressure reduction in MFS. Irrespective of loss of downstream ATR1 signaling involving TGF-β, our C1039G$^{+/-}$ ATR1$^{-/-}$ model shows a decrease in MAP. As such, this draws into question the clinical use of blood pressure lowering medications, such as β-blockers, ACE inhibitors, and ARBs in MFS patients [154]. Essentially, our findings that the loss of AngII vasopressor responses and reduction in MAP does not reduce aneurysm contradict the hypothesis that decreased hemodynamic stress attenuates MFS aortic pathology. However, our findings thereby do lend credence to conflicting reports on effectiveness of anti-hypertensives in MFS patients including recent trials of atenolol and losartan [116, 162, 174].

Importantly, by performing studies over a range of ages in different groups of mice, including aortic root analysis at three, six, and nine months of age with additional histological analysis at six and twenty two months of age, we are able to conclude that the loss of ATR1 expression with a resulting decrease in MAP does not effect aneurysm development or long-term progression of pathology. While mice at nine months of age do show a lesser degree of aortic root dilation relative to control, this corresponds to a previously reported pattern in the

C1039G$^{+/-}$ strain [104]. Notably, work focused on the early stages of MFS aneurysm in the C1039G$^{+/-}$ strain has identified pathological signaling mechanisms of caspases and microRNAs that were shown to be specific to early stages of aneurysm development in the C1039G$^{+/-}$ strain [46, 205]. While we did not directly study time-points earlier than three months of age, disease progression was unchanged. Thus, this suggests that even if ATR1 deficiency was beneficial at time points earlier than three months, it does not have a lasting benefit. However, early time points, prior to three months on age, could be addressed in future experiments.

Of note, throughout the presented studies, use of ATR1$^{-/-}$ mice shows no cofounding phenotype as no difference was observed in aortic root diameter, histology of the aortic root or lungs parenchyma in ATR1$^{-/-}$ controls. However, while we show clear success in ATR1 genotyping and functional deficiency of ATR1 by demonstrating lack of response to AngII infusion in C1039G$^{+/-}$ATR1$^{-/-}$ and C1039G$^{+/+}$ATR1$^{-/-}$ animals, it is notable that we were unable to assess ATR1 levels by Western blot or direct staining on tissue sections. While staining for the ATR1 receptor was attempted with multiple commercially available antibodies on Western blots of aortic and lung lysates, we were largely unable to detect ATR1 in ATR1$^{+/+}$ control mice and also detected bands at multiple molecular weights inconsistent with the known molecular weight of ATR1. Moreover, we also observed the same bands seen on blots from ATR1$^{+/+}$ mice in ATR1$^{-/-}$ mice purchased directly form The Jackson Laboratory [181]. However, the results of these unsuccessful experiments were validated in recent studies showing that commercially available antibodies for ATR1 are non-specific [206]; Benicky *et al.* showed that six commercially available antibodies from large vendors including Santa Cruz Biotechnology Inc. and Abcam detected non-specific banding in ATR1$^{+/+}$ controls and ATR1$^{-/-}$ animals. Furthermore, the difficulty associated with ATR antibodies was also recently shown to extend to

ATR2 antibodies in which, Hafko *et al.* showed a pattern of non-specific staining in both $ATR2^{+/+}$ and $ATR2^{-/-}$ animals which was inconsistent with AngII receptor binding and gene expression studies [24].

Although the development of a novel ATR1 antibody was considered to aid our studies, discussion with Dr. A. Daugherty (Editor-in-Chief, *Atherosclerosis, Thrombosis, Vascular Biology & Therapeutics,* Director of the Saha Cardiovascular Research Centre, University of Kentucky) revealed that his lab has been attempting to do so at great expense for a number of years with many different approaches and collaborations with no success. Given the highly regarded expertise of Dr. Daugherty in the field of AngII/ATR signaling, we concluded that development of a novel and specific ATR1 antibody was outside of the scope and funding capacity of this project. However, future studies of this $C1039G^{+/-}$ $ATR1^{-/-}$ model could potentially look at the downstream regulation of pathways regulated by ATR1/ATR2 given the availability of antibodies to investigate levels of activation of both canonical and non-canonical downstream TGF-β signaling.

Given our surprising results of no reduction in severity of MFS phenotype upon ATR1 knockout, we deemed use of inducible and tissue specific ATR1 knockout animal models [207, 208] to be outside of the scope of the study; initially, the anticipated next step in investigating ATR1 penetrance and tissue specific effects in MFS was the use of such models as they would allow us to discerning the tissue specific target of future pharmaceuticals and the ideal time-points to reduce ATR1 signaling in order to best combat MFS pathology. However, given the complete lack of benefit resulting from ATR1 knockout, this approach was negated. Albeit, an interesting alternative approach to further investigation of ATR1 in MFS if desired may be through use of mice that over-express ATR1α. Although we have established that loss of ATR1

expression is not beneficial, increased expression may still have a deleterious effect. However, mice that have multiple copies of ATR1α show significant changes in renin-angiotensin signaling that are not reported to be representative of MFS [209].

While we found no benefit to ATR1 deficiency, the laboratory of Francesco Ramirez recently demonstrated a role for ATR1 in a more severe, cardiac centric model of MFS; the MgR murine model spontaneously develops dilated cardiomyopathy (DCM). Cook *et al.* report the ability of ATR1 deficiency, using the same $ATR1^{-/-}$ murine model employed in the studies above, to prevent DCM in the MgR MFS murine model. The authors generally concluded this is through a mechano-sensing mechanism. However, MFS-associated cardiomyopathy is a rare phenotype, thereby bringing the applicability of this study to overall MFS into question. Likely this report is a better commentary on of the effects of deficient extracellular matrix composition (as a result of a large mutation in fibrillin seen in MgR mice) on DCM. Moreover, Cook *et al.* do not report on the effect of ATR1 deficiency on the aortic root [180]. Therefore, owing to the lack of aneurysm data and the use of a different MFS murine model, it is difficult to compare this work to our current findings. Moreover, the aortic root, as studied in our current work, has a unique embryonic origin [210]. As such, our study provides unique insight into role of ATR1 in MFS aortic root aneurysm.

Collectively, our findings present a non-ATR1/AngII driven axis for MFS pathology by presenting a comprehensive analysis of the pathological features of MFS in the $C1039G^{+/-}$ murine model lacking ATR1 with resulting decreases in BP and no functional response to AngII. Given this over-arching conclusion, our findings also suggest that the use of losartan may not be mediated through blood pressure reduction and ATR1 blockade. As such, this possibility is investigated and presented in Chapter 5.

Chapter 5: Do Pleiotropic or Off-target Effects Govern the Therapeutic Benefit of Losartan in Marfan Syndrome?

5.1 Introduction

ARBs are traditionally described as a class of drugs that mediate reduction in blood pressure through inhibition of AngII binding to angiotensin receptors. Notably, there are a number of pleiotropic and off-target or non-angiotensin receptor blockade mediated effects attributed to the use of ARBs. For example, telmisartan, and to a lesser extent, other ARBs, is known to mediate many of its effects through the activation of proliferator-activated receptor-γ (PPAR-γ) [211, 212]. These off-target benefits of telmisartan are linked to NO and improved endothelial function in clinical studies [213] and telmisartan was also found to phosphorylate serine/threonine-specific kinase, protein kinase B (PKB, more commonly referred to as AKT), which is an upstream regulator of eNOS [214]. Moreover, treatment of cultured COS7 cells with telmisartan was shown to have anti-proliferative effects independent of ATR1 expression. In addition, telmisartan is noted to have anti-proliferative and anti-apoptotic effects on ECs [215], known to reduce ROS signaling, shown to reduce oxidative stress, and found to treat endothelial dysfunction in a rat model [216]. Furthermore, the ability to combat endothelial dysfunction and increase NO are also noted as functions of valsartan and irbesartan [217, 218]. However, how much of these effects are off-target remains largely unknown due to the lack of studies that investigate the use of ARBs in the absence of angiotensin receptors.

Despite the intriguing pleiotropic and off-target effects of many ARBs such as valsartan and telmisartan, the most salient ARB to the current study is the potential off-target effects of losartan. Within the study of MFS pathology, losartan is proposed and generally assumed to function as a classic ARB and mediates its effect through specific blockade of ATR1 (Figure 10).

However, the potential for therapeutic benefit as a result of off-target effects have been demonstrated in the past. In 2005, Watanabe *et al.* demonstrated the ability of losartan to activate AKT in bovine aortic endothelial cells [219]. This activation was found to be dependent on vascular endothelial growth factor receptor type II (VEGFR2). Most importantly, from an endothelial dysfunction perspective, this activation also resulted in a downstream increase in phosphorylation of endothelial nitric oxide synthase (eNOS). However, the resulting effect on NO production was not studied. However, losartan was also utilized in a rat model of transient cerebral ischemia and was found to reduce infarct size through an AKT mediated phosphorylation of eNOS [220]. Furthermore, losartan was found to attenuate inducible nitric oxide synthase [221] activation. Yet, it is important to note that these two latter findings did not conclude that such a mechanism was not mediated through the ATR1 receptor. Collectively, these studies present a means by which losartan may act independently of ATR1 in MFS.

Given the potential for ATR1-independent effects of losartan and the lack of benefit of ATR1 knockout seen in our studies, this suggests that losartan may in fact act off-target in MFS. One potential mechanism of such an effect may be through the VEGFR2/AKT/eNOS axis as detailed in studies presented above (Figure 20). Moreover, the likelihood that activation of the VEGFR2/AKT/eNOS axis in MFS may be therapeutic (ie. prevent or reduce progression of aortic aneurysm) is also supported by a number of studies. For example, improved NO bioavailability is associated with improved endothelial function and decreased inflammation, remodeling and oxidative stress, all of which may combat pathophysiological components of MFS-associated aneurysm [107, 127-129, 131]. Furthermore, activation of the AKT/NOS/NO axis may improve the pathological contribution of TGF-β to MFS pathogenesis as established by blocking antibodies [27]; NO inhibits downstream gene activation resulting from TGF-β/Smad

signaling by preventing Smad-2/3 nuclear transmigration and enhancing Smad degradation [222]. Additionally, NO is known to inhibit phosphorylation of ERK, a pathway previously demonstrated to central to mitigating pathological TGF-β signaling in MFS aortic aneurysm in mice [44].

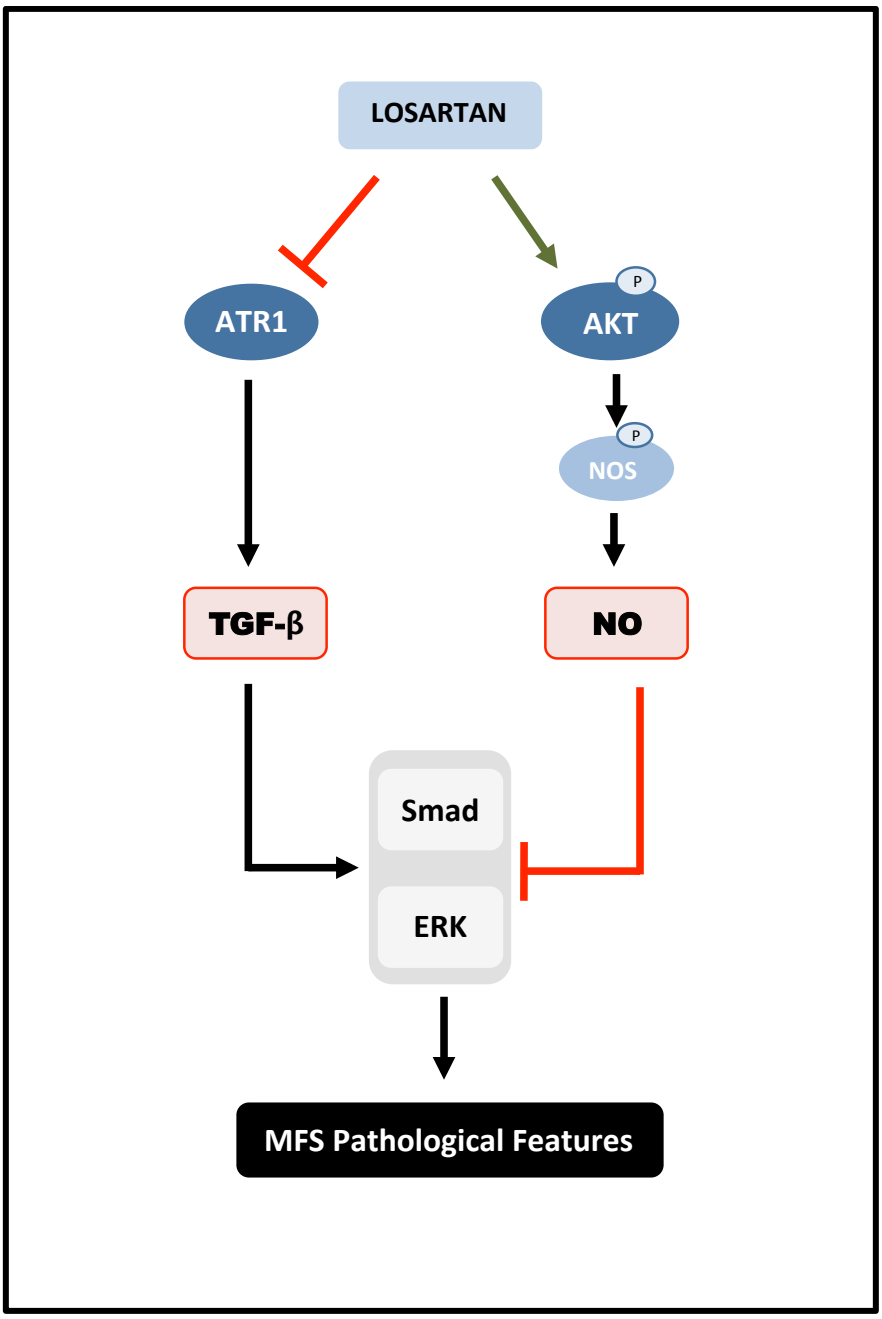

Figure 20: Potential off-target effects of losartan in MFS.
While losartan is proposed to function through specific blockade of ATR1, alternative mechanisms propose that losartan functions through activation of the VEGFR2/AKT/eNOS axis. Activation of this axis may benefit MFS pathology through reduction of pathological TGF-β signaling, inflammation, MMP activity and oxidative stress.

5.2 Experimental Approach and Chapter Specific Aims

In Chapter 4, it was established that loss of ATR1 deficiency does not mitigate aortic aneurysm, airspace enlargement or kyphosis observed in the C1039G$^{+/-}$ MFS strain. Given this lack of benefit resulting from ATR1 deficiency in the face of previous reports of effectiveness of losartan, which is proposed to occur through ATR1 [104], a clear paradox is presented. To address this, we aimed to answer the question of whether treatment of MFS aneurysm with losartan requires the expression of ATR1. As pharmacological principles dictate that losartan should have no benefit in the absence of ATR1, we hypothesized that losartan would benefit C1039G$^{+/-}$ mice but have no effect in C1039G$^{+/-}$ATR1$^{-/-}$ mice. In the event of finding that losartan acted in an ATR1-independent manner, we aimed to determine the potential off-target mechanism of losartan using loss of function models both *in vitro* and *in vivo*.

5.3 Results

5.3.1 Losartan Mediates Reduction in Aortic Root Aneurysm Independently of ATR1

Whether losartan requires expression of its proposed receptor, ATR1, to mediate reduction of aortic root aneurysm was assessed by losartan treatment of C1039G$^{+/-}$ and C1039G$^{+/-}$ ATR1$^{-/-}$ animals. Consistent with previously reports, we observed significant reduction in aneurysm in C1039G$^{+/-}$ mice treated with losartan (Figure 21A, B). Surprisingly, similar therapeutic benefit was seen in C1039G$^{+/-}$ATR1$^{-/-}$ mice, despite a lack of functional ATR1 expression (Figure 21A, B). Further, reduction in aneurysm development was accompanied by prevention of aortic wall pathology in both C1039G$^{+/-}$ and C1039G$^{+/-}$ATR1$^{-/-}$ mice (Figure 21C), thereby indicating that the therapeutic effect of losartan in aneurysm prevention is an ATR1-independent event.

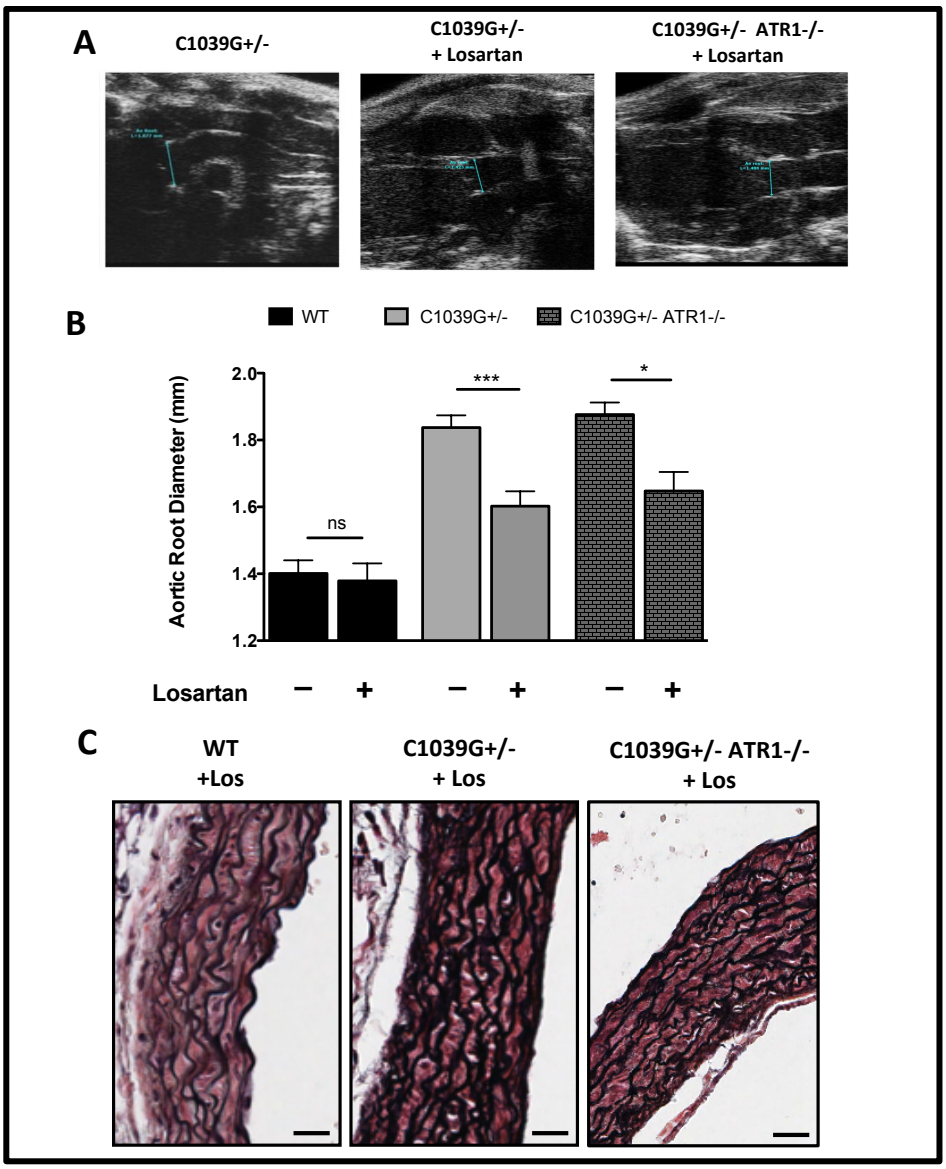

Figure 21: Losartan mediates reduction in aortic aneurysm independently of ATR1. Treatment of losartan treated C1039G$^{+/-}$ and C1039G$^{+/-}$ ATR1$^{-/-}$ was assessed by B- and AM-mode echocardiograms by a blinded technician at three months of age (**A**). Quantification of echocardiograms revealed losartan to mediate reduction in aortic root diameter in both C1039G$^{+/-}$ and C1039G$^{+/-}$ ATR1$^{-/-}$ (**B**) where WT n=8, WT +losartan n=4, C1039G$^{+/-}$ n=9, C1039G$^{+/-}$ +losartan n=11, C1039G$^{+/-}$ ATR1$^{-/-}$ n=5, C1039G$^{+/-}$ ATR1$^{-/-}$ +losartan n=5. Representative images of aortic root histology in losartan treated C1039G$^{+/+}$, C1039G$^{+/-}$, and C1039G$^{+/-}$ ATR1$^{-/-}$ mice at six months of age (**C**) (scale bar=25μm) stained with Movat's pentachrome (elastic fibers = black) that indicate reduction in elastic fiber fragmentation relative to untreated animals. Where ns= not significantly different, *p<0.05, ***p<0.001.

The argument that the effects of losartan that we propose are off-target may in fact be mediated by the beta isoform of the ATR1 receptor is valid and required further analysis. Given the paucity of specific antibodies available, to confirm loss of ATR1 receptor expression in our models, we assessed AngII binding in aortic root sections. Robust staining was found in wild-type myocardium surrounding the aortic root (Figure 22A), which was partly inhibited by losartan, indicating positive ATR1 expression. In the absence of myocardium (to prevent AngII scavenging) AngII binding was much weaker in the aortic root and mostly inhibited by losartan (Figure 22B) indicating lower ATR1 levels. However, use of $ATR1^{-/-}$ aortic root sections showed no losartan-sensitive AngII staining (Figure 22C), thereby validating the absence of ATR1 expression and supporting the conclusion that our observed effect of losartan in $C1039G^{+/-}ATR1^{-/-}$ is the result off-target effects.

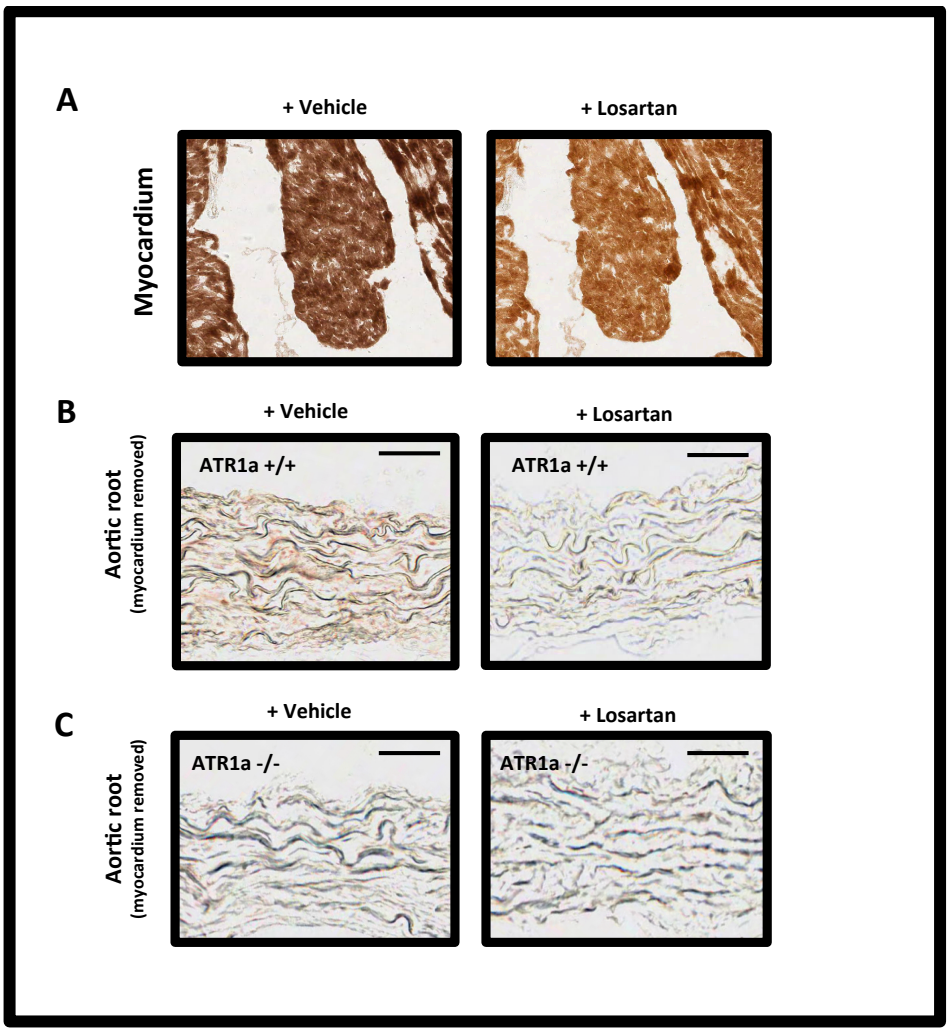

Figure 22: Loss of losartan-sensitive AngII binding in the aortic root of ATR1-null mice. Representative images of staining using biotin-conjugated AngII which was bound to myocardium and aortic root sections with (+Losartan) and without Losartan (+Vehicle). The resulting signal is interpreted as the levels of ATR1/2 present. In wild type myocardium strong binding is noted, which losartan reduced by approximately fifty percent (A). In aortic root sections of wild type mice ($ATR1a^{+/+}$) less AngII staining is noted relative to myocardium but is still inhibited by losartan (B). In aortic root sections of ATR1-alpha deficient animals ($ATR1a^{-/-}$) less AngII staining is seen, of which none is inhibited by losartan (C).

5.3.2 Losartan Mediates Increased NO Production via VEGFR2

Having established that losartan mediates reduction of MFS aneurysm in an ATR1-independent manner, an alternative mechanism for the therapeutic benefit of losartan was investigated. Previously, losartan has been reported to activate the eNOS pathway [219, 220].

However, whether losartan increases NO bioavailability is unknown. To investigate this, we studied NO-release *in vitro*. This revealed that pre-treatment of BAECs with losartan for 48 or 72 hours in the absence of AngII significantly increased ionophore-induced NO release in a time and dose dependent manner (Figure 23A). Furthermore, losartan increased NO levels without pre-treatment wherein losartan was given acutely in combination with ionophore (Figure 23B).

As a potential mediator of losartan-induced NO release, we investigated the role of VEGF receptor type 2 (VEGFR2) in BAECs [219]. To do so, BAECs were treated with VEGFR2 siRNA, which achieved an 88% knockdown compared with scrambled sequence control (Figure 23C). Subsequently, studies of acute ionophore induced NO release in siRNA treated BAECs failed to show increased NO release with losartan treatment (Figure 23D), thus supporting the conclusion that losartan activates protective NO release in a VEGFR2-dependent fashion, independently of AngII/ATR1.

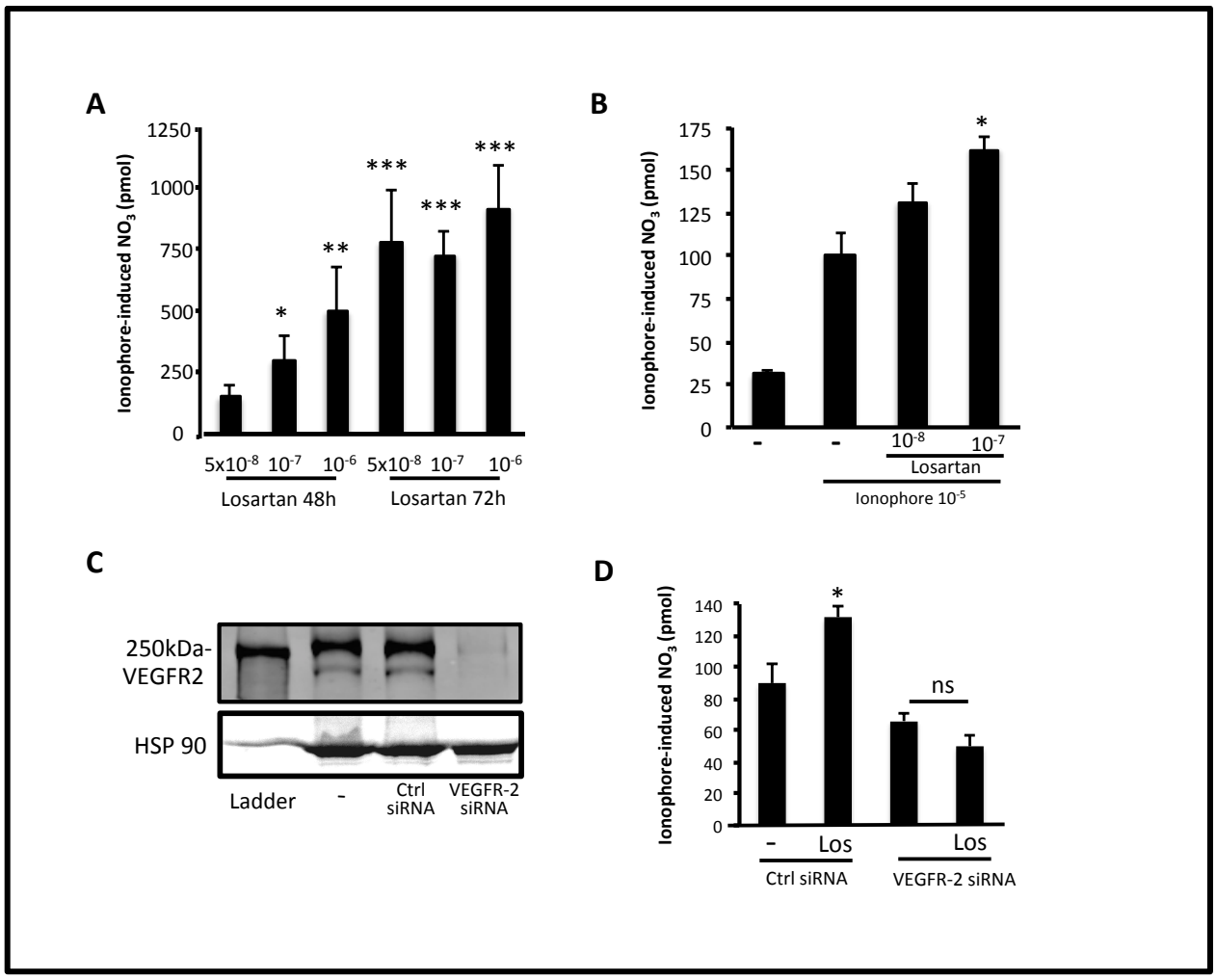

Figure 23: Losartan increases NO release *in vitro* in endothelial cells in a VEGFR2-dependent manner.

The ability of losartan to increase NO *in vitro* was determined through measurement of ionophore-induced nitrite in BAECs pre-treated with Losartan ($5x10^{-8}$M, $5x10^{-7}$M, and $5x10^{-6}$M) for 48- or 72-hours (**A**) which showed a dose and time dependent increase in nitrite with losartan treatment. A similar increase was seen with acute losartan treatment ($5x10^{-8}$M and $5x10^{-7}$M) (**B**). To determine regulation of increased nitrite levels with losartan treatment, ionophore-induced nitrite release was studied in BAECs treated with VEGFR2 siRNA compared to untreated (-negative) BAECs, and BAECs treated with a scrambled siRNA sequence (Ctrl siRNA). VEGFR2 siRNA treated BAECs showed large reduction in VEGFR2 expression (250kDA) relative to controls on western blot using an Hsp90 loading control (90kDA) (**C**). Further, VEGFR2 siRNA treated ECs showed no increase in ionophore-induced nitrate with acute losartan treatment (**D**). For ionophore-induced nitrite studies values represent 1hr accumulation of nitrate for pre-treated cells and 15 minute accumulation for acutely treated cells expressed as mean release ±SEM with each condition performed in triplicate within the experiment.***$p<0.001$ **$p<0.01$, *$p<0.05$.

5.3.3 Reduction of Aortic Aneurysm in MFS by Losartan is NOS-dependent

Others have reported that losartan can function to increase activation of the eNOS pathway and combat endothelial dysfunction in an off-target manner [219, 220, 223, 224]. These findings are further supported by our data showing an off-target effect of losartan *in vivo* and the ability of losartan to increase NO *in vitro.* Further, eNOS-derived NO is a potent TGF-β modulator and decreased NO bioavailability has been reported in MFS C1039G$^{+/-}$ mice [51, 127, 222]. Therefore, to investigate the hypothesis that the off-target effect of losartan on MFS aneurysm is mediated through NO/NOS, C1039G$^{+/-}$ mice were treated with losartan in combination with NOS inhibitor L-NAME. While L-NAME alone had no effect on aortic root diameter in C1039G$^{+/-}$ animals, we observed that L-NAME completely antagonized the benefits of losartan (Figure 24A, B), thus supporting a NOS-dependent effect of losartan in treatment of MFS aneurysm *in vivo.*

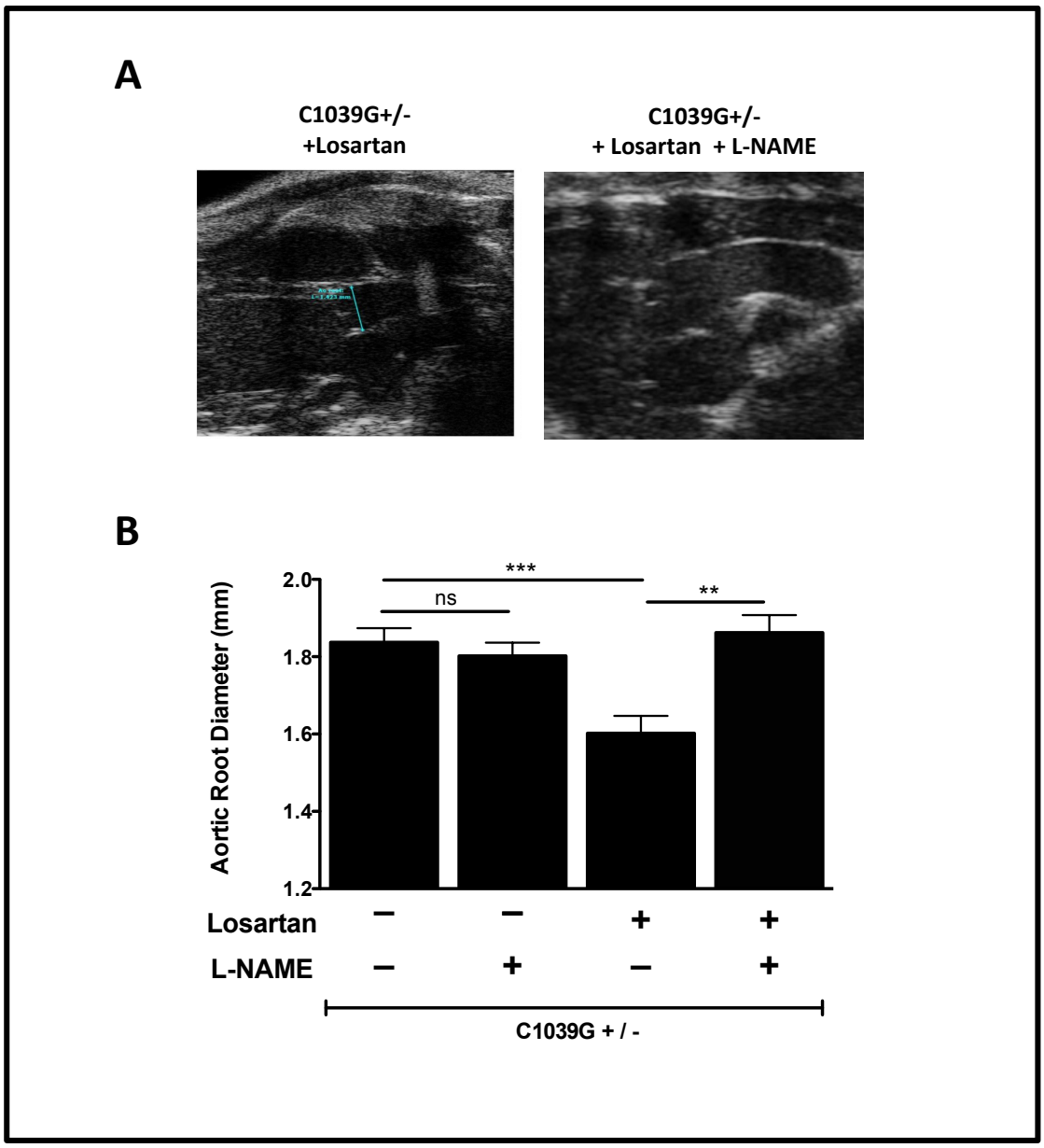

Figure 24: Losartan mediates reduction in aneurysm in a NOS-dependent manner.
To determine dependence of losartan to reduce aortic aneurysm on NOS, mice were treated with losartan in combination with NOS blocker L-NAME. While losartan reduced aortic root diameter, combination treatment with losartan and L-NAME had no effect of aortic root aneurysm (**A, B**) at three months of age wherein aortic root diameters represent mean aortic root diameter ±SEM as determined from multiple measurements by a blinded technician where $C1039G^{+/-}$ n=9, $C1039G^{+/-}$ +L-NAME n=5, $C1039G^{+/-}$ +losartan n=5, $C1039G^{+/-}$ +losartan +L-NAME n=5). **p<0.01, ***p<0.001.

5.3.4 Losartan Corrects NO Levels in C1039G$^{+/-}$ Mice and NO Correlates to Aneurysm Size

Having established the ability of losartan to increase NO release *in vitro* and the NOS dependency of losartan *in vivo*, we next investigated NO levels *in vivo*. Analysis of total NO (nitrate and nitrite) from plasma of fasted mice revealed a significantly decreased NO levels in C1039G$^{+/-}$ compared to WT controls (Figure 25A). Analysis of aneurysm size versus total plasma NO in a subset of mice revealed an inverse linear correlation between decreased plasma NO and aortic root dilation (Figure 25B). While this established that a notable decline in NO levels was associated with MFS pathology, how this would be impacted by losartan treatment was unknown. However, analysis of total plasma NO in losartan treated C1039G$^{+/-}$ mice demonstrated that losartan corrected NO levels *in vivo* (Figure 25A). Furthermore, a clear relationship between aortic root diameter and total plasma NO is still seen upon addition of losartan treated animals (Figure 25C) to our initial analysis (Figure 25B). Hence, these findings suggest a role for decreased NO levels in the pathology of MFS aortic aneurysm that is treated by losartan.

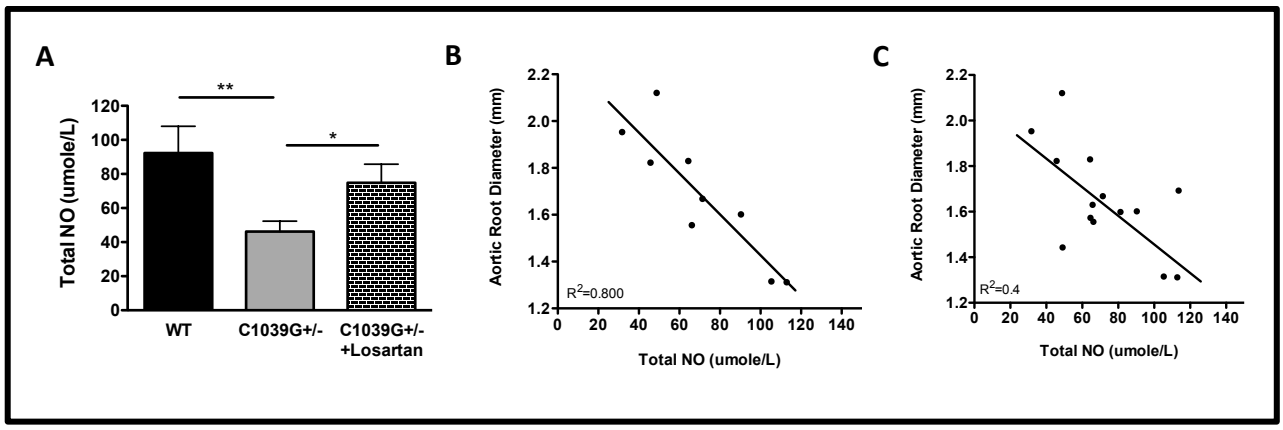

Figure 25: MFS mice show reduced NO levels that correlate to aortic aneurysm size and are corrected with losartan.
Total plasma NO levels in WT ($C1039G^{+/+}$), $C1039G^{+/-}$ and losartan treated $C1039G^{+/-}$ mice was determined at six months of age in fasted mice (**A**) and shows significant reduction in NO in $C1039G^{+/-}$ mice that is corrected with losartan where WT n=5, $C1039G^{+/-}$ n=9, and $C1039G^{+/-}$ +losartan n=5 with values for each animal average from assays run in duplicate. Furthermore, a relationship is seen between aortic root diameter and total plasma NO at six months of age in WT vs. $C1039G^{+/-}$ animals (**B**) which holds upon addition of losartan treated animals to this analysis (**C**). *p<0.05, **p<0.01.

5.3.5 Losartan Does Not Mediate Therapeutic Benefit Through Phosphorylation of eNOS Residue Serine 1176

Having confirmed the ATR1-independent effect of losartan and established the benefit of losartan in reducing aneurysm to be NOS dependent, we sought to define this mechanism further. Notably, serine 1176 (S1176) is one of the main activation phosphorylation sites of eNOS and may mediate our observed increase in NO from losartan [219]. To determine the importance of this phosphorylation site in mediating the therapeutic benefit of losartan, we utilized MFS mice containing an eNOS knock-in that makes S1176 unable to be phosphorylated via substitution of an alanine residue (S1176A). Measurement of aortic root diameter in these mice ($C1309G^{+/-}$ S1176A) with and without losartan treatment revealed that losartan was still able to mediate aortic root reduction (Figure 26). Therefore, we concluded that losartan mediates its therapeutic benefit via NOS, but this does not require phosphorylation of S1176.

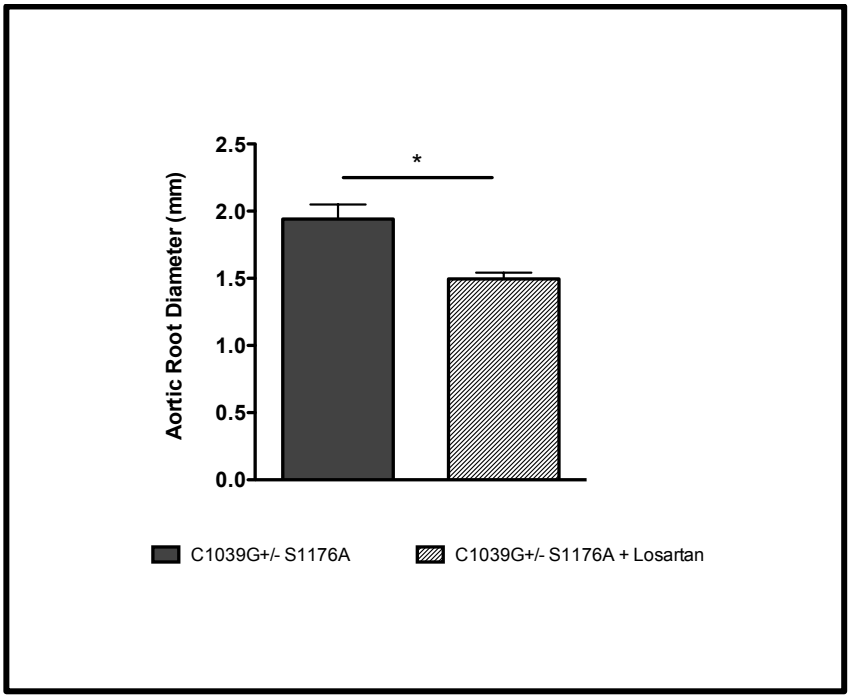

Figure 26: The action of losartan in preventing aneurysm in C1039G$^{+/-}$ mice is not mediated through phosphorylation of eNOS Ser1176.
Analysis of aortic root diameter via echocardiograms by a blinded technician in MFS mice with an unphosphorylatable S1176 residue (C1039G$^{+/-}$ S1176A) compared to those treated with losartan (C1039G$^{+/-}$ S1176A + Losartan) demonstrates the ability of losartan to significantly reduce aneurysm independently from the ability of S1176 phosphorylation. Values represented mean aortic root diameter averaged from AM- and B-mode echocardiograms. *$p<0.05$.

5.4 Discussion

Overall, the data presented clearly identify the ability of losartan to mediate reduction in aortic pathology independently of ATR1, its proposed cellular target, and thereby supports the conclusion that losartan functions in an off-target manner in MFS. As such, this is the first study to show a therapeutic off-target effect of losartan in MFS *in vivo*. While this is a key finding for our understanding of MFS pathology, the argument that optimizing off-target effects may require high doses of drug is important to address. In this respect, it is notable that the dosage of losartan utilized in these studies was 0.6g/L is drinking water and has frequently been used in the

C1039G$^{+/-}$ mouse line [44, 93, 104] and higher doses (1.2g/L) have been used in murine models of MFS without toxicity and showing dose dependent improvement [103]. This suggests that the dose of losartan used here was conservative and the potential to increase the beneficial or off-target effects generated by losartan could be amplified at higher dosages in future experiments. This, in some aspects, may also be true in MFS patients; a key criticism of the landmark trial of atenolol vs. losartan recently published by Lacro *et al.* in the New England Journal of Medicine [174] is that unequal reduction in blood pressure was observed between groups and an increased dosage of losartan should be used in future trials to equalize this discrepancy.

Importantly, the conclusion that losartan functions in an off-target manner to prevent aortic aneurysm in MFS is also supported by our studies of AngII binding in myocardium and aortic root sections. Of note, the observation of distinct staining within the myocardium is supportive of the previously discussed findings of the effect of ATR1 deficiency in a MFS model of DCM [180]. However, in contrast to AngII binding in myocardium seen in the current study, relatively less AngII staining was observed in the aortic root and inhibited by losartan. Yet, the most salient component of these binding studies is the lack of binding of AngII that was inhibited by losartan in the aortic root of ATR1-alpha deficient mice. This finding supports the conclusion that the observed reduction of aortic root diameter in C1039G$^{+/-}$ ATR1$^{-/-}$ mice is not mediated through blockade of ATR1-beta.

While the conclusion of an off-target losartan effect is central to helping explain conflicting results for the use losartan in MFS, it also posed a new and complex question: what is the alternative mechanism of losartan in preventing MFS aneurysm? Answering this question is of key importance for future therapy development, potential stratification of MFS patients, and shedding new light on MFS pathology. In considering the answer to this question, the observed

ability of losartan to mediate increased NO release with acute or chronic treatment *in vitro* in a VEGFR2 dependent manner is consistent with previous findings of the signaling mechanism of losartan metabolites [219]. Specifically, the authors demonstrated the ability of losartan, and both its metabolites (EXP3174 and EXP3179), to activate AKT by stimulating phosphorylation of Ser473, which subsequently led to an increase in phosphorylation of eNOS at Ser1179 in BAECs. Notably, we did complete initial ionophore-induced NO release studies using EXP3174 and EXP3179 metabolites and akin to activation of the AKT/eNOS pathway activation reported by Watanabe *et al.*, we found that both metabolites were able to stimulate NO-release but found either metabolite alone to be similar to losartan (Appendix B). Our findings are also similar to Watanabe *et al.* in that we found NO release to be dependent on VEGFR2 expression. VEGF receptors control a number of signaling pathways within endothelial cells associated with TGF-β and are also expressed in cell types of tissues that correspond to systemic phenotypes of MFS including the retina and lens of the eye, skeletal muscle, skin and bone [225]. Moreover, blockade of VEGF receptors has been a tactic associated with cancer therapies, which relates to MFS and our presented findings in some aspects; the use of sugen (SU5416), an inhibitor of VEGF signaling, has been associated with MFS like phenotypes including emphysema that was linked to a decrease in downstream phosphorylation of AKT [226] [227]. Moreover, sugen and VEGF inhibitors carry an FDA warning regarding aneurysm and inhibition of VEGF has been associated with aneurysm rupture [228]. Notably, while it is highly likely that increased NO release is the result of increase NOS activity, we did not complete an L-NAME control for this set of *in vitro* experiments and as such is a limitation of our study and should be completed upon further *in vitro* analysis in future directions. Moreover, as an extension of our *in vitro* findings of the VEGFR2/NO axis regulation by losartan in BAECs, future experiments would be useful to

determine the ability of losartan to increase NO in MFS-derived endothelial cells either from C1039G$^{+/-}$ murine models or human samples from surgical cases. However, we indirectly approached this using an *in vivo* model; treatment of C1039G$^{+/-}$ with losartan in combination with L-NAME clearly established the effect of losartan in MFS *in vivo* to be NOS-dependent. As such, this represents the first report of a definitive therapeutic benefit of losartan in MFS that is off-target. However, despite this strong finding, it raised a new question of the means by which losartan mediates aneurysm prevention *in vivo*.

As others have suggested that endothelial dysfunction is a critical regulator of MFS aortic pathology [51, 127, 128], we sought to define a parameter of endothelial dysfunction *in vivo* in our model. Our findings of decreased plasma NO in MFS is suggestive of endothelial dysfunction and the correction plasma NO levels were achieved by losartan. Not only does this mesh with our findings of NOS-dependent aneurysm reduction, it recapitulates our findings of increased NO release in EC culture with losartan treatment. However, the means by which NO is increased *in vivo* by losartan remains a point for future study. In this respect, our finding of sustained utility of losartan in S1176A mice was surprising. As S1176 is one of the main phosphorylation sites of eNOS, and a site shown *in vitro* to be phosphorylated during losartan treatment, the phosphorylation of S1176 by losartan was a probable mechanism of increased NO *in vivo* in MFS [184, 188, 189, 219]. Notably, due to our desire to specifically compare the impact of losartan in the presence of the S1176A phospho-mutant, recommendations to reduce animal use when possible, and excess cost, no separate WT and C1039G$^{+/-}$ groups was completed within this set of experiments and values. However, values for C1039G$^{+/-}$ S1176A mice were consistent with previous groups as well as a response to losartan. Despite a therapeutic benefit of losartan in the presence of the S1176A phospho-mutant, alternative

phosphorylation sites of eNOS may be responsible for increased production of NO such as Ser116, Ser635, and Thr497, which have been shown to be phosphorylated by VEGF driven stimuli [229]. Moreover, increased NO production may be related to increased eNOS expression, reduced NO scavenging or changes to eNOS co-factors [230]. As such, study of these potential alternative phosphorylation sites or mechanisms remains an opportunity for future investigation.

Irrespective of the mechanism of losartan-mediated reduction in aneurysm, the data presented speak to a role of endothelial function MFS *in vivo* that correlates to the extent of aneurysm progression as suggested by our finding of a correlation between plasma NO levels and aneurysm size. As such, investigation of therapeutic approaches for mediating increased NO and improving endothelial function would shed light on future treatment directions for MFS. Moreover, given reports regarding the ability ARBs, other that losartan, to mediate therapeutic effects via NO [214, 218, 220], complete study of the potential for improvement of endothelial function by ARBs as a class would be well placed. While we utilized NO levels as an indicator of endothelial function/dysfunction and correlated to the degree of aneurysm, other indices of endothelial function may be useful; analysis of endothelial activation, levels of reactive oxygen species, and assessment of vasoactive responses all represent alternative indices of endothelial health [127, 128, 231]. While future work along these lines will be useful in animal models such as those presented in this work, our findings also speak to the potential for studying endothelial dysfunction in a more detailed manner in patient populations. In this respect, we have approached this by looking at flow mediated dilation (FMD) in a MFS patient population treated with losartan (Appendix C) via sub-stratification of data obtained in patients detailed in a recent publication by Sandor *et al.* in the *International Journal of Cardiology* [130]. While Sandor *et al.* examined parameters of vascular function in MFS and showed a trend towards decreased aortic

pulse wave velocity, an indicator of improved vascular function as a result of decreasing aortic stiffness, we analyzed these data to look at FMD. This analysis showed that patients who experienced an improvement in FMD with losartan treatment all showed a regression of aortic root diameter. Conversely, those patients who had a decrease in FMD showed progression of aortic root aneurysm. As improvement of FMD represents an improvement in endothelial function, this finding suggests that a subset of MFS patients experience improved endothelial function with losartan treatment and this is associated with a reduction in rate of progression of aortic aneurysm. Further to this point, and similar to the suggestion that losartan should be titrated against blood pressure when trialed against atenolol, it may be useful to titrate losartan against FMD. As we find a relationship between improved FMD and regression of aortic size, treatment with losartan based on FMD is an important potential approach to explore in future trials. If confirmed, this finding may drastically change the guidelines utilized for treating and monitoring aortic aneurysm in MFS patients. Moreover, this would mark a change in perspectives on the role of endothelial function in MFS and highlight the role of NO, endothelial function and off-target effects of losartan in MFS. Collectively, this point is supported by the presented work as overall we conclude from our *in vitro* studies in ECs, experiments in $C1039G^{+/-}$ mice, and initial analysis of a patient population support the conclusion that losartan acts to treat aortic aneurysm in an off-target NOS-dependent manner in MFS to improve endothelial function.

Chapter 6: Role of Nitric Oxide in Treatment of Marfan Syndrome

6.1 Introduction

The data presented in Chapter 4 and Chapter 5 establish that the loss of ATR1 expression does not have an impact on MFS pathology and that losartan treats MFS aneurysm in an ATR1-independent and NOS-dependent manner that corrects NO levels in MFS mice. This mechanism is in line with reports of abnormal eNOS expression and endothelial function in MFS and the ability of losartan to improve vascular function in patients [127, 128, 130]. Moreover, our group has previously demonstrated the importance of NO in vascular homeostasis in the context of atherosclerosis [231]. However, we have not yet moved past the study of losartan mediated NO to explore the impact of altering nitric oxide levels on MFS pathology. Study of how altering NO levels in the context of MFS, other than by treatment with losartan, may shed light on the role of NO and endothelial function in MFS pathology and treatment. Moreover, clearly demonstrating that increasing NO is therapeutic in MFS would direct future pharmaceutical development and clinical trials.

A focus on NO levels in MFS is clearly important; as previously discussed, NO has the potential to mitigate pathogenic TGF-β via downstream inactivation of Smad and ERK signaling (Figure 18). Furthermore, endothelial dysfunction and reduced levels of NO are associated with MFS pathology specifically in C1039G$^{+/-}$ mice [128] [127]. More broadly, low NO availability and oxidative stress is also associated with increased MMP activity [232, 233] as well VSMCs apoptosis [234] [235]. Exploring the impact of altered NO levels in murine models is often achieved by genetic manipulation including the previous successful use of eNOS deficient models (eNOS$^{-/-}$) [194, 195] as well as models that have altered eNOS activity (eNOS^{S1176A} and eNOS^{S1176D}) and those that over-express eNOS via a transgene (eNOS Tg) [189, 193]. However,

genetic manipulation is highly unlikely to be translated to human systems in the near future and thereby supports the development and use of pharmacological means of increasing NO and/or decreasing oxidative stress. Although many pharmaceuticals currently in use produce increased NO levels, they do so in an exogenous manner that generates NO boluses. However, our group has previously published on the use of CavNOxin, a peptide mimetic of the caveolin-1 scaffold domain containing key point mutations that allow for increased endogenous NO production (Figure 9) that also reduces oxidative stress markers [231]. As such, the use of CavNOxin in MFS presents is a potentially interesting alternative therapeutic approach to genetic manipulation.

6.2 Experimental Approach and Chapter Specific Aims

To investigate the impact of altering NO levels in MFS independent of the use of losartan, we aimed to use genetic models of altered eNOS activity and expression within the C1039G$^{+/-}$ MFS murine model. Moreover, the use of CavNOxin was explored to investigate the role of pharmaceutical means of increasing endogenous NO in MFS. Overall, using these approaches we aimed to determine the therapeutic implications of altering NOS activity and/or NO levels in the context of MFS.

6.3 Results

6.3.1 Marfan Models with Increased eNOS Activity and eNOS Expression Have Improved Aortic Aneurysm

To determine if prevention of aneurysm in C1039G$^{+/-}$ animals was possible through increased production of NO, we generated C1039G$^{+/-}$ mice with increased eNOS activity via a phospho-mimetic 1176 Ser-to-Asp (S1176D) eNOS gene knock-in. Evaluation of these mice by

echocardiogram revealed a significant reduction in the aortic root diameter similar to that seen with losartan treatment in C1039G$^{+/-}$ with expression of the S1176D mutation (C1039G$^{+/-}$ S1176D, Figure 27A). Furthermore, the ascending aorta in this group of animals was also examined and showed, that C1039G$^{+/-}$ mice were found to have a significant increase in ascending aorta diameter. Moreover, akin to findings in the aortic root, a significant reduction in ascending aortic aneurysm was seen in C1039G$^{+/-}$ S1176D mice. (Figure 27B), thereby supporting the conclusion that increased activation of endogenous eNOS is therapeutic in the context of MFS aneurysm.

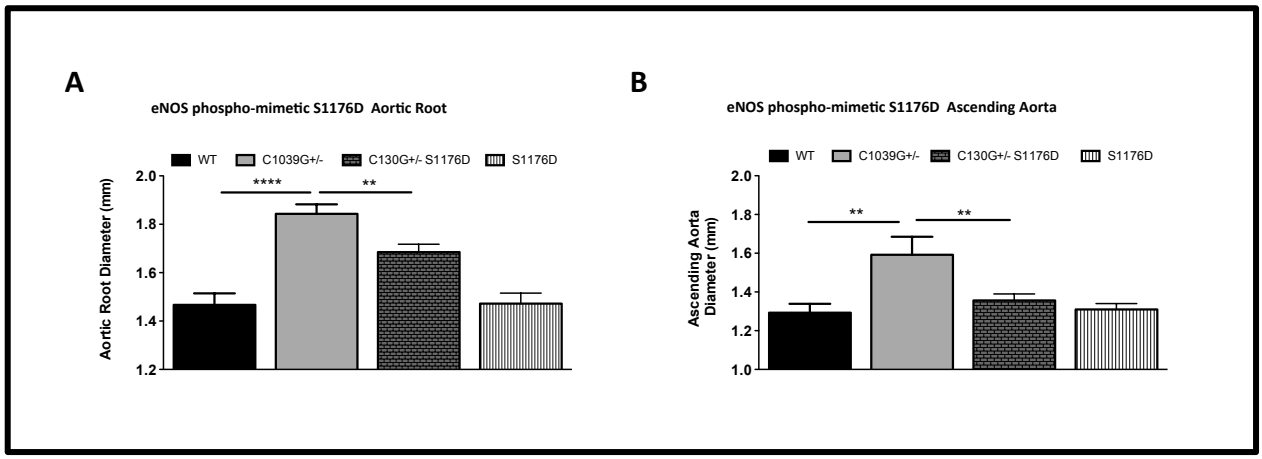

Figure 27: eNOS Ser-1176-Asp (S1176D) knock-in prevents aortic root and ascending aorta aneurysm in C1039G$^{+/-}$ mice.
Analysis of aortic root diameter via echocardiograms by a blinded technician in MFS mice with a constitutively active eNOS (C1039G$^{+/-}$ S1176D) showed significantly decreased aortic root diameter at three months of age (**A**) where WT n=11, C1039G$^{+/-}$ n=15, C1039G$^{+/-}$ S1176D n=13, S1176D n=9. Echocardiography also revealed a significant increased in ascending aortic diameter in C1039G$^{+/-}$ animals compared to controls at three months of age (**B**) that was corrected in C1039G$^{+/-}$ S1176D mice where WT n=5, C1039G$^{+/-}$ n=7, C1039G$^{+/-}$ S1176D n=9, S1176D n=6. Values for each group represent mean vessel diameter ±SEM where values for each animal studied were averaged from multiple measurements. **p<0.01, ****p<0.0001.

To augment echocardiogram findings of reduced aortic aneurysm in C1039G$^{+/-}$ S1176D animals, histology of the aortic root was analyzed. While a significant increase in elastic fiber fragmentation was seen in C1039G$^{+/-}$ animals, there was an observable reduction in fragmentation seen in C1039G$^{+/-}$ S1176D mice (Figure 28A, B). Moreover, while staining of levels of phopho-Smad2 showed no difference between groups (data not shown), a decrease phospho-ERK staining can be appreciated in C1039G$^{+/-}$ S1176D animals compared to C1039G$^{+/-}$ mice (Figure 28C). Therefore, histological findings within the aorta of C1039G$^{+/-}$ S1176D mice (Figure 28) demonstrate a reduction in MFS pathology that corresponds to echocardiogram findings (Figure 27).

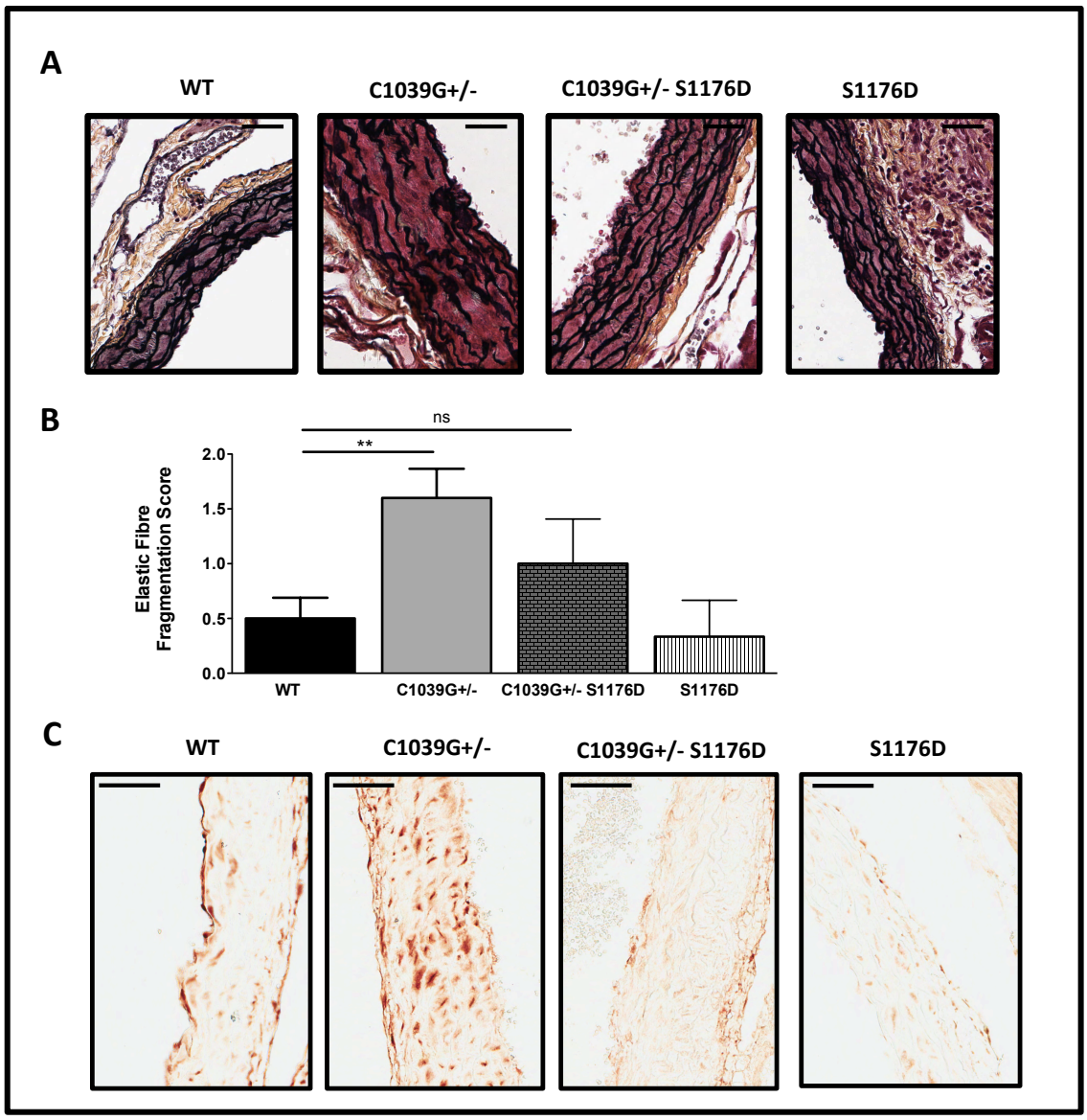

Figure 28: eNOS Ser-1176-Aps (S1176D) knock-in prevents MFS aortic root pathology. In addition to reduction in aortic aneurysm (Figure 25), analysis of aortic root pathology in C1039G$^{+/-}$ S1176D mice showed reduction in elastic fibre fragmentation to levels non-significantly different than control (WT n=8, C1039G$^{+/-}$ n=10, C1039G$^{+/-}$ S1176D n=4, S1176D n=3) (**A, B**) as scored by aortic root sections stained with Movat's pentachrome. Furthermore, reduction in phospho-ERK staining is seen in representative aortic root sections of C1039G$^{+/-}$ S1176D mice compared to C1039G$^{+/-}$ mice (**C**). Scale bar=100um, **p<0.01, ns= not significantly different.

Of note, upon dissection of hearts prior to embedding for histology, a gross size difference was noted in those containing an S1176D eNOS phospho-mutant knock-in. On one hand, this may simply be related to a preferential stage of the cardiac cycle arrest post-sacrifice. However, it may also reflect an overall difference in heart size that could potentially confound our finding of the benefit of eNOS phospho-mutant knock-in in MFS mice. Therefore, to address this possibility, hearts from S1176D and WT controls were evaluated for differences in weight and by four-chamber view echocardiograms to evaluate changes in ventricle size and cardiac function parameters. Analysis of weight revealed no difference between S1176D hearts and controls (Figure 29). In addition, no difference in left ventricle systolic or diastolic diameter (Figure 30A, B) or volume (Figure 30C, D) was observed. Furthermore, analysis of cardiac function showed no difference in cardiac output, ejection fraction, fractional shortening or stroke volume (Figure 30 E-H). Given these findings of similar cardiac parameters, in combination with similarity of WT and S1176D aortic root size and ascending aorta size (Figure 27A, B), this supports a conclusion that no confounding phenotype in the S1176D strain mediated the observed improvement in aortic diameter.

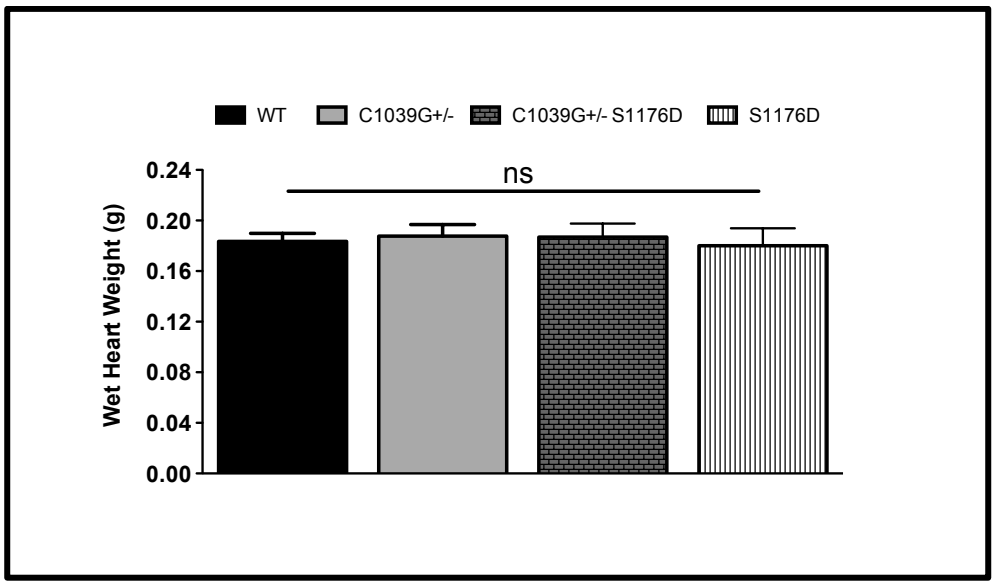

Figure 29: Heart weight does not differ between C1039G$^{+/-}$ S1176D mice and controls. Comparison of isolated and fixed heart weight in C1039G$^{+/-}$ S1176D mice and controls revealed no significant (ns) difference between any of the groups. Weights represent average wet weights ±SEM where WT n=7, C1039G$^{+/-}$ n=11, C1039G$^{+/-}$ S1176D n=13, and S1176D n=11.

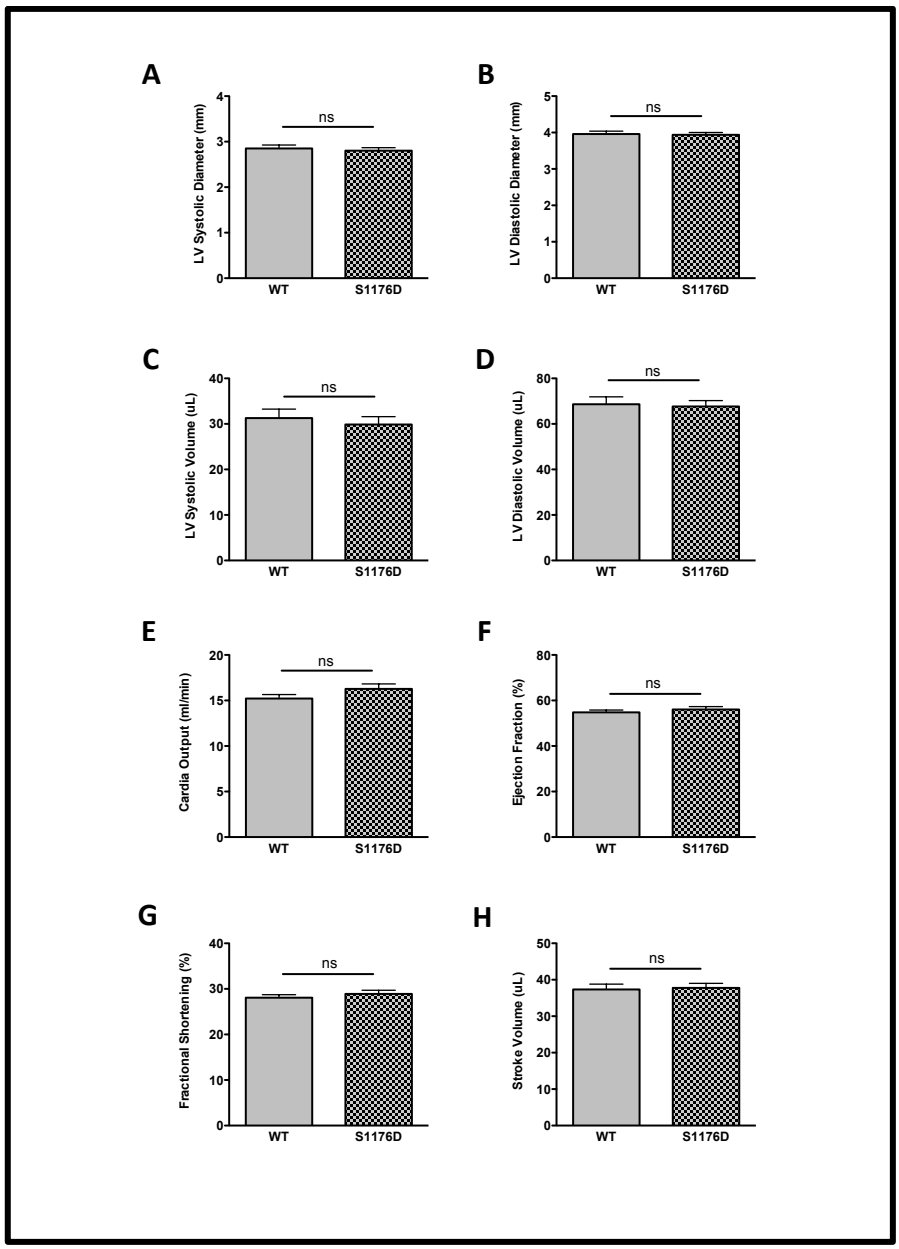

Figure 30: Echocardiogram analysis of cardiac parameters of S1176D mice.
Echocardiograms to determine left ventricle (LV) diameter in systole (**A**) and diastole (**B**) as well as LV volume in systole (**C**) and diastole (**D**) in WT and S1176D mice revealed no significant difference in ventricle size. Furthermore, no significant difference was seen between WT and S1176D mice in the cardiac parameters of cardiac output (**E**), ejection fraction (**F**), fractional shortening (**G**), or stroke volume (**H**). In all graphs WT n=5 and S1176D n=8 where ns= not significantly different and values represent groups averages ±SEM.

To support findings of the benefit of increased eNOS activity via an eNOS phospho-mutant knock-in MFS-associated aortic aneurysm, additional models of eNOS over-expression and NO production were evaluated. Specifically, C1039G$^{+/-}$ mice hemizygous for an eNOS transgene (eNOS Tg^{+}) were assessed. Echocardiogram analysis of aortic root diameter of these mice showed a significant reduction in aortic root diameter in C1039$^{+/-}$ eNOS Tg^{+} mice compared to C1039G$^{+/-}$ mice (Figure 31A). Furthermore, analysis of the survival of the first fifty experimental mice generated in this line showed that while approximately 20% of the C1039G$^{+/-}$ animals died, none of those expressing the eNOS transgene (C1039G$^{+/-}$ eNOS Tg^{+}) died (Figure 31B). Further, C1039G$^{+/-}$ mice treated with CavNOxin, a caveolin-1 peptide antagonist that mediates an increase in endogenous NO production as described above, showed a significant decrease in aortic root diameter (Figure 31C).

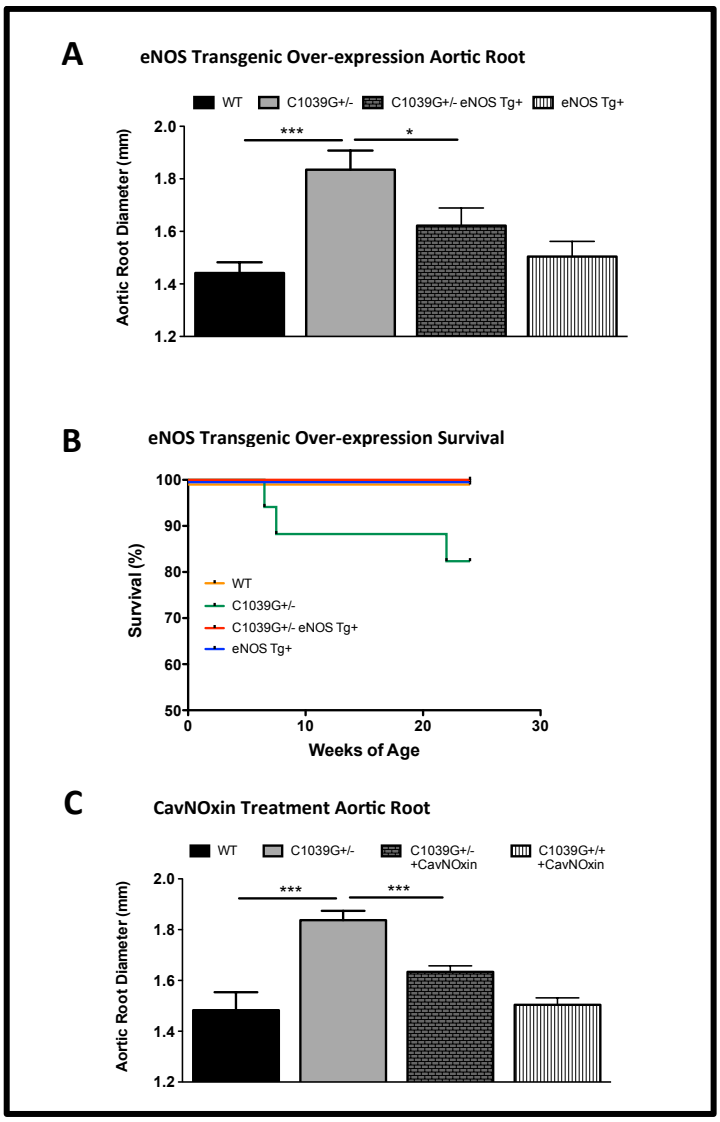

Figure 31: Expression of an eNOS transgene or treatment with CavNOxin reduces aortic root aneurysm in C1039G$^{+/-}$ mice.

Analysis of aortic root diameter at three months of age via echocardiograms by a blinded technician in C1039G$^{+/-}$ mice hemizygous for an eNOS trangene (C1039G$^{+/-}$ eNOS Tg^{+}) showed a significant reduction in aortic root diameter (**A**) where WT n=7, C1039G$^{+/-}$ n=10, C1039G$^{+/-}$ eNOS Tg^{+} n=7, eNOS Tg^{+} n=7. Analysis of survival within C1039G$^{+/-}$ eNOS Tg^{+} mice and littermate controls showed a trend towards increased survivability of C1039G$^{+/-}$ eNOS Tg^{+} over C1039G$^{+/-}$ mice (**B**). Treatment of C1039G$^{+/-}$ mice with CavNOxin also significantly reduced aortic root diameter at three months of age (**C**) where WT n=6, C1039G$^{+/-}$ n=9 C1039G$^{+/-}$ +CavNOxin n=8, C1039G$^{+/+}$ +CavNOxin n=6. Echocardiogram values mean diameter represent multiple measurements averaged per mouse taken in AM- and B-mode ±SEM. *p<0.05, ***p<0.001.

6.3.2 Evaluation of TGF-β Plasma Levels

To support our findings of the ability of models of increased NO levels to reduce MFS pathology, we attempted to evaluate active TGF-β levels. However, active TGF-β levels were not detected in either whole or platelet poor plasma using two different enzyme linked absorbent assays (Biolegend, Legend Max Free Active TGF-β1 ELISA Kit or R&D Biosystems Quantikine TGF- β1 ELISA Kit). This was in stark contrast to previous reports by the laboratory of Dr. H. Dietz who reported on circulating plasma level of TGF-β in the C1039G$^{+/-}$ mouse strain [103]. However, using the R&D Biosystems Quantikine TGF- β1 ELISA Kit, latent TGF-β was detectable in platelet poor plasma following activation and was assayed to compare plasma from WT, C1039G$^{+/-}$ and C1039G$^{+/-}$ S1176D mice. While a trend was suggested, no significant difference was found (Figure 32).

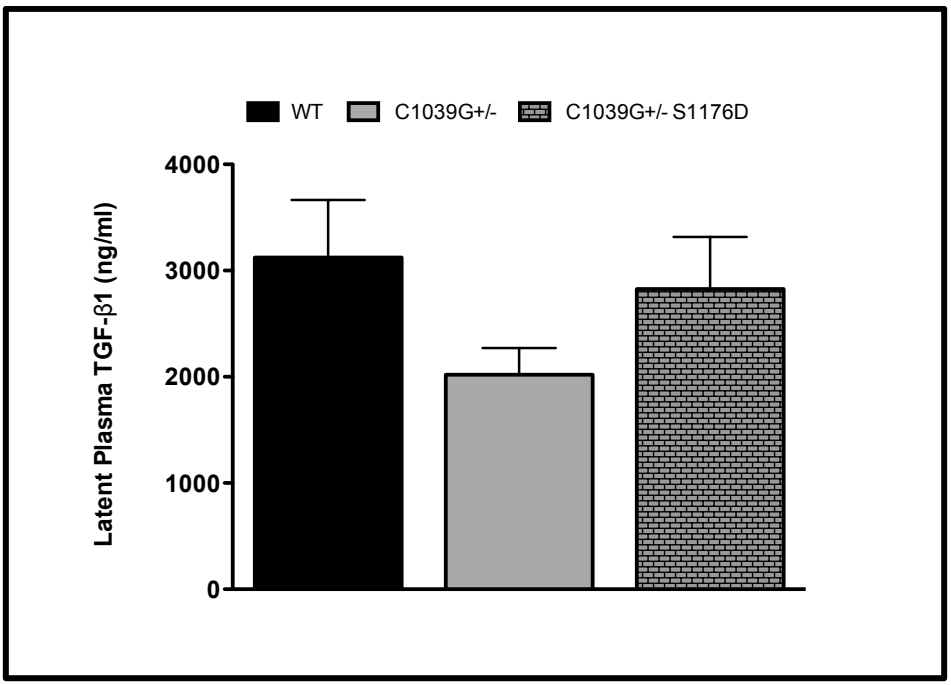

Figure 32: Circulating plasma levels of latent TGF-β levels in C1039G$^{+/-}$ S1176D mice. Comparison of latent plasma levels of TGF-β was completed by Quantikine (R&D Biosystems) ELISA for TGF-β on activated platelet poor plasma in WT, C1039G$^{+/-}$ and C1039G$^{+/-}$ S1176D mice. Values for each group represent mean ±SEM where values from each animal were determine from samples run in duplicate and n=8 for all groups. No significant difference was found between groups.

6.3.3 Evaluation of MFS Models with Reduced NOS Activity

To evaluate the converse model of the phospho-mimetic S1176D eNOS knock-in mouse, we also studied aortic root aneurysm in C1039G$^{+/-}$ 'phospho-dead' 1176 Ser-to-Ala (S1176A) eNOS knock-in mice (C1039G$^{+/-}$ S1176A) that exhibit a decreased level of eNOS activity [189]. Notably, C1039G$^{+/-}$ S1176A mice showed a trend towards increased aortic root diameter over C1039G$^{+/-}$ mice (Figure 33A) at six months of age. However, this did not reach significance ($p=0.09$) for the number of animals evaluated. In addition to this model of decreased eNOS activity, eNOS knockout mice (eNOS$^{-/-}$) were utilized to evaluate the effect of complete eNOS deficiency on C1039G$^{+/-}$ associated aortic root aneurysm. Unfortunately, this line of eNOS

deficient MFS mice (C1039G$^{+/-}$ eNOS$^{-/-}$) was very difficult to generate owing to low litter frequency and small litter sizes. In addition, of the mice that were produced, a much lower than anticipated number of C1039G$^{+/-}$ eNOS$^{-/-}$ mice were produced. As a result, only two animals were evaluated by echocardiogram and no conclusion regarding impact on aortic root aneurysm could be drawn (Figure 33B).

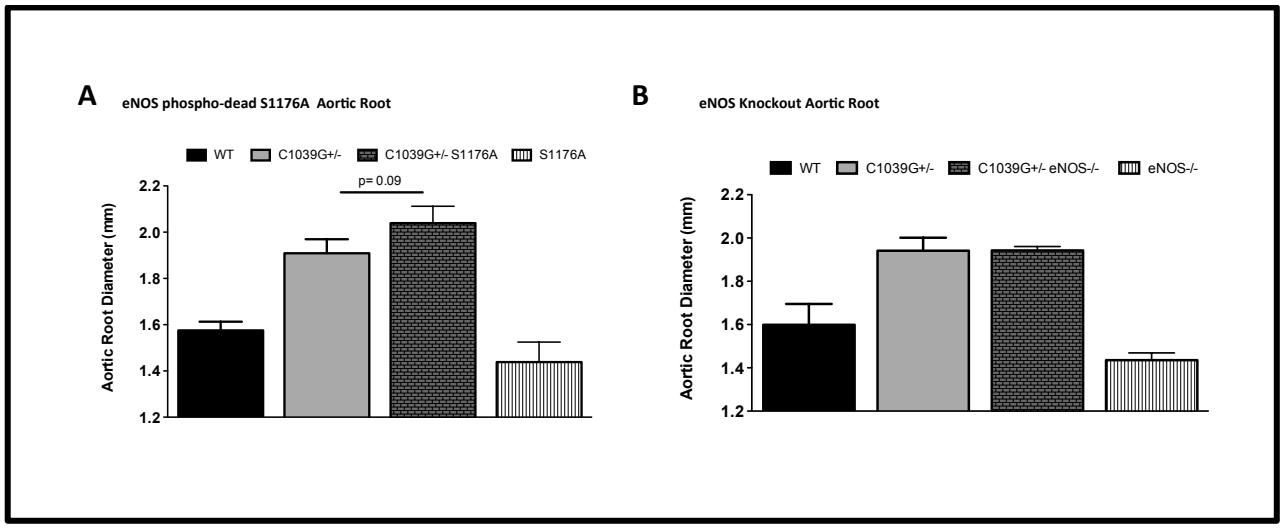

Figure 33: Impact of decreased eNOS activity and eNOS knockout on MFS aneurysm. Analysis of aortic root diameter was via echocardiogram was completed on MFS mice with decreased eNOS activity (C1039G$^{+/-}$ S1176A) and littermate controls (**A**) at six months of age, which showed no significant difference between groups. However, a trend toward significance was seen between C1039G$^{+/-}$ and C1039G$^{+/-}$ S1176A mice where WT n=9, C1039G$^{+/-}$ n=10, C1039G$^{+/-}$ S1176A n=9, and S1176 n=5. Subsequently, echocardiogram evaluation of MFS lacking eNOS expression (C1039G$^{+/-}$ eNOS$^{-/-}$) was completed at six months of age (**B**). However, owing to low animal numbers (WT n=5, C1039G$^{+/-}$ n=4, C1039G$^{+/-}$ eNOS n=2, eNOS$^{-/-}$ n=3) no conclusion regarding significance was drawn. For all groups (**A, B**) aortic root diameter values represent mean aortic diameter ±SEM where values for each animal studied were averaged from AM- and B-mode echocardiograms performed by a blinded technician.

6.4 Discussion

Overall, the data presented in this chapter identifies methods that increase NO to be of therapeutic benefit in reducing aortic aneurysm in the C1039G$^{+/-}$ strain of MFS mice. As our multi-faceted approach used models employing eNOS over-expression (eNOS transgenic model) and increased eNOS activity using both a genetic approach (S1176D knock-in model) and a pharmacological approach (CavNOxin treatment), we are able to conclude that eNOS-derived NO is therapeutic. While eNOS-specific effect of using an eNOS transgenic and eNOS S1176D approaches is apparent, we recently established the actions of CavNOxin to be eNOS-specific in the context of atherosclerosis. Specifically, CavNOxin was found to reduce atherosclerosis in high fat diet fed ApoE deficiency mice. However, use of ApoE deficient mice also deficient in eNOS rendered CavNOxin ineffective at preventing development of atherosclerosis [231]. Notably, the effectiveness of CavNOxin in this model was associated with a reduction in oxidative stress as demonstrated by decreased levels of superoxide, nitrotyrosine (NT) and lipid peroxidation. These are notable oxidative stress markers and levels of NT and 4-HNE (lipid peroxidation marker) would be a potential future use of additional paraffin slides cut at the level of aneurysm with in the aortic root of our MFS models. Yet, while we did not stain markers of oxidative stress in the aortic wall, we did attempt to evaluate levels of isoprostane, which is a marker of oxidative stress as isoprostanes result from the free-radical peroxidation of arachidonic acid [236, 237]. Unfortunately, our analysis of 8-isoprostane in the plasma of our mice was not successful and an alternative approach may be to repeat this analysis in future groups of animals using urine as we have previously reported the success of this assay [231]. In addition to histological markers of oxidative stress we have previously shown to be responsive to CavNOxin (superoxide, NT, 4-HNE)[231], other markers of oxidative stress shown to be elevated in MFS

could be an option such as total ROS and protein carbonyl content [129]. Moreover, given our previous findings of reduced NO in the plasma of MFS mice and the success of reducing aneurysm severity using models of eNOS over-expression and hyper-activation, a consideration of the role of ROS in the future is warranted. ROS may scavenge NO and result in the observed reduction of NO-availability and the benefit of increasing NO levels observed in our C1039G$^{+/-}$ S1176D and C1039G$^{+/-}$ eNOS Tg^{+} mice as well as in C1039G$^{+/-}$ mice treated with CavNOxin. This would also be consistent with findings demonstrating increased levels of oxidative stress markers in isolated C1039G$^{+/-}$ aortas [128]. If in fact increased ROS contributes to reduced NO and endothelial dysfunction in MFS, then investigating methods to reduce ROS may be additive to developing new therapeutic approaches in MFS. In addition, other markers of oxidative stress including 8-hydroxydeoxyguanosine (8-OHdG), the oxidation product of DNA, [238] have been shown to be elevated in models of aneurysm, albeit not MFS associated aneurysm, but reduction in expression levels also has been shown to correlate with reduced levels of MMP-2 and MMP-9 that are know to play a role in MFS pathology [239].

Given our success at reducing MFS aortic root diameter with CavNOxin, this presents the potential for exploring the therapeutic utility and continued development of small molecules designed to increase NO and/or attenuate oxidative stress [240]. Initially, the most obvious form of therapeutic to increased levels of NO is the use of NO donors and NO releasing drugs that increase levels of nitric oxide either requiring or directly releasing NO respectively [241, 242]. The most obvious of these is inhaled nitric oxide, although this has mostly been studied in the lungs and never been looked at in MFS [243]. Moreover, sodium nitroprusside has never been trialed in MFS but suffers from the disadvantage of creating a bolus of NO and thus has dynamics of administration to consider. Furthermore, toxicity and mutagenesis are drawbacks to

use [241, 244]. Organic nitrates and nitrite esters such as nitroglycerin, isosorbide dinitrate and nicorandil are another option in potential use for MFS but also have never been studied in this context. Moreover, this may have a severe drawback in MFS as these drugs are associated with AngII-induced superoxide levels through deregulation of eNOS, a factor that our data suggests may contribute to MFS pathology [245, 246]. In addition to NO donors and releasing agents, activators of soluble guanylate cyclase (sGC) act essentially activate the downstream normally stimulated by eNOS/NO signaling as they increased the activity of sGC that generates cyclic GMP. Although sGC activators have been studied in cardiovascular disease contexts including heart failure, their use has yet to be reported in MFS aneurysm or aneurysm pathology in general [247]. However, targeting of the downstream NO pathway, including the use of phosphodiesterase 5 inhibitors if discussed in the appendix below. Yet, eNOS transcription enhancers are another groups of drugs that could be used to increased NO levels in MFS; AVE9488 and AVE3085 that have been shown to increase eNOS levels and reduce atherosclerotic plaque burden in ApoE deficient mice in an eNOS-dependent manner [248]. Midostaurin, a PKC inhibitor, has also been shown to reduce atherosclerotic plaque in ApoE deficient mice via reduction of oxidative stress, and prevention of eNOS uncoupling, thereby increasing NO bio-availability and combating endothelial dysfunction [249]. Moreover, anti-oxidants such as those derived from fruits and plants like resveratrol and red wine extract, have been shown to increase expression of eNOS and production of NO [250] [251]. In fact, very recently, resveratrol was shown to reduce aortic aneurysm in C1039G$^{+/-}$ animals [252]. However, this was not linked to oxidative stress directly. Yet, red wine phenols have also been shown to block AngII induced MMP-2 activation; however this was also associated with a decline in eNOS and VEGF levels that resulted from AngII stimulation [253].

Similar to considering the use of small molecules to increase NO in MFS, as well as related to our studies of losartan and the benefit of increasing NO, Caymen Chemical now sells a version of losartan, NO-losartan A. This compound is designed to have both anti-hypertensive ATR1 blocking effects and vasodilatory effects mediated through NO production [254]. NO-losartan A is a compound based on the work of Breschi *et al.* in which NO-donor side chains (either m-nitrooxymethylbenzoate or 5-nitrooxypentanoate) were added to the structure of losartan [255] or its metabolites [256]. However, there are no reports of the use of NO-losartan A in MFS to date.

Despite the need to investigate ROS and NO interplay further in our model in the future, we did investigate the impact of increased NOS activity on TGF-β associated signaling and found reduction of phospho-ERK staining in the aortic wall of C1039G$^{+/-}$ S1176D mice. Increased activation/phosphorylation of ERK is mediated by TGF-β via signaling through Ras and Mek1 and ultimately leads to an increase in expression of components associated with MFS pathology including MMPs, TGF-β, connective tissue growth factor (which is associated with increased ECM deposition in the aortic wall) and thrombospondin-1 (which can increase activation of TGF-β) [257]. Therefore supporting the conclusion that reduction in phospho-ERK staining in MFS S1176D mice demonstrates an ability of NO to reduce MFS-associated pathological signaling.

A more global means of determining the impact of our models of increased NO on TGF-β was through analysis of plasma levels of TGF-β as these have been reported previously to be elevated in C1039G$^{+/-}$ animals [103]. Notably, while we attempted to assay levels of active TGF-β in plasma we were unsuccessful as we were not able to detect active TGF-β in plasma using two different approaches. Given the reported successful detection by Matt *et al.* this was

surprising but also slightly confusing [103]; the authors report use of the Quantikine TGF-β1 immuno-assay (R&D Systems, Minneapolis, Minn; catalog No. MB100M). However, this assay is not commercially available and in direct discussions with customer service representatives of the company, this product number and assay were never manufactured. Therefore, we were unable to repeat the experiment presented in Matt *et al*. and had to conclude we were unable to detect active TGF-β in plasma. However, we were able to detect levels of latent TGF-β in plasma post-acidic activation of samples in which active TGF-β was not detectable. While this demonstrates no significant difference between groups, it presents a trend towards decreased latent TGF-β in C1039G$^{+/-}$ mice versus WT ($p=0.08$). As Neptune *et al.* suggest that increased TGF-β in the MgΔ MFS model is the result of greater activation versus increased secretion and production of TGF-β, the lower levels of latent TGF-β in C1039G$^{+/-}$ may result from an increased level of activation [27]. However, this requires further study.

The development of models with reduced eNOS activity (MFS S1176A model) or loss of eNOS expression (MFS eNOS$^{-/-}$ mice) was hypothesized to be a means of studying exacerbation of aortic aneurysm in the C1039G$^{+/-}$ line. However, we did not observe a significant increase in aortic root aneurysm in C1039G$^{+/-}$ S1176A despite a trend towards significance. As C1039G$^{+/-}$ already show reduced production of NO and reduced phosphorylation of eNOS in the thoracic aorta, the inability to phosphorylate S1176 may not be sufficient to make a bad situation worse [127]. However, it may be of interest to utilize the S1176A model in the context of a more severe MFS model that has as reported early lethality to explore the consequence of the S1176A substitution on increasing incidence of mortality and shortened lifespan. Increased mortality, is actually suggested by our experience with C1039G$^{+/-}$ eNOS$^{-/-}$ mice; our inability to generate sufficient mice to study due to infrequent litter production, small litter size, and less than

expected C1039G$^{+/-}$ eNOS$^{-/-}$ mice based on Mendelian genetics is suggestive of an *in utero* or early post-natal lethality. While we did not formally study this, our overall inability to generate enough C1039G$^{+/-}$ eNOS$^{-/-}$ animals to comment on the effect of eNOS deficiency on aortic aneurysm (Figure 33B) speaks to an overall incurred detriment.

Despite being unable to draw a conclusion on the impact of eNOS knockout, the data presented in this chapter do outline a number of novel and important conclusions regarding NO in MFS pathology and treatment; our findings support the conclusion that drugs targeting endothelial dysfunction and increased production of NO are of benefit in preventing aortic aneurysm in MFS. Moreover increased eNOS activity resulted in a decrease in pathological markers within the aortic wall such as elastic fiber fragmentation and activation of TGF-β signaling through ERK. As such these findings support a focus on on-going development and testing of pharmaceutical approaches, such as CavNOxin, which can increase eNOS activity and NO levels in MFS.

Chapter 7: Summary Conclusions, Study Impact, and Future Directions

7.1 Overall Study Conclusions

Overall, the data presented address the overall aims set out for the study:

- Develop a novel model of MFS lacking ATR1 expression
- Determine the impact of loss of ATR1 expression on MFS pathological features including aortic root aneurysm, kyphosis, and airspace enlargement.
- Confirm the ATR1 specificity of losartan in MFS.
- Characterize lung airspace enlargement in models of MFS
- Evaluate lung function parameters in MFS

In fulfilling these aims, the presented studies effectively allow us to address our hypotheses that:

- A model of MFS lacking ATR1 expression would be protected from development of MFS aortic and lung pathology.
- As a MFS model deficient in ATR1 lacks the proposed target of losartan, losartan would have no therapeutic benefit in preventing aortic root aneurysm a model of MFS lacking ATR1.

Therefore, overall, the presented work provides a new understanding of the role of ATR1 and use of losartan in MFS, propose a new therapeutic mechanism and potential targets for treatment of MFS, and expands our knowledge regarding the phenotype of the C1039G$^{+/-}$ murine model. In doing so, this work moves the field forward towards a more comprehensive understanding of MFS and serves to direct future work. While evaluation of lung function and airspace enlargement is ongoing, the current state of this component of the study does show a number of interesting results that are detailed below.

7.1.1 ATR1 Independent MFS Pathology

By demonstrating that ATR1 does not play a role in development of MFS pathology in C1039G$^{+/-}$ mice, we have prompted discussion regarding the exact pathological mechanism driving MFS pathology. In an attempt to answer the question: "How much of MFS pathology is ATR1 dependent?" the studies conducted present the conclusion that none of the pathology we considered (aortic root aneurysm, emphysema-like lung destruction, kyphosis) is ATR1 dependent. While the work of the laboratory of Dr. H. Dietz presents the role of ATR1 in MFS through studies looking at losartan and in studies of the protective effects of ATR2 [44, 104], confirmation of the role of ATR1 through loss-of-function studies, such as the ones demonstrated herein, were never completed. Given the multi-system (cardiac, pulmonary, and skeletal) evidence provided here, our findings argue that reconsideration of the role of ATR1 is needed but also brings about the larger question of the use of ARBs in attempting to grapple with the best approach to treat MFS. Moreover, our data from MFS ATR1-deficient mice also support the conclusion that reasonable reduction in MAP has no benefit in MFS as the resulting decrease in blood pressure from ATR1 deficiency had no therapeutic benefit. This in turn, as discussed in more detail below, speaks to the potential of new trial designs in MFS in which drugs are selected and titrated to achieve a more significant reduction in blood pressure and optimize the potential for non-ATR1 dependent effects.

7.1.2 Off-target Effects of Losartan and Endothelial Function in MFS

The new mechanism proposed by our collective studies is shown in Figure 34 wherein ATR1 signaling does not impact MFS pathology and losartan is proposed to work through a VEGFR2 / NOS dependent mechanism. Furthermore, augmentation of NO using genetic

strategies (S1176D phospho-mutant, eNOS transgene) or pharmaceutical approaches (CavNOxin) acts to block MFS aneurysm. Overall, this is the first study to show losartan to act off-target in MFS and identifies clear pathways for future study and drug development via augmented NO production to improve endothelial function.

However, the utility of repeating these studies in other models of MFS is notable. Alternative models of MFS are representative of other phenotypes of MFS such as those outlined in Table 2 and may shed light on whether the off-target effects of losartan are specific to particular mutation types.

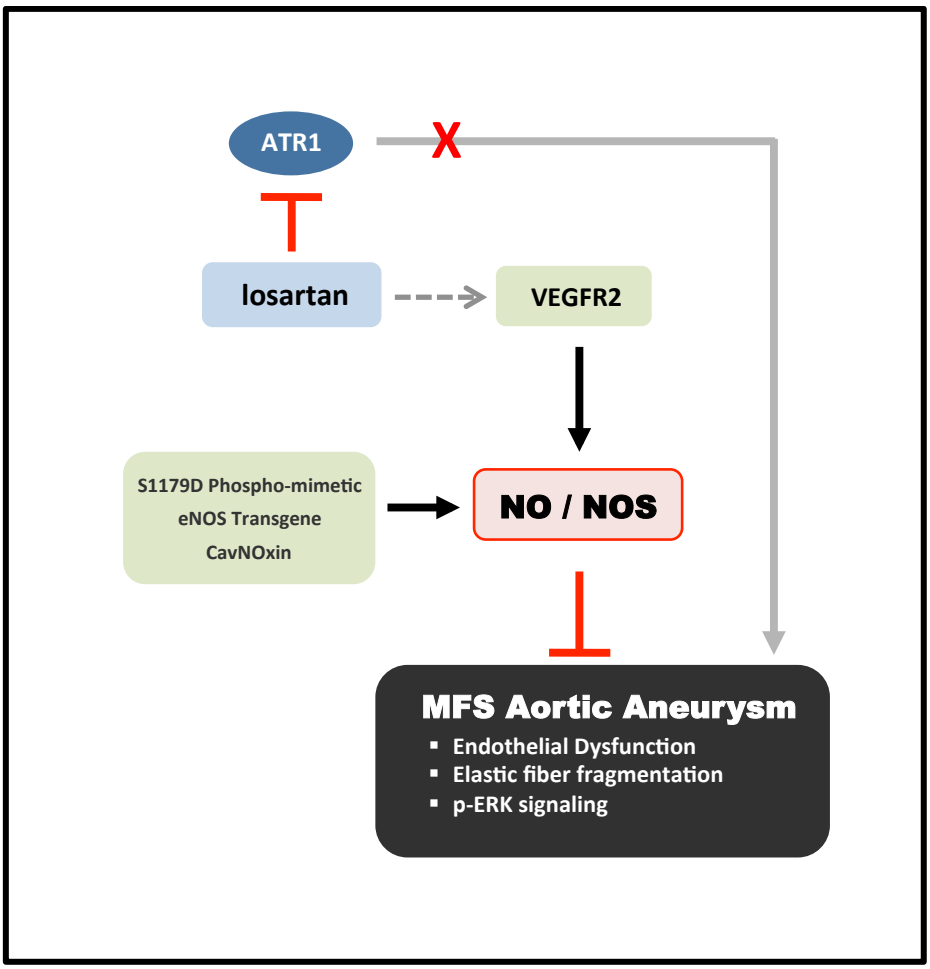

Figure 34: Schematic representation of study conclusions regarding the role of ATR1, off-target effects of losartan, and impact of NO and NOS signaling in C1039G$^{+/-}$ MFS mice. Conclusions from the presented study demonstrate a lack of effects of ATR1 in MFS pathology. Furthermore, losartan does not act through ATR1 but instead mediates inhibition of aortic aneurysm via a NOS-dependent mechanism governed upstream by VEGFR2. In addition, use of strategies to improve NO levels or NOS function in MFS using S1176D phosho-mimetic, eNOS transgene or CavNOxin successfully reduce aortic aneurysm signaling and pathology

7.1.3 Impact on the Current Management of MFS

Our data support the conclusion that moderate MAP lowering, such as that achieved with ARBs, is of questionable benefit in MFS. Since current gold-standard β-blocker (atenolol) therapy drastically reduces MAP, with appreciable clinical effect, our findings of the off-target effects of losartan justify studying atenolol in MFS in combination with losartan owing to

potential synergy. As large recent clinical trials fail to find a superiority of either losartan or atenolol and thereby stress the need for further improvement of MFS treatment paradigms over what either atenolol or losartan can provide, the potential combination of the two drugs is worth exploring and supported by our study [258, 259] [118, 162, 260]. In fact, during the course of our study, Chiu *et al.* demonstrated that the use of losartan in combination with a β-blocker was superior to use of β-blockers alone in slowing the rate of aortic root growth in pediatric MFS patients [161]. Yet, a subsequent study by Milleron *et al.* [162] found a non-significant effect on the rate of aneurysm growth from adding losartan to standard therapy was found by in an older group of patients. While, not significant, the rate of aneurysm progression was lower with in the losartan treated group. This may be because the synergy of losartan and atenolol is best mediated at early stages of disease in younger patients. This may also explain conflicting losartan clinical trial results using patients of variable ages, as age is a key modulator of endothelial function. Overall however, the mechanistic detail behind these results is unknown and supports continued study of the synergy between β-blocker and losartan therapy as proposed by our presented work.

Extrapolating our findings to MFS patients would make use of losartan in MFS the first example of a disease managed by specifically improving endothelial function, as the effects of losartan appear independent of blood pressure reduction. A number of techniques exist for evaluation of endothelial function. In the research laboratory setting this is classically evaluated using vaso-active profiling of intravital microscopy preparation of blood vessels or myography using isolated vessel setups or vessels rings on wire myographs. However, the translation of this into patient populations requires the addition of parameters assessing endothelial function in MFS clinical trials going forward. As detailed in our collaborators' recent trial [130] and our sub-stratification of their patient population (Appendix D), endothelial function can be measured

and analyzed a number of ways and points towards a recommendation for future trials to evaluate aspects such as pulse wave velocity, flow mediated dilation, and arterial stiffness. Moreover, MFS patients could benefit from studies correlating endothelial function using a EndoPAT system which as been shown to provide an indicator of endothelial function in a variety of studies including erectile dysfunction, pre-eclampsia, and diabetes and has the advantage of being a relatively quick, highly portable, non-invasive approach that requires less dedicated medical staff commitment [261-263]. Additionally, analysis using emerging technologies such as CT-based computational fluid dynamics to assess aortic wall dynamics with rate of disease progression may be of use in predicting risk and evaluating impact of treatment [264]. Blood-borne markers of endothelial function may also be a means of tracking endothelial function in MFS patients. Analyses of factors such as c-reactive protein, Von Willibrand factor, soluble adhesion molecule levels, and endothelial microparticles have all been proposed in setting of vascular disease and may serve well in the future investigation of MFS [265-267]

Regardless of how endothelial function is measured in future clinical trials, our findings stress the need for further clinical development of endothelial function-enhancing medications or approaches for MFS; increased endothelial function is linked to improved NO bioavailability, decreased inflammation, remodeling and oxidative stress. Notably, endothelial function improvements would promote homeostasis of aortic SMC layers as shown by our group [231] and supported by lower MFS severity in phospho-eNOS-mimetic mice (S1176D) presented in this study. Yet, development of new pharmaceuticals to specifically combat endothelial function and their translation into the clinic will require further study. However, repurposing of some current drugs may also be an avenue of investigation. For example, the use of the statin pravastatin, which acts by inhibiting HMG-CoA reductase to lower cholesterol and is

predominately used to combat cardiovascular disease associated with hypercholesterolemia, is a consideration; pravastatin has also been shown to reduce aortic root aneurysm in the C1039G MFS strain [268] [269]; McLoughlin *et al.* showed that treatment of C1039G$^{+/-}$ mice with 0.5g/L of pravastatin or 0.6g/L of losartan had similar reduction in aneurysm size in MFS mice compared to untreated controls. While the authors postulate this may be through a pleiotropic anti-inflammatory effect or results for a reduction in MMP levels, these factors have not been investigated. Notably, the authors do not consider the potential effect that pravastatin may be having on the endothelium. Statins have been shown to improve endothelial function through a number of mechanisms including increased expression of eNOS, increased production of NOS cofactors, stimulation of pathways including AKT leading to phosphorylation and thus enhanced activity of eNOS as well as reduction in ROS and suppression of inflammatory cytokines and activation of the endothelium [270-281].

As our data and previous clinical studies support the potential benefit of increasing NO/NOS signaling in MFS and an additive effect of losartan in combination with β-blockers has been reported, compounds which both lower blood pressure and increase NO may be ideal [161]. So-called "third generation" β-blockers represent such groups of compounds as those they act as β-adrenergic receptor antagonists with vasodilatory properties [176]. In fact, one such compound, nebivolol, is now part of a clinical trial of MFS, however data from this trial are not currently available [282]. Nebivolol acts as both a β1-blocker and mediates vasodilation in a NO-dependent manner as a consequent of increased eNOS activation by acting as a β3-receptor agonist [176, 282]. As such, nebivolol represents a potentially exciting new therapeutic direction, but has not been studied in MFS murine models.

7.2 Additional On-going Studies

The studies presented have a number of related concepts and avenues foe investigation. Many of these constitute on-going experiments in our research group. Below, we detail, in brief, the aims and preliminary results of some of these studies with data and study details given in the appendices. The completion of these studies will serve to further our understanding of MFS pathology, the function of NO in MFS, and pathology within the lung in MFS.

7.2.1 Pulmonary Pathology

The primary focus of MFS research remains on determining the mechanisms and potential treatment of aortic aneurysm and predicting risk of dissection. While this is valid given the life-threatening associated outcomes or aortic aneurysm, there is great interplay between the pulmonary and cardiovascular systems that warrants consideration of the impact of pulmonary pathology on cardiovascular pathology in the overall evaluation of MFS. For example, it was recently demonstrated that the presence of lung inflammation caused an increase in aneurysm severity in murine models of AngII or calcium chloride induced abdominal aortic aneurysm [283] and many factors of lung inflammation are thought to contribute to facets of cardiovascular disease as recently reviewed by members of our research group [284]. In addition to the interplay between lung and cardiovascular disease, a greater focus needs to be put on systemic manifestations of MFS outside the aorta. As our ability to identify, treat, and support patients with MFS increases, so does life expectancy. This in turn brings about the potential that less studied systemic features of MFS, such as pulmonary pathology, will become of increasing clinical significance, impact quality of life, and complicate care.

Losartan is also currently being evaluated for the treatment of chronic obstructive pulmonary disease in humans. This trial is based on the work of Podowski *et al.* in which the authors demonstrated increased levels of TGF-β in mice exposed to cigarette smoke and in patients with COPD. Subsequently, the authors outlined the ability of both neutralizing TGF-β antibody or losartan to prevent inflammation, reduce oxidative stress markers, and prevent airspace enlargement and decline in lung function in a mouse model of smoke induced lung injury [285]. Although the results of the human trials of losartan in COPD are not yet published, they were recently presented at the 2015 CHEST Annual Meeting and showed a 0.32% regression of emphysema extent in losartan treated patients versus a 2.18% progression in patients receiving placebo over the course of one year ($p=0.064$) with studies currently ongoing [286]. Notably, other ARBs have also shown utility in the treatment of emphysema; irbesartan was shown to reduce airspace enlargement and improved lung function and running distance in a mouse model of elatase-induced emphysema [287]. Therefore, given the relatively little knowledge we have regarding pulmonary MFS pathology relative to that of aortic pathology, and to explore the role of losartan in NO in MFS pulmonary pathology, studies are ongoing in our laboratory to provide a more comprehensive understanding of MFS pulmonary disease. These studies focus on aneurysm of the pulmonary artery, altered lung function in MFS, and evaluation of the utility of using losartan to improve lung function and airspace enlargement in MFS (Appendix D). As a component of these studies we also present the evaluation of the use of sildenafil, most commonly known and marketed as Viagra, which is an inhibitor of phospho-diesterase 5 (PDE5). While the use of sildenafil is most famous for the treatment of erectile dysfunction, PDE5 inhibitors are also considered an option for treatment of pulmonary hypertension [288] including that associated with COPD [230]. Moreover, sildenafil is also

effective at preventing smoke induced injury in lungs of animal smoking models [289, 290]. Therefore, we are currently continuing to evaluate the impact of sildenafil on pulmonary and aortic aneurysm, airspace enlargement and lung function in the MFS C1039G strain.

7.2.2 Coronary Artery Dissection

During evaluation of histology of the aortic root throughout our study, serial sections were sectioned, stained, and reviewed at 50μm intervals from below the aortic valve throughout the aortic root to obtain the desired section for scoring of elastic fibers in the sinus of Valsalva. As a result of this thorough and sequential protocol, sections of the coronary ostia were observed. Interestingly, a notable rate of mild to severe dissection was found in many slides. Upon breaking of the code used to blind samples to those evaluating the sections, we observed that dissection was predominately a feature of C1039G$^{+/-}$ MFS mice. Subsequently, we are continuing to study the rate of coronary dissection and evaluating the effect of losartan treatment, ATR1 deficiency, and impact of additional gene manipulation (eNOS S1176D and eNOS transgenic mice) on the rate and severity of dissection. Preliminary data and on-going study details are given in Appendix E.

7.3 Final Thoughts

The evolution of our understanding of MFS has grown significantly in the last 20 years. The field has identified the causative gene mutation associated with MFS, provided comprehensive phenotypic studies, improved on its ability to diagnose and manage patients, and developed many *in vitro* and *in vivo* models to study MFS. Despite this, the field is still in search of a means to drastically improve MFS pathology, reduce patient risk, and mitigate the need for

surgical intervention. Much hope was placed on the use of losartan, but recent clinical trials have had less success than expected and failed to show superiority over previous approaches. This has stirred up much controversy regarding the pursuit of ATR1 blockade and targeting of TGF-β signalling in MFS. The studies presented in this thesis address key questions in this controversy by shedding new light on the role of ATR1 in MFS and in identifying losartan to act off-target in treating MFS aortic aneurysm. Finally, we clearly demonstrate the NOS-dependent function of losartan as well as the potential of targeting NO, and by association endothelial function, in MFS. As such, these findings both further our understanding of MFS pathology as well as provide novel points for consideration in future studies of MFS.

Bibliography

1. Hecht, F. and R.K. Beals, *Hecht F, Beals RK "New" syndrome of congenital contractural arachnodactyly originally described by Marfan i n 1896. Pediatrics 49:574-579. .* Pediatrics, 1972. **49**: p. 574-579.

2. Marfan, A.B., *Un cas de déformation congénitale des quartre membres, plus prononcée aux extrémitiés, caractérisée par l'allongement des os avec un certain degré d'amincissement".* Bulletins et memoires de la Société medicale des hôspitaux de Paris, 1896. **13**(3rd Series): p. 220-226.

3. Pyeritz, R.E. and V.A. McKusick, *The Marfan syndrome: diagnosis and management.* N Engl J Med, 1979. **300**(14): p. 772-7.

4. Pyeritz, R.E. and V.A. McKusick, *Basic defects in Marfan syndrome.* N Engl J Med, 1981. **305**(17): p. 1011-2.

5. Judge, D.P. and H.C. Dietz, *Marfan's syndrome.* Lancet, 2005. **366**(9501): p. 1965-76.

6. Sakai, L.Y., D.R. Keene, and E. Engvall, *Fibrillin, a new 350-kD glycoprotein, is a component of extracellular microfibrils.* J Cell Biol, 1986. **103**(6 Pt 1): p. 2499-509.

7. Sakai, L.Y., et al., *Purification and partial characterization of fibrillin, a cysteine-rich structural component of connective tissue microfibrils.* J Biol Chem, 1991. **266**(22): p. 14763-70.

8. Keene, D.R., et al., *Extraction of extendable beaded structures and their identification as fibrillin-containing extracellular matrix microfibrils.* J Histochem Cytochem, 1991. **39**(4): p. 441-9.

9. Ramirez, F. and H.C. Dietz, *Fibrillin-rich microfibrils: Structural determinants of morphogenetic and homeostatic events.* J Cell Physiol, 2007. **213**(2): p. 326-30.

10. Handford, P.A., et al., *Fibrillin: from domain structure to supramolecular assembly.* Matrix Biol, 2000. **19**(6): p. 457-70.

11. Reinhardt, D.P., et al., *Fibrillin-1: organization in microfibrils and structural properties.* J Mol Biol, 1996. **258**(1): p. 104-16.

12. Mariko, B., et al., *Microfibrils and fibrillin-1 induce integrin-mediated signaling, proliferation and migration in human endothelial cells.* Am J Physiol Cell Physiol, 2010. **299**(5): p. C977-87.

13. Hollister, D.W., et al., *Immunohistologic abnormalities of the microfibrillar-fiber system in the Marfan syndrome.* N Engl J Med, 1990. **323**(3): p. 152-9.

14. Schaefer, G.B. and M. Godfrey, *Quantitation of fibrillin immunofluorescence in fibroblast cultures in the Marfan syndrome.* Clin Genet, 1995. **47**(3): p. 144-9.

15. Milewicz, D.M., et al., *Marfan syndrome: defective synthesis, secretion, and extracellular matrix formation of fibrillin by cultured dermal fibroblasts.* J Clin Invest, 1992. **89**(1): p. 79-86.

16. Kainulainen, K., et al., *Location on chromosome 15 of the gene defect causing Marfan syndrome.* N Engl J Med, 1990. **323**(14): p. 935-9.

17. Dietz, H.C., et al., *The Marfan syndrome locus: confirmation of assignment to chromosome 15 and identification of tightly linked markers at 15q15-q21.3.* Genomics, 1991. **9**(2): p. 355-61.

18. Tsipouras, P., et al., *Marfan syndrome is closely linked to a marker on chromosome 15q1.5----q2.1.* Proc Natl Acad Sci U S A, 1991. **88**(10): p. 4486-8.

19. Dietz, H.C., et al., *Marfan syndrome caused by a recurrent de novo missense mutation in the fibrillin gene.* Nature, 1991. **352**(6333): p. 337-9.

20. Burchett, M.E., I.F. Ling, and S. Estus, *FBN1 isoform expression varies in a tissue and development-specific fashion.* Biochem Biophys Res Commun, 2011. **411**(2): p. 323-8.

21. Schrijver, I., et al., *Cysteine substitutions in epidermal growth factor-like domains of fibrillin-1: distinct effects on biochemical and clinical phenotypes.* Am J Hum Genet, 1999. **65**(4): p. 1007-20.

22. Zhang, H., et al., *Structure and expression of fibrillin-2, a novel microfibrillar component preferentially located in elastic matrices.* J Cell Biol, 1994. **124**(5): p. 855-63.

23. Carta, L., et al., *Fibrillins 1 and 2 perform partially overlapping functions during aortic development.* J Biol Chem, 2006. **281**(12): p. 8016-23.

24. Hafko, R., et al., *Commercially available angiotensin II At(2) receptor antibodies are nonspecific.* PLoS One, 2013. **8**(7): p. e69234.

25. Isogai, Z., et al., *Latent transforming growth factor beta-binding protein 1 interacts with fibrillin and is a microfibril-associated protein.* J Biol Chem, 2003. **278**(4): p. 2750-7.

26. Judge, D.P., et al., *Evidence for a critical contribution of haploinsufficiency in the complex pathogenesis of Marfan syndrome.* J Clin Invest, 2004. **114**(2): p. 172-81.

27. Neptune, E.R., et al., *Dysregulation of TGF-beta activation contributes to pathogenesis in Marfan syndrome.* Nat Genet, 2003. **33**(3): p. 407-11.

28. Foundation, T.M. *Calculatin of Systemic Score*. 2014 [cited 2016 Aug 26, 2016]; Available from: https://www.marfan.org/dx/score.

29. Beighton, P., et al., *International Nosology of Heritable Disorders of Connective Tissue, Berlin, 1986.* Am J Med Genet, 1988. **29**(3): p. 581-94.

30. De Paepe, A., et al., *Revised diagnostic criteria for the Marfan syndrome.* Am J Med Genet, 1996. **62**(4): p. 417-26.

31. Loeys, B.L., et al., *The revised Ghent nosology for the Marfan syndrome.* J Med Genet, 2010. **47**(7): p. 476-85.

32. Colan, S.D., et al., *Validation and re-evaluation of a discriminant model predicting anatomic suitability for biventricular repair in neonates with aortic stenosis.* J Am Coll Cardiol, 2006. **47**(9): p. 1858-65.

33. Devereux, R.B., et al., *Normal limits in relation to age, body size and gender of two-dimensional echocardiographic aortic root dimensions in persons >/=15 years of age.* Am J Cardiol, 2012. **110**(8): p. 1189-94.

34. Chubb, H. and J.M. Simpson, *The use of Z-scores in paediatric cardiology.* Ann Pediatr Cardiol, 2012. **5**(2): p. 179-84.

35. Awais, M., et al., *Aneurysms of medium-sized arteries in Marfan syndrome.* Ann Vasc Surg, 2013. **27**(8): p. 1188.e5-7.

36. Yoshida Rde, A., et al., *Modified "stent-graft sandwich" technique for treatment of isolated common iliac artery aneurysm in patient with Marfan syndrome.* Ann Vasc Surg, 2012. **26**(3): p. 419.e7-9.

37. Yoshida Rde, A., et al., *Retrograde endovascular treatment of internal iliac aneurysm in a patient with Marfan syndrome.* Vascular, 2010. **18**(4): p. 235-41.

38. Flanagan, P.V., J. Geoghegan, and T.J. Egan, *Iliac artery aneurysm in Marfan's syndrome.* Eur J Vasc Surg, 1990. **4**(3): p. 323-4.

39. Morisaki, K., et al., *Subclavian artery aneurysm in Marfan syndrome.* Ann Vasc Surg, 2012. **26**(5): p. 731.e1-4.

40. Mariucci, E.M., et al., *Dilation of peripheral vessels in Marfan syndrome: importance of thoracoabdominal MR angiography.* Int J Cardiol, 2013. **167**(6): p. 2928-31.

41. Veldhoen, S., et al., *Exact monitoring of aortic diameters in Marfan patients without gadolinium contrast: intraindividual comparison of 2D SSFP imaging with 3D CE-MRA and echocardiography.* Eur Radiol, 2015. **25**(3): p. 872-82.

42. Canadas, V., et al., *Marfan syndrome. Part 2: treatment and management of patients.* Nat Rev Cardiol, 2010. **7**(5): p. 266-76.

43. Okamura, H., et al., *Assessment of elastin deficit in a Marfan mouse aneurysm model using an elastin-specific magnetic resonance imaging contrast agent.* Circ Cardiovasc Imaging, 2014. **7**(4): p. 690-6.

44. Habashi, J.P., et al., *Angiotensin II type 2 receptor signaling attenuates aortic aneurysm in mice through ERK antagonism.* Science, 2011. **332**(6027): p. 361-5.

45. Holm, T.M., et al., *Noncanonical TGFbeta signaling contributes to aortic aneurysm progression in Marfan syndrome mice.* Science, 2011. **332**(6027): p. 358-61.

46. Merk, D.R., et al., *miR-29b participates in early aneurysm development in Marfan syndrome.* Circ Res, 2012. **110**(2): p. 312-24.

47. Segura, A.M., et al., *Immunohistochemistry of matrix metalloproteinases and their inhibitors in thoracic aortic aneurysms and aortic valves of patients with Marfan's syndrome.* Circulation, 1998. **98**(19 Suppl): p. II331-7; discussion II337-8.

48. Ikonomidis, J.S., et al., *Expression of matrix metalloproteinases and endogenous inhibitors within ascending aortic aneurysms of patients with Marfan syndrome.* Circulation, 2006. **114**(1 Suppl): p. I365-70.

49. Xiong, W., et al., *Doxycycline delays aneurysm rupture in a mouse model of Marfan syndrome.* J Vasc Surg, 2008. **47**(1): p. 166-72; discussion 172.

50. Chung, A.W., et al., *Long-term doxycycline is more effective than atenolol to prevent thoracic aortic aneurysm in marfan syndrome through the inhibition of matrix metalloproteinase-2 and -9.* Circ Res, 2008. **102**(8): p. e73-85.

51. Yang, H.H., et al., *Long-term effects of losartan on structure and function of the thoracic aorta in a mouse model of Marfan syndrome.* Br J Pharmacol, 2009. **158**(6): p. 1503-12.

52. Guo, G., et al., *Indomethacin Prevents the Progression of Thoracic Aortic Aneurysm in Marfan Syndrome Mice.* Aorta (Stamford), 2013. **1**(1): p. 5-12.

53. Xiong, W., et al., *MMP-2 regulates Erk1/2 phosphorylation and aortic dilatation in Marfan syndrome.* Circ Res, 2012. **110**(12): p. e92-e101.

54. Cui, J.Z., et al., *Quantification of aortic and cutaneous elastin and collagen morphology in Marfan syndrome by multiphoton microscopy.* J Struct Biol, 2014. **187**(3): p. 242-53.

55. He, R., et al., *Characterization of the inflammatory cells in ascending thoracic aortic aneurysms in patients with Marfan syndrome, familial thoracic aortic aneurysms, and sporadic aneurysms.* J Thorac Cardiovasc Surg, 2008. **136**(4): p. 922-9, 929.e1.

56. Ju, X., et al., *IL-6 regulates extracellular matrix remodeling associated with aortic dilation in a fibrillin-1 hypomorphic mgR/mgR mouse model of severe Marfan syndrome.* J Am Heart Assoc, 2014. **3**(1): p. e000476.

57. Ng, C.M., et al., *TGF-beta-dependent pathogenesis of mitral valve prolapse in a mouse model of Marfan syndrome.* J Clin Invest, 2004. **114**(11): p. 1586-92.

58. Fuzellier, J.F., et al., *Surgical management of mitral regurgitation associated with Marfan's syndrome.* Ann Thorac Surg, 1998. **66**(1): p. 68-72.

59. Brown, O.R., et al., *Aortic root dilatation and mitral valve prolapse in Marfan's syndrome: an ECHOCARDIOgraphic study.* Circulation, 1975. **52**(4): p. 651-7.

60. Geirsson, A., et al., *Modulation of transforming growth factor-beta signaling and extracellular matrix production in myxomatous mitral valves by angiotensin II receptor blockers.* Circulation, 2012. **126**(11 Suppl 1): p. S189-97.

61. Kielty, C.M., et al., *Marfan syndrome: fibrillin expression and microfibrillar abnormalities in a family with predominant ocular defects.* J Med Genet, 1995. **32**(1): p. 1-6.

62. Nahum, Y. and A. Spierer, *Ocular features of Marfan syndrome: diagnosis and management.* Isr Med Assoc J, 2008. **10**(3): p. 179-81.

63. Nemet, A.Y., et al., *Current concepts of ocular manifestations in Marfan syndrome.* Surv Ophthalmol, 2006. **51**(6): p. 561-75.

64. Dominguez, R., R.A. Weisgrau, and M. Santamaria, *Pulmonary hyperinflation and emphysema in infants with the Marfan syndrome.* Pediatr Radiol, 1987. **17**(5): p. 365-9.

65. Bolande, R.P. and A.S. Tucker, *PULMONARY EMPHYSEMA AND OTHER CARDIORESPIRATORY LESIONS AS PART OF THE MARFAN ABIOTROPHY.* Pediatrics, 1964. **33**: p. 356-66.

66. Dwyer, E.M., Jr. and F. Troncale, *SPONTANEOUS PNEUMOTHORAX AND PULMONARY DISEASE IN THE MARFAN SYNDROME. REPORT OF TWO CASES AND REVIEW OF THE LITERATURE.* Ann Intern Med, 1965. **62**: p. 1285-92.

67. Wood, J.R., et al., *Pulmonary disease in patients with Marfan syndrome.* Thorax, 1984. **39**(10): p. 780-4.

68. Hall, J.R., et al., *Pneumothorax in the Marfan syndrome: prevalence and therapy.* Ann Thorac Surg, 1984. **37**(6): p. 500-4.

69. Karpman, C., G.L. Aughenbaugh, and J.H. Ryu, *Pneumothorax and bullae in Marfan syndrome.* Respiration, 2011. **82**(3): p. 219-24.

70. Tanoue, L.T., *Pulmonary involvement in collagen vascular disease: a review of the pulmonary manifestations of the Marfan syndrome, ankylosing spondylitis, Sjogren's syndrome, and relapsing polychondritis.* J Thorac Imaging, 1992. **7**(2): p. 62-77.

71. Reye, R.D. and P.M. Bale, *Elastic tissue in pulmonary emphysema in Marfan syndrome.* Arch Pathol, 1973. **96**(6): p. 427-31.

72. Lipton, R.A., R.A. Greenwald, and N.S. Seriff, *Pneumothorax and bilateral honeycombed lung in Marfan syndrome. Report of a case and review of the pulmonary abnormalities in this disorder.* Am Rev Respir Dis, 1971. **104**(6): p. 924-8.

73. Chisholm, J.C., N.S. Cherniack, and R.W. Carton, *Results of pulmonary function testing in 5 persons with the Marfan syndrome.* J Lab Clin Med, 1968. **71**(1): p. 25-8.

74. Fuleihan, F.J., S.K. Suh, and R.H. Shepard, *SOME ASPECTS OF PULMONARY FUNCTION IN THE MARFAN SYNDROME.* Bull Johns Hopkins Hosp, 1963. **113**: p. 320-9.

75. Streeten, E.A., E.A. Murphy, and R.E. Pyeritz, *Pulmonary function in the Marfan syndrome.* Chest, 1987. **91**(3): p. 408-12.

76. Cipriano, G.F., et al., *Safety and cardiovascular behavior during pulmonary function in patients with Marfan syndrome.* Clin Genet, 2010. **78**(1): p. 57-65.

77. Corsico, A.G., et al., *Pulmonary involvement in patients with Marfan Syndrome.* Panminerva Med, 2014. **56**(2): p. 177-82.

78. Giske, L., et al., *Pulmonary function, working capacity and strength in young adults with Marfan syndrome.* J Rehabil Med, 2003. **35**(5): p. 221-8.

79. Dyhdalo, K. and C. Farver, *Pulmonary histologic changes in Marfan syndrome: a case series and literature review.* Am J Clin Pathol, 2011. **136**(6): p. 857-63.

80. Lee, J.J., et al., *Losartan Attenuates Degradation of Aorta and Lung Tissue Micromechanics in a Mouse Model of Severe Marfan Syndrome.* Ann Biomed Eng, 2016.

81. da Palma, R.K., et al., *Increased upper airway collapsibility in a mouse model of Marfan syndrome.* Respir Physiol Neurobiol, 2015. **207**: p. 58-60.

82. Cistulli, P.A. and C.E. Sullivan, *Sleep apnea in Marfan's syndrome. Increased upper airway collapsibility during sleep.* Chest, 1995. **108**(3): p. 631-5.

83. Loeys, B.L., G. Mortier, and H.C. Dietz, *Bone lessons from Marfan syndrome and related disorders: fibrillin, TGF-B and BMP at the balance of too long and too short.* Pediatr Endocrinol Rev, 2013. **10 Suppl 2**: p. 417-23.

84. Smaldone, S. and F. Ramirez, *Fibrillin microfibrils in bone physiology.* Matrix Biol, 2016. **52-54**: p. 191-7.

85. Ramirez, F. and D.B. Rifkin, *Extracellular microfibrils: contextual platforms for TGFbeta and BMP signaling.* Curr Opin Cell Biol, 2009. **21**(5): p. 616-22.

86. Kohlmeier, L., C. Gasner, and R. Marcus, *Bone mineral status of women with Marfan syndrome.* Am J Med, 1993. **95**(6): p. 568-72.

87. Kohlmeier, L., et al., *The bone mineral status of patients with Marfan syndrome.* J Bone Miner Res, 1995. **10**(10): p. 1550-5.

88. Gray, J.R., et al., *Osteoporosis and the Marfan syndrome.* Postgrad Med J, 1993. **69**(811): p. 373-5.

89. Tobias, J.H., N. Dalzell, and A.H. Child, *Assessment of bone mineral density in women with Marfan syndrome.* Br J Rheumatol, 1995. **34**(6): p. 516-9.

90. Kanis, J.A., et al., *Risk of hip fracture according to the World Health Organization criteria for osteopenia and osteoporosis.* Bone, 2000. **27**(5): p. 585-90.

91. Nistala, H., et al., *Differential effects of alendronate and losartan therapy on osteopenia and aortic aneurysm in mice with severe Marfan syndrome.* Hum Mol Genet, 2010. **19**(24): p. 4790-8.

92. Percheron, G., et al., *Muscle strength and body composition in adult women with Marfan syndrome.* Rheumatology (Oxford), 2007. **46**(6): p. 957-62.

93. Cohn, R.D., et al., *Angiotensin II type 1 receptor blockade attenuates TGF-beta-induced failure of muscle regeneration in multiple myopathic states.* Nat Med, 2007. **13**(2): p. 204-10.

94. Haine, E., et al., *Muscle and Bone Impairment in Children With Marfan Syndrome: Correlation With Age and FBN1 Genotype.* J Bone Miner Res, 2015. **30**(8): p. 1369-76.

95. Annes, J.P., J.S. Munger, and D.B. Rifkin, *Making sense of latent TGFbeta activation.* J Cell Sci, 2003. **116**(Pt 2): p. 217-24.

96. Koli, K., et al., *Latency, activation, and binding proteins of TGF-beta.* Microsc Res Tech, 2001. **52**(4): p. 354-62.

97. Munger, J.S., et al., *Latent transforming growth factor-beta: structural features and mechanisms of activation.* Kidney Int, 1997. **51**(5): p. 1376-82.

98. Ribeiro, S.M., et al., *The activation sequence of thrombospondin-1 interacts with the latency-associated peptide to regulate activation of latent transforming growth factor-beta.* J Biol Chem, 1999. **274**(19): p. 13586-93.

99. Yu, Q. and I. Stamenkovic, *Cell surface-localized matrix metalloproteinase-9 proteolytically activates TGF-beta and promotes tumor invasion and angiogenesis.* Genes Dev, 2000. **14**(2): p. 163-76.

100. Ailawadi, G., J.L. Eliason, and G.R. Upchurch, Jr., *Current concepts in the pathogenesis of abdominal aortic aneurysm.* J Vasc Surg, 2003. **38**(3): p. 584-8.

101. Wang, Y., et al., *TGF-beta activity protects against inflammatory aortic aneurysm progression and complications in angiotensin II-infused mice.* J Clin Invest, 2010. **120**(2): p. 422-32.

102. Dai, J., et al., *Overexpression of transforming growth factor-beta1 stabilizes already-formed aortic aneurysms: a first approach to induction of functional healing by endovascular gene therapy.* Circulation, 2005. **112**(7): p. 1008-15.

103. Matt, P., et al., *Circulating transforming growth factor-beta in Marfan syndrome.* Circulation, 2009. **120**(6): p. 526-32.

104. Habashi, J.P., et al., *Losartan, an AT1 antagonist, prevents aortic aneurysm in a mouse model of Marfan syndrome.* Science, 2006. **312**(5770): p. 117-21.

105. Lindsay, M.E. and H.C. Dietz, *Lessons on the pathogenesis of aneurysm from heritable conditions.* Nature, 2011. **473**(7347): p. 308-16.

106. Mori, T., et al., *Role and interaction of connective tissue growth factor with transforming growth factor-beta in persistent fibrosis: A mouse fibrosis model.* J Cell Physiol, 1999. **181**(1): p. 153-9.

107. Radonic, T., et al., *Inflammation aggravates disease severity in Marfan syndrome patients.* PLoS One, 2012. **7**(3): p. e32963.

108. Schultz-Cherry, S. and J.E. Murphy-Ullrich, *Thrombospondin causes activation of latent transforming growth factor-beta secreted by endothelial cells by a novel mechanism.* J Cell Biol, 1993. **122**(4): p. 923-32.

109. Konishi, H., et al., *Novel subtype of human angiotensin II type 1 receptor: cDNA cloning and expression.* Biochem Biophys Res Commun, 1994. **199**(2): p. 467-74.

110. de Gasparo, M., et al., *International union of pharmacology. XXIII. The angiotensin II receptors.* Pharmacol Rev, 2000. **52**(3): p. 415-72.

111. Oliverio, M.I., et al., *Reduced growth, abnormal kidney structure, and type 2 (AT2) angiotensin receptor-mediated blood pressure regulation in mice lacking both AT1A and AT1B receptors for angiotensin II.* Proc Natl Acad Sci U S A, 1998. **95**(26): p. 15496-501.

112. Oliverio, M.I., et al., *Angiotensin II responses in AT1A receptor-deficient mice: a role for AT1B receptors in blood pressure regulation.* Am J Physiol, 1997. **272**(4 Pt 2): p. F515-20.

113. George, A.J., W.G. Thomas, and R.D. Hannan, *The renin-angiotensin system and cancer: old dog, new tricks.* Nat Rev Cancer, 2010. **10**(11): p. 745-59.

114. Oro, C., H. Qian, and W.G. Thomas, *Type 1 angiotensin receptor pharmacology: signaling beyond G proteins.* Pharmacol Ther, 2007. **113**(1): p. 210-26.

115. Horiuchi, M., J. Iwanami, and M. Mogi, *Regulation of angiotensin II receptors beyond the classical pathway.* Clin Sci (Lond), 2012. **123**(4): p. 193-203.

116. Yacoub, M. and M. Radford, *COMPARE and Pediatric Heart Network Investigator trials: Losartan finally validated in humans with Marfan, but much work remains!* Glob Cardiol Sci Pract, 2014. **2014**(4): p. 371-8.

117. Forteza, A., et al., *Efficacy of losartan vs. atenolol for the prevention of aortic dilation in Marfan syndrome: a randomized clinical trial.* Eur Heart J, 2016. **37**(12): p. 978-85.

118. Lacro, R.V., et al., *Atenolol versus losartan in children and young adults with Marfan's syndrome.* N Engl J Med, 2014. **371**(22): p. 2061-71.

119. Li, Y., X.H. Li, and H. Yuan, *Angiotensin II type-2 receptor-specific effects on the cardiovascular system.* Cardiovasc Diagn Ther, 2012. **2**(1): p. 56-62.

120. Rajagopalan, S., et al., *Angiotensin II-mediated hypertension in the rat increases vascular superoxide production via membrane NADH/NADPH oxidase activation. Contribution to alterations of vasomotor tone.* J Clin Invest, 1996. **97**(8): p. 1916-23.

121. Griendling, K.K., et al., *Angiotensin II stimulates NADH and NADPH oxidase activity in cultured vascular smooth muscle cells.* Circ Res, 1994. **74**(6): p. 1141-8.

122. Zafari, A.M., et al., *Role of NADH/NADPH oxidase-derived H2O2 in angiotensin II-induced vascular hypertrophy.* Hypertension, 1998. **32**(3): p. 488-95.

123. Pueyo, M.E., et al., *Angiotensin II stimulates the production of NO and peroxynitrite in endothelial cells.* Am J Physiol, 1998. **274**(1 Pt 1): p. C214-20.

124. Rodriguez-Puyol, M., et al., *Angiotensin II induces a rapid and transient increase of reactive oxygen species.* Antioxid Redox Signal, 2002. **4**(6): p. 869-75.

125. Cingolani, O.H., et al., *In vivo key role of reactive oxygen species and NHE-1 activation in determining excessive cardiac hypertrophy.* Pflugers Arch, 2011. **462**(5): p. 733-43.

126. Ogawa, S., et al., *Angiotensin II Type 1 Receptor Blockers Reduce Urinary Angiotensinogen Excretion and the Levels of Urinary Markers of Oxidative Stress and Inflammation in Patients with Type 2 Diabetic Nephropathy.* Biomark Insights, 2009. **4**: p. 97-102.

127. Chung, A.W., et al., *Endothelial dysfunction and compromised eNOS/Akt signaling in the thoracic aorta during the progression of Marfan syndrome.* Br J Pharmacol, 2007. **150**(8): p. 1075-83.

128. Yang, H.H., C. van Breemen, and A.W. Chung, *Vasomotor dysfunction in the thoracic aorta of Marfan syndrome is associated with accumulation of oxidative stress.* Vascul Pharmacol, 2010. **52**(1-2): p. 37-45.

129. Fiorillo, C., et al., *Evidence for oxidative stress in plasma of patients with Marfan syndrome.* Int J Cardiol, 2010. **145**(3): p. 544-6.

130. Sandor, G.G., et al., *A randomized, double blind pilot study to assess the effects of losartan vs. atenolol on the biophysical properties of the aorta in patients with Marfan and Loeys-Dietz syndromes.* Int J Cardiol, 2015. **179**: p. 470-5.

131. Seppelt, P.C., et al., *Loss of Endothelial Barrier in Marfan Mice (mgR/mgR) Results in Severe Inflammation after Adenoviral Gene Therapy.* PLoS One, 2016. **11**(2): p. e0148012.

132. Daugherty, A., M.W. Manning, and L.A. Cassis, *Angiotensin II promotes atherosclerotic lesions and aneurysms in apolipoprotein E-deficient mice.* J Clin Invest, 2000. **105**(11): p. 1605-12.

133. Van Herck, J.L., et al., *Impaired fibrillin-1 function promotes features of plaque instability in apolipoprotein E-deficient mice.* Circulation, 2009. **120**(24): p. 2478-87.

134. Davies, R.R., et al., *Yearly rupture or dissection rates for thoracic aortic aneurysms: simple prediction based on size.* Ann Thorac Surg, 2002. **73**(1): p. 17-27; discussion 27-8.

135. Davies, J.E. and T.M. Sundt, *Surgery insight: the dilated ascending aorta--indications for surgical intervention.* Nat Clin Pract Cardiovasc Med, 2007. **4**(6): p. 330-9.

136. Erbel, R. and H. Eggebrecht, *Aortic dimensions and the risk of dissection.* Heart, 2006. **92**(1): p. 137-42.

137. Bentall, H. and A. De Bono, *A technique for complete replacement of the ascending aorta.* Thorax, 1968. **23**(4): p. 338-9.

138. Benedetto, U., et al., *Surgical management of aortic root disease in Marfan syndrome: a systematic review and meta-analysis.* Heart, 2011. **97**(12): p. 955-8.

139. David, T.E., et al., *Results of aortic valve-sparing operations.* J Thorac Cardiovasc Surg, 2001. **122**(1): p. 39-46.

140. Treasure, T., *The evolution of aortic root surgery for Marfan syndrome.* Interact Cardiovasc Thorac Surg, 2010. **10**(3): p. 353-5.

141. Treasure, T. and J.R. Pepper, *Aortic root surgery in Marfan syndrome.* Heart, 2011. **97**(12): p. 951-2.

142. Treasure, T., et al., *Personalized external aortic root support: a review of the current status.* Eur J Cardiothorac Surg, 2016. **50**(3): p. 400-4.

143. Pepper, J., et al., *Histology of a Marfan aorta 4.5 years after personalized external aortic root support.* Eur J Cardiothorac Surg, 2015. **48**(3): p. 502-5.

144. Pepper, J., et al., *External aortic root support for Marfan syndrome: early clinical results in the first 20 recipients with a bespoke implant.* J R Soc Med, 2010. **103**(9): p. 370-5.

145. Bito, Y., et al., *Surgical approach to left subclavian artery aneurysm in Marfan syndrome.* Gen Thorac Cardiovasc Surg, 2009. **57**(7): p. 376-8.

146. Elefteriades, J.A., *Natural history of thoracic aortic aneurysms: indications for surgery, and surgical versus nonsurgical risks.* Ann Thorac Surg, 2002. **74**(5): p. S1877-80; discussion S1892-8.

147. Hino, Y., et al., *Extended replacement of the thoracic aorta.* Eur J Cardiothorac Surg, 2013. **43**(1): p. 176-81; discussion 181.

148. Murashita, T., et al., *[A case of redo operation for ascending aortic aneurysm after modified Bentall operation for Marfan syndrome associated with type A acute dissecting aortic aneurysm].* Kyobu Geka, 1996. **49**(7): p. 579-82.

149. Bucci, M., et al., *In vivo delivery of the caveolin-1 scaffolding domain inhibits nitric oxide synthesis and reduces inflammation.* Nat Med, 2000. **6**(12): p. 1362-7.

150. Phomakay, V., et al., *beta-Blockers and angiotensin converting enzyme inhibitors: comparison of effects on aortic growth in pediatric patients with Marfan syndrome.* J Pediatr, 2014. **165**(5): p. 951-5.

151. Williams, A., et al., *Effects of atenolol, perindopril and verapamil on haemodynamic and vascular function in Marfan syndrome - a randomised, double-blind, crossover trial.* Eur J Clin Invest, 2012. **42**(8): p. 891-9.

152. Yang, Y., Y. Cui, and D.Q. Peng, *ARB may be superior to ACEI on treatment of Marfan's syndrome by blocking TGF-beta mediated activation of ERK.* Int J Cardiol, 2012. **155**(3): p. 482-3.

153. Castro, M.M., et al., *Matrix metalloproteinase inhibitor properties of tetracyclines: therapeutic potential in cardiovascular diseases.* Pharmacol Res, 2011. **64**(6): p. 551-60.

154. Hartog, A.W., et al., *Current and future pharmacological treatment strategies with regard to aortic disease in Marfan syndrome.* Expert Opin Pharmacother, 2012. **13**(5): p. 647-62.

155. Brooke, B.S., et al., *Angiotensin II blockade and aortic-root dilation in Marfan's syndrome.* N Engl J Med, 2008. **358**(26): p. 2787-95.

156. Pees, C., et al., *Usefulness of losartan on the size of the ascending aorta in an unselected cohort of children, adolescents, and young adults with Marfan syndrome.* Am J Cardiol, 2013. **112**(9): p. 1477-83.

157. Groenink, M., et al., *Losartan reduces aortic dilatation rate in adults with Marfan syndrome: a randomized controlled trial.* Eur Heart J, 2013. **34**(45): p. 3491-500.

158. Franken, R., et al., *Circulating transforming growth factor-beta as a prognostic biomarker in Marfan syndrome.* Int J Cardiol, 2013. **168**(3): p. 2441-6.

159. Franken, R., et al., *The revised role of TGF-beta in aortic aneurysms in Marfan syndrome.* Neth Heart J, 2015. **23**(2): p. 116-21.

160. Franken, R., et al., *Beneficial Outcome of Losartan Therapy Depends on Type of FBN1 Mutation in Marfan Syndrome.* Circ Cardiovasc Genet, 2015. **8**(2): p. 383-8.

161. Chiu, H.H., et al., *Losartan added to beta-blockade therapy for aortic root dilation in Marfan syndrome: a randomized, open-label pilot study.* Mayo Clin Proc, 2013. **88**(3): p. 271-6.

162. Milleron, O., et al., *Marfan Sartan: a randomized, double-blind, placebo-controlled trial.* Eur Heart J, 2015. **36**(32): p. 2160-6.

163. Nordon, I.M., et al., *Pathophysiology and epidemiology of abdominal aortic aneurysms.* Nat Rev Cardiol, 2011. **8**(2): p. 92-102.

164. Roger, V.L., et al., *Heart disease and stroke statistics--2012 update: a report from the American Heart Association.* Circulation, 2012. **125**(1): p. e2-e220.

165. Baxter, B.T., M.C. Terrin, and R.L. Dalman, *Medical management of small abdominal aortic aneurysms.* Circulation, 2008. **117**(14): p. 1883-9.

166. Stather, P.W., et al., *A review of current reporting of abdominal aortic aneurysm mortality and prevalence in the literature.* Eur J Vasc Endovasc Surg, 2014. **47**(3): p. 240-2.

167. Miyake, T. and R. Morishita, *Pharmacological treatment of abdominal aortic aneurysm.* Cardiovasc Res, 2009. **83**(3): p. 436-43.

168. Kurosawa, K., J.S. Matsumura, and D. Yamanouchi, *Current status of medical treatment for abdominal aortic aneurysm.* Circ J, 2013. **77**(12): p. 2860-6.

169. Pereira, L., et al., *Pathogenetic sequence for aneurysm revealed in mice underexpressing fibrillin-1.* Proc Natl Acad Sci U S A, 1999. **96**(7): p. 3819-23.

170. Pereira, L., et al., *Targetting of the gene encoding fibrillin-1 recapitulates the vascular aspect of Marfan syndrome.* Nat Genet, 1997. **17**(2): p. 218-22.

171. Charbonneau, N.L., et al., *In vivo studies of mutant fibrillin-1 microfibrils.* J Biol Chem, 2010. **285**(32): p. 24943-55.

172. Dietz, H.C., et al., *Clustering of fibrillin (FBN1) missense mutations in Marfan syndrome patients at cysteine residues in EGF-like domains.* Hum Mutat, 1992. **1**(5): p. 366-74.

173. Gould, R.A., et al., *Multi-scale biomechanical remodeling in aging and genetic mutant murine mitral valve leaflets: insights into Marfan syndrome.* PLoS One, 2012. **7**(9): p. e44639.

174. Lacro, R.V., et al., *Atenolol versus losartan in children and young adults with Marfan's syndrome.* N Engl J Med, 2014. **371**(22): p. 2061-71.

175. Turner, J.A. and N.N. Stanley, *Fragile lung in the Marfan syndrome.* Thorax, 1976. **31**(6): p. 771-5.

176. Fongemie, J. and E. Felix-Getzik, *A Review of Nebivolol Pharmacology and Clinical Evidence.* Drugs, 2015. **75**(12): p. 1349-71.

177. Laboratory, T.J. *B6.129-Fbn1tmHcd/J*. 2016 2016 [cited 2016 July 5, 2016]; Available from: https://www.jax.org/strain/012885.

178. Laboratory, T.J. *C57 BL/6J*. 2016 2016 [cited 2016 July 9, 2016]; Available from: https://www.jax.org/strain/000664.

179. Schwill, S., et al., *The fibrillin-1 hypomorphic mgR/mgR murine model of Marfan syndrome shows severe elastolysis in all segments of the aorta.* J Vasc Surg, 2013. **57**(6): p. 1628-36, 1636.e1-3.

180. Cook, J.R., et al., *Abnormal muscle mechanosignaling triggers cardiomyopathy in mice with Marfan syndrome.* J Clin Invest, 2014. **124**(3): p. 1329-39.

181. Laboratory, T.J. *B6.129P2-Agtr1atm1Unc/J*. 2016 2016 [cited 2016 July 24, 2016]; Available from: https://www.jax.org/strain/002682.

182. Cassis, L.A., et al., *Bone marrow transplantation reveals that recipient AT1a receptors are required to initiate angiotensin II-induced atherosclerosis and aneurysms.* Arterioscler Thromb Vasc Biol, 2007. **27**(2): p. 380-6.

183. Daugherty, A., et al., *Hypercholesterolemia stimulates angiotensin peptide synthesis and contributes to atherosclerosis through the AT1A receptor.* Circulation, 2004. **110**(25): p. 3849-57.

184. Dimmeler, S., et al., *Activation of nitric oxide synthase in endothelial cells by Akt-dependent phosphorylation.* Nature, 1999. **399**(6736): p. 601-5.

185. Fulton, D., et al., *Regulation of endothelium-derived nitric oxide production by the protein kinase Akt.* Nature, 1999. **399**(6736): p. 597-601.

186. Dudzinski, D.M., et al., *The regulation and pharmacology of endothelial nitric oxide synthase.* Annu Rev Pharmacol Toxicol, 2006. **46**: p. 235-76.

187. Chen, Z.P., et al., *AMP-activated protein kinase phosphorylation of endothelial NO synthase.* FEBS Lett, 1999. **443**(3): p. 285-9.

188. Schleicher, M., et al., *The Akt1-eNOS axis illustrates the specificity of kinase-substrate relationships in vivo.* Sci Signal, 2009. **2**(82): p. ra41.

189. Kashiwagi, S., et al., *eNOS phosphorylation on serine 1176 affects insulin sensitivity and adiposity.* Biochem Biophys Res Commun, 2013. **431**(2): p. 284-90.

190. Michell, B.J., et al., *The Akt kinase signals directly to endothelial nitric oxide synthase.* Curr Biol, 1999. **9**(15): p. 845-8.

191. Atochin, D.N., et al., *The phosphorylation state of eNOS modulates vascular reactivity and outcome of cerebral ischemia in vivo.* J Clin Invest, 2007. **117**(7): p. 1961-7.

192. McCabe, T.J., et al., *Enhanced electron flux and reduced calmodulin dissociation may explain "calcium-independent" eNOS activation by phosphorylation.* J Biol Chem, 2000. **275**(9): p. 6123-8.

193. van Haperen, R., et al., *Functional expression of endothelial nitric oxide synthase fused to green fluorescent protein in transgenic mice.* Am J Pathol, 2003. **163**(4): p. 1677-86.

194. Laboratory, T.J. *B6.129P2-Nos3tm1Unc/J*. 2016 2016 [cited 2016 July 5, 2016]; Available from: https://www.jax.org/strain/002684.

195. Shesely, E.G., et al., *Elevated blood pressures in mice lacking endothelial nitric oxide synthase.* Proc Natl Acad Sci U S A, 1996. **93**(23): p. 13176-81.

196. Tranguch, S. and Y. Huet-Hudson, *Decreased viability of nitric oxide synthase double knockout mice.* Mol Reprod Dev, 2003. **65**(2): p. 175-9.

197. Bhandari, V., et al., *Essential role of nitric oxide in VEGF-induced, asthma-like angiogenic, inflammatory, mucus, and physiologic responses in the lung.* Proc Natl Acad Sci U S A, 2006. **103**(29): p. 11021-6.

198. Bernatchez, P., et al., *A noninhibitory mutant of the caveolin-1 scaffolding domain enhances eNOS-derived NO synthesis and vasodilation in mice.* J Clin Invest, 2011. **121**(9): p. 3747-55.

199. Bernatchez, P.N., et al., *Dissecting the molecular control of endothelial NO synthase by caveolin-1 using cell-permeable peptides.* Proc Natl Acad Sci U S A, 2005. **102**(3): p. 761-6.

200. Sellers, S.L., A.E. Trane, and P.N. Bernatchez, *Caveolin as a potential drug target for cardiovascular protection.* Front Physiol, 2012. **3**: p. 280.

201. Hirota, J.A., R. Ellis, and M.D. Inman, *Regional differences in the pattern of airway remodeling following chronic allergen exposure in mice.* Respir Res, 2006. **7**: p. 120.

202. Su, J.Z., et al., *Effect of AT2 receptor on expression of AT1 and TGF-beta receptors in VSMCs from SHR.* Hypertension, 2002. **40**(6): p. 853-8.

203. Ito, M., et al., *Regulation of blood pressure by the type 1A angiotensin II receptor gene.* Proc Natl Acad Sci U S A, 1995. **92**(8): p. 3521-5.

204. Masri A, K.V., Svensson L, Alashi A, Schoenhagen P, Roselli E, Johnston D, Rodriguez LL, Griffin BP, Desai M.Y., *Aortic cross-sectional area/height ratio and outcomes in patients with bicuspid aortic valve and a dilated ascending aorta.* Circulation: Cardiovascular Imaging, 2017.

205. Emrich, F.C., et al., *Enhanced caspase activity contributes to aortic wall remodeling and early aneurysm development in a murine model of Marfan syndrome.* Arterioscler Thromb Vasc Biol, 2015. **35**(1): p. 146-54.

206. Benicky, J., et al., *Six commercially available angiotensin II AT1 receptor antibodies are non-specific.* Cell Mol Neurobiol, 2012. **32**(8): p. 1353-65.

207. Rateri, D.L., et al., *Endothelial cell-specific deficiency of Ang II type 1a receptors attenuates Ang II-induced ascending aortic aneurysms in LDL receptor-/- mice.* Circ Res, 2011. **108**(5): p. 574-81.

208. Poduri, A., et al., *Fibroblast Angiotensin II Type 1a Receptors Contribute to Angiotensin II-Induced Medial Hyperplasia in the Ascending Aorta.* Arterioscler Thromb Vasc Biol, 2015. **35**(9): p. 1995-2002.

209. Le, T.H., et al., *Physiological impact of increased expression of the AT1 angiotensin receptor.* Hypertension, 2003. **42**(4): p. 507-14.

210. Cheung, C., et al., *Generation of human vascular smooth muscle subtypes provides insight into embryological origin-dependent disease susceptibility.* Nat Biotechnol, 2012. **30**(2): p. 165-73.

211. Benson, S.C., et al., *Identification of telmisartan as a unique angiotensin II receptor antagonist with selective PPARgamma-modulating activity.* Hypertension, 2004. **43**(5): p. 993-1002.

212. Schupp, M., et al., *Angiotensin type 1 receptor blockers induce peroxisome proliferator-activated receptor-gamma activity.* Circulation, 2004. **109**(17): p. 2054-7.

213. Jung, A.D., et al., *The effect of telmisartan on endothelial function and arterial stiffness in patients with essential hypertension.* Korean Circ J, 2009. **39**(5): p. 180-4.

214. Yuen, C.Y., et al., *Telmisartan inhibits vasoconstriction via PPARgamma-dependent expression and activation of endothelial nitric oxide synthase.* Cardiovasc Res, 2011. **90**(1): p. 122-9.

215. Siragusa, M. and W.C. Sessa, *Telmisartan exerts pleiotropic effects in endothelial cells and promotes endothelial cell quiescence and survival.* Arterioscler Thromb Vasc Biol, 2013. **33**(8): p. 1852-60.

216. Knorr, M., et al., *Nitroglycerin-induced endothelial dysfunction and tolerance involve adverse phosphorylation and S-Glutathionylation of endothelial nitric oxide synthase: beneficial effects of therapy with the AT1 receptor blocker telmisartan.* Arterioscler Thromb Vasc Biol, 2011. **31**(10): p. 2223-31.

217. Su, K.H., et al., *Valsartan regulates the interaction of angiotensin II type 1 receptor and endothelial nitric oxide synthase via Src/PI3K/Akt signalling.* Cardiovasc Res, 2009. **82**(3): p. 468-75.

218. Negro, R., *Endothelial effects of antihypertensive treatment: focus on irbesartan.* Vasc Health Risk Manag, 2008. **4**(1): p. 89-101.

219. Watanabe, T., et al., *Losartan metabolite EXP3179 activates Akt and endothelial nitric oxide synthase via vascular endothelial growth factor receptor-2 in endothelial cells: angiotensin II type 1 receptor-independent effects of EXP3179.* Circulation, 2005. **112**(12): p. 1798-805.

220. Liu, H., et al., *Losartan, an angiotensin II type 1 receptor blocker, ameliorates cerebral ischemia-reperfusion injury via PI3K/Akt-mediated eNOS phosphorylation.* Brain Res Bull, 2012. **89**(1-2): p. 65-70.

221. Mizuguchi, T., et al., *Heterozygous TGFBR2 mutations in Marfan syndrome.* Nat Genet, 2004. **36**(8): p. 855-60.

222. Saura, M., et al., *Nitric oxide regulates transforming growth factor-beta signaling in endothelial cells.* Circ Res, 2005. **97**(11): p. 1115-23.

223. Inoue, K., et al., *Nitric oxide mediates inhibitory effect of losartan on angiotensin-induced contractions in hamster but not rat aorta.* J Renin Angiotensin Aldosterone Syst, 2000. **1**(2): p. 180-3.

224. Sleem, M., et al., *Combination therapy with losartan and L-carnitine protects against endothelial dysfunction of streptozotocin-induced diabetic rats.* Eur J Pharmacol, 2014. **744**: p. 10-7.

225. Ferrara, N., H.P. Gerber, and J. LeCouter, *The biology of VEGF and its receptors.* Nat Med, 2003. **9**(6): p. 669-76.

226. Kasahara, Y., et al., *Inhibition of VEGF receptors causes lung cell apoptosis and emphysema.* J Clin Invest, 2000. **106**(11): p. 1311-9.

227. Abe, K., et al., *Formation of plexiform lesions in experimental severe pulmonary arterial hypertension.* Circulation, 2010. **121**(25): p. 2747-54.

228. Baek, S.U. and S.I. Kwon, *Rupture of abdominal aortic aneurysm after intravitreal bevacizumab injection: a case report.* J Med Case Rep, 2014. **8**: p. 48.

229. Boo, Y.C., et al., *Shear stress stimulates phosphorylation of eNOS at Ser(635) by a protein kinase A-dependent mechanism.* Am J Physiol Heart Circ Physiol, 2002. **283**(5): p. H1819-28.

230. Vitulo, P., et al., *Sildenafil in severe pulmonary hypertension associated with chronic obstructive pulmonary disease: A randomized controlled multicenter clinical trial.* J Heart Lung Transplant, 2016.

231. Sharma, A., et al., *Direct Endothelial Nitric Oxide Synthase Activation Provides Atheroprotection in Diabetes-Accelerated Atherosclerosis.* Diabetes, 2015. **64**(11): p. 3937-50.

232. Ridnour, L.A., et al., *Nitric oxide regulates matrix metalloproteinase-9 activity by guanylyl-cyclase-dependent and -independent pathways.* Proc Natl Acad Sci U S A, 2007. **104**(43): p. 16898-903.

233. Meschiari, C.A., et al., *Nitric oxide attenuates matrix metalloproteinase-9 production by endothelial cells independent of cGMP- or NFkappaB-mediated mechanisms.* Mol Cell Biochem, 2013. **378**(1-2): p. 127-35.

234. Bennett, M.R., *Apoptosis of vascular smooth muscle cells in vascular remodelling and atherosclerotic plaque rupture.* Cardiovasc Res, 1999. **41**(2): p. 361-8.

235. Li, P.F., R. Dietz, and R. von Harsdorf, *Reactive oxygen species induce apoptosis of vascular smooth muscle cell.* FEBS Lett, 1997. **404**(2-3): p. 249-52.

236. Morrow, J.D., *The isoprostanes - unique products of arachidonate peroxidation: their role as mediators of oxidant stress.* Curr Pharm Des, 2006. **12**(8): p. 895-902.

237. Fam, S.S. and J.D. Morrow, *The isoprostanes: unique products of arachidonic acid oxidation-a review.* Curr Med Chem, 2003. **10**(17): p. 1723-40.

238. Yu, J., et al., *Glucagon-like peptide-1 prevented abdominal aortic aneurysm development in rats.* Surg Today, 2016. **46**(9): p. 1099-107.

239. Bao, W., et al., *Orally administered dipeptidyl peptidase-4 inhibitor (alogliptin) prevents abdominal aortic aneurysm formation through an antioxidant effect in rats.* J Vasc Surg, 2014. **59**(4): p. 1098-108.

240. Forstermann, U. and H. Li, *Therapeutic effect of enhancing endothelial nitric oxide synthase (eNOS) expression and preventing eNOS uncoupling.* Br J Pharmacol, 2011. **164**(2): p. 213-23.

241. Napoli, C. and L.J. Ignarro, *Nitric oxide-releasing drugs.* Annu Rev Pharmacol Toxicol, 2003. **43**: p. 97-123.

242. Miller, M.R. and I.L. Megson, *Recent developments in nitric oxide donor drugs.* Br J Pharmacol, 2007. **151**(3): p. 305-21.

243. Griffiths, M.J. and T.W. Evans, *Inhaled nitric oxide therapy in adults.* N Engl J Med, 2005. **353**(25): p. 2683-95.

244. Birnboim, H.C. and H. Privora, *Depletion of intracellular glutathione reduces mutations by nitric oxide-donating drugs.* Nitric Oxide, 2000. **4**(5): p. 496-504.

245. Munzel, T., et al., *Hydralazine prevents nitroglycerin tolerance by inhibiting activation of a membrane-bound NADH oxidase. A new action for an old drug.* J Clin Invest, 1996. **98**(6): p. 1465-70.

246. Munzel, T., et al., *Evidence for enhanced vascular superoxide anion production in nitrate tolerance. A novel mechanism underlying tolerance and cross-tolerance.* J Clin Invest, 1995. **95**(1): p. 187-94.

247. Breitenstein, S., et al., *Novel sGC Stimulators and sGC Activators for the Treatment of Heart Failure.* Handb Exp Pharmacol, 2017. **243**: p. 225-247.

248. Wohlfart, P., et al., *Antiatherosclerotic effects of small-molecular-weight compounds enhancing endothelial nitric-oxide synthase (eNOS) expression and preventing eNOS uncoupling.* J Pharmacol Exp Ther, 2008. **325**(2): p. 370-9.

249. Li, H., et al., *Midostaurin upregulates eNOS gene expression and preserves eNOS function in the microcirculation of the mouse.* Nitric Oxide, 2005. **12**(4): p. 231-6.

250. Leikert, J.F., et al., *Red wine polyphenols enhance endothelial nitric oxide synthase expression and subsequent nitric oxide release from endothelial cells.* Circulation, 2002. **106**(13): p. 1614-7.

251. Wallerath, T., et al., *Resveratrol, a polyphenolic phytoalexin present in red wine, enhances expression and activity of endothelial nitric oxide synthase.* Circulation, 2002. **106**(13): p. 1652-8.

252. Hibender, S., et al., *Resveratrol Inhibits Aortic Root Dilatation in the Fbn1C1039G/+ Marfan Mouse Model.* Arterioscler Thromb Vasc Biol, 2016. **36**(8): p. 1618-26.

253. Walter, A., et al., *Angiotensin II induces the vascular expression of VEGF and MMP-2 in vivo: preventive effect of red wine polyphenols.* J Vasc Res, 2008. **45**(5): p. 386-94.

254. Chemical, C. *NO-Losartan A*. 2016 [cited 2016 Aug 26, 2016]; Available from: https://www.caymanchem.com/product/10006456.

255. Breschi, M.C., et al., *NO-sartans: a new class of pharmacodynamic hybrids as cardiovascular drugs.* J Med Chem, 2004. **47**(23): p. 5597-600.

256. Breschi, M.C., et al., *New NO-releasing pharmacodynamic hybrids of losartan and its active metabolite: design, synthesis, and biopharmacological properties.* J Med Chem, 2006. **49**(8): p. 2628-39.

257. Lee, M.K., et al., *TGF-beta activates Erk MAP kinase signalling through direct phosphorylation of ShcA.* Embo j, 2007. **26**(17): p. 3957-67.

258. Mueller, G.C., et al., *Retrospective analysis of the effect of angiotensin II receptor blocker versus beta-blocker on aortic root growth in paediatric patients with Marfan syndrome.* Heart, 2014. **100**(3): p. 214-8.

259. Moberg, K., et al., *The Ghent Marfan Trial--a randomized, double-blind placebo controlled trial with losartan in Marfan patients treated with beta-blockers.* Int J Cardiol, 2012. **157**(3): p. 354-8.

260. Singh, M.N. and R.V. Lacro, *Recent Clinical Drug Trials Evidence in Marfan Syndrome and Clinical Implications.* Can J Cardiol, 2016. **32**(1): p. 66-77.

261. Bahouth, Z., et al., *Endothelial Function Assessment in Patients with Erectile Dysfunction.* Isr Med Assoc J, 2015. **17**(11): p. 682-6.

262. Meeme, A., et al., *Endothelial dysfunction and arterial stiffness in pre-eclampsia demonstrated by the EndoPAT method.* Cardiovasc J Afr, 2016. **27**: p. 1-7.

263. Sagara, M., et al., *Impact of teneligliptin on oxidative stress and endothelial function in type 2 diabetes patients with chronic kidney disease: a case-control study.* Cardiovasc Diabetol, 2016. **15**: p. 76.

264. Cheruvu, C., et al., *Beyond Stenosis With Fractional Flow Reserve Via Computed Tomography and Advanced Plaque Analyses for the Diagnosis of Lesion-Specific Ischemia.* Can J Cardiol, 2016.

265. Paudel, K.R., N. Panth, and D.W. Kim, *Circulating Endothelial Microparticles: A Key Hallmark of Atherosclerosis Progression.* Scientifica (Cairo), 2016. **2016**: p. 8514056.

266. Anwar, A., et al., *Novel biomarkers for pulmonary arterial hypertension.* Respir Res, 2016. **17**(1): p. 88.

267. Chen, J., et al., *Interrelationship of Multiple Endothelial Dysfunction Biomarkers with Chronic Kidney Disease.* PLoS One, 2015. **10**(7): p. e0132047.

268. Sirtori, C.R., *Pharmacology and mechanism of action of the new HMG-CoA reductase inhibitors.* Pharmacol Res, 1990. **22**(5): p. 555-63.

269. McLoughlin, D., et al., *Pravastatin reduces Marfan aortic dilation.* Circulation, 2011. **124**(11 Suppl): p. S168-73.

270. Beckman, J.A. and M.A. Creager, *The nonlipid effects of statins on endothelial function.* Trends Cardiovasc Med, 2006. **16**(5): p. 156-62.

271. Bellosta, S., et al., *Non-lipid-related effects of statins.* Ann Med, 2000. **32**(3): p. 164-76.

272. Ma, S. and C.C. Ma, *Recent developments in the effects of nitric oxide-donating statins on cardiovascular disease through regulation of tetrahydrobiopterin and nitric oxide.* Vascul Pharmacol, 2014. **63**(2): p. 63-70.

273. Williams, J.K., et al., *Pravastatin has cholesterol-lowering independent effects on the artery wall of atherosclerotic monkeys.* J Am Coll Cardiol, 1998. **31**(3): p. 684-91.

274. Margaritis, M., K.M. Channon, and C. Antoniades, *Statins as regulators of redox state in the vascular endothelium: beyond lipid lowering.* Antioxid Redox Signal, 2014. **20**(8): p. 1198-215.

275. Zhu, B., et al., *Effects of simvastatin on oxidative stress in streptozotocin-induced diabetic rats: a role for glomeruli protection.* Nephron Exp Nephrol, 2005. **101**(1): p. e1-8.

276. Ota, H., et al., *Induction of endothelial nitric oxide synthase, SIRT1, and catalase by statins inhibits endothelial senescence through the Akt pathway.* Arterioscler Thromb Vasc Biol, 2010. **30**(11): p. 2205-11.

277. Settergren, M., L. Ryden, and J. Pernow, *Letter by Settergren et al regarding article, "Evidence for statin pleiotropy in humans: differential effects of statins and ezetimibe on rho-associated coiled-coil containing protein kinase activity, endothelial function, and inflammation".* Circulation, 2009. **120**(9): p. e68; author reply e69-70.

278. Wagner, A.H., et al., *Improvement of nitric oxide-dependent vasodilatation by HMG-CoA reductase inhibitors through attenuation of endothelial superoxide anion formation.* Arterioscler Thromb Vasc Biol, 2000. **20**(1): p. 61-9.

279. Zapolska-Downar, D., et al., *Simvastatin modulates TNFalpha-induced adhesion molecules expression in human endothelial cells.* Life Sci, 2004. **75**(11): p. 1287-302.

280. Hattori, Y., et al., *HMG-CoA reductase inhibitor increases GTP cyclohydrolase I mRNA and tetrahydrobiopterin in vascular endothelial cells.* Arterioscler Thromb Vasc Biol, 2003. **23**(2): p. 176-82.

281. Aoki, C., et al., *Fluvastatin upregulates endothelial nitric oxide synthase activity via enhancement of its phosphorylation and expression and via an increase in tetrahydrobiopterin in vascular endothelial cells.* Int J Cardiol, 2012. **156**(1): p. 55-61.

282. Gambarin, F.I., et al., *Rationale and design of a trial evaluating the effects of losartan vs. nebivolol vs. the association of both on the progression of aortic root dilation in Marfan syndrome with FBN1 gene mutations.* J Cardiovasc Med (Hagerstown), 2009. **10**(4): p. 354-62.

283. Liu, C.L., et al., *Allergic Lung Inflammation Aggravates Angiotensin II-Induced Abdominal Aortic Aneurysms in Mice.* Arterioscler Thromb Vasc Biol, 2016. **36**(1): p. 69-77.

284. Van Eeden, S., et al., *The relationship between lung inflammation and cardiovascular disease.* Am J Respir Crit Care Med, 2012. **186**(1): p. 11-6.

285. Podowski, M., et al., *Angiotensin receptor blockade attenuates cigarette smoke-induced lung injury and rescues lung architecture in mice.* J Clin Invest, 2012. **122**(1): p. 229-40.

286. ZOLER, M.L. *CHEST: Losartan slows emphysema progression in pilot trial*. 2015 [cited 2016 Aug 26, 2016]; Available from: http://www.chestphysician.org/specialty-focus/pulmonary-medicine/article/chest-losartan-slows-emphysema-progression-in-pilot-trial/eb08c330a6dd31338544295f36247dfc.html.

287. Raupach, T., et al., *Local and systemic effects of angiotensin receptor blockade in an emphysema mouse model.* Pulm Pharmacol Ther, 2011. **24**(2): p. 215-20.

288. Hoeper, M.M., et al., *Treatment of pulmonary hypertension.* Lancet Respir Med, 2016. **4**(4): p. 323-36.

289. Argun Baris, S., et al., *The effects of sildenafil on smoke induced lung inflammation in rats.* Malays J Pathol, 2016. **38**(1): p. 39-44.

290. Dominguez-Fandos, D., et al., *Sildenafil in a cigarette smoke-induced model of COPD in the guinea-pig.* Eur Respir J, 2015. **46**(2): p. 346-54.

291. Diet, L. *Standard Diets*. 2016 [cited 2016 August 31, 2016]; Available from: http://www.labdiet.com/Products/StandardDiets/.

292. Kramer, C., et al., *Angiotensin II receptor-independent antiinflammatory and antiaggregatory properties of losartan: role of the active metabolite EXP3179.* Circ Res, 2002. **90**(7): p. 770-6.

293. Fortuno, A., et al., *Losartan metabolite EXP3179 blocks NADPH oxidase-mediated superoxide production by inhibiting protein kinase C: potential clinical implications in hypertension.* Hypertension, 2009. **54**(4): p. 744-50.

294. Rossi, G.P., *Losartan metabolite EXP3179: an AT1-receptor-independent treatment strategy for patients with the metabolic syndrome?* Hypertension, 2009. **54**(4): p. 710-2.

295. Henkin, S., et al., *Spontaneous coronary artery dissection and its association with heritable connective tissue disorders.* Heart, 2016. **102**(11): p. 876-81.

296. Williams-Phillips, S., *Marfan's syndrome: pre-pubertal aortic rupture with left coronary artery aneurysms and fistulas.* West Indian Med J, 2012. **61**(9): p. 937-40.

297. Fattori, R., et al., *Spontaneous coronary artery dissection in a young woman with Loeys-Dietz syndrome.* Am J Med Genet A, 2012. **158a**(5): p. 1216-8.

298. Alvira, C.M., et al., *Inhibition of transforming growth factor beta worsens elastin degradation in a murine model of Kawasaki disease.* Am J Pathol, 2011. **178**(3): p. 1210-20.

299. Lee, A.M., et al., *Role of TGF-beta Signaling in Remodeling of Noncoronary Artery Aneurysms in Kawasaki Disease.* Pediatr Dev Pathol, 2015. **18**(4): p. 310-7.

300. Shimizu, C., et al., *Transforming growth factor-beta signaling pathway in patients with Kawasaki disease.* Circ Cardiovasc Genet, 2011. **4**(1): p. 16-25.

Appendix A: Laboratory Animal Diet Formulations

A.1 Breeding Diet (LabDiet 5058) Formulation Sheet

Breeding diet formulations were used to support husbandry of animals [291].

PicoLab® Mouse Diet 20 — 5058*
PicoLab® Mouse 20 EXT — 5R58*

DESCRIPTION

PicoLab® Mouse Diet 20 is a formulation providing 20% protein for mouse colonies that require extra levels of energy needed for maximum production in post-partum breeding. This diet is a complete life cycle diet formulated using managed formulation, delivering Constant Nutrition®. This is paired with the selection of highest quality ingredients to assure minimal inherent biological variation in long-term studies. Irradiation treatment and special 3-ply packaging provide virtually bacteria-free dietary control.

Features and Benefits

- Managed Formulation delivers Constant Nutrition®
- Formulated with 20% protein for mouse breeding colonies
- Designed to meet the energy needs of breeding mouse colonies, transgenic strains, and mice exposed to higher stress levels
- Irradiation gives reliable microbial control and eliminates the need for autoclaving

Product Forms Available	***Catalog #***
• 5058: Oval pellet, 3/8"x5/8"x1"	0007689
• 5R58: Extruded Particle	0047039
• Meal (ground pellets), special order	0006953
Other Versions Available	***Catalog #***
• 5062 Pico-Vac® Mouse Diet 20	0006955

GUARANTEED ANALYSIS

Crude protein not less than	20.0%
Crude fat not less than	9.0%
Crude fiber not more than	4.0%
Ash not more than	6.5%
Moisture not more than	12.0%

INGREDIENTS

Whole wheat, ground corn, dehulled soybean meal, wheat germ, fish meal, corn gluten meal, brewers dried yeast, porcine animal fat preserved with BHA, soybean oil, porcine animal fat preserved with BHA and BHT, calcium carbonate, condensed whey, salt, condensed whey solubles, dry whey protein concentrate, DL-methionine, mono and diglycerides of edible fats, choline chloride, menadione dimethylpyrimidinol bisulfite (source of vitamin K), pyridoxine hydrochloride, cholecalciferol, vitamin A acetate, biotin, dl-alpha tocopheryl acetate (form of vitamin E), folic acid, thiamine mononitrate, calcium pantothenate, vitamin B_{12} supplement, riboflavin supplement, nicotinic acid, casein, manganous oxide, zinc oxide, ferrous carbonate, copper sulfate, zinc sulfate, calcium iodate, cobalt carbonate, sodium selenite.

FEEDING DIRECTIONS

Feed ad libitum to mice. Plenty of fresh, clean water should be available to the animals at all times.

Mice-Adult mice will eat up to 5 grams of pelleted ration daily. Some of the larger strains may eat as much as 8 grams per day per animal. Feed should be available on a free choice basis in wire feeders above the floor of the cage.

For information regarding shelf life please visit www.labdiet.com.

CHEMICAL COMPOSITION[1]

Nutrients[2]	
Protein, %	**21.8**
Arginine, %	1.21
Cystine, %	0.40
Glycine, %	0.94
Histidine, %	0.52
Isoleucine, %	0.91
Leucine, %	1.80
Lysine, %	1.12
Methionine, %	0.58
Phenylalanine, %	0.98
Tyrosine, %	0.66
Threonine, %	0.80
Tryptophan, %	0.24
Valine, %	1.00
Serine, %	1.03
Aspartic Acid, %	2.06
Glutamic Acid, %	4.55
Alanine, %	1.33
Proline, %	1.52
Taurine, %	0.03
Fat (ether extract), %	**9.0**
Fat (acid hydrolysis), %	**10.2**
Cholesterol, ppm	208
Linoleic Acid, %	2.11
Linolenic Acid, %	0.22
Arachidonic Acid, %	0.03
Omega-3 Fatty Acids, %	0.43
Total Saturated Fatty Acids, %	2.59
Total Monounsaturated Fatty Acids, %	2.85
Fiber (Crude), %	**2.3**
Neutral Detergent Fiber[3], %	10.8
Acid Detergent Fiber[4], %	3.1
Nitrogen-Free Extract (by difference), %	**51.9**
Starch, %	35.2
Glucose, %	0.16
Fructose, %	0.16
Sucrose, %	0.74
Lactose, %	0.71
Total Digestible Nutrients,%	**82.7**
Gross Energy, kcal/gm	**4.63**
Physiological Fuel Value[5], kcal/gm	**3.76**
Metabolizable Energy, kcal/gm	**3.45**

Minerals	
Ash, %	**4.9**
Calcium, %	0.81
Phosphorus, %	0.61
Phosphorus (non-phytate), %	0.34
Potassium, %	0.72
Magnesium, %	0.16
Sulfur, %	0.26
Sodium, %	0.26
Chloride, %	0.45
Fluorine, ppm	9.9
Iron, ppm	180
Zinc, ppm	120
Manganese, ppm	120
Copper, ppm	17
Cobalt, ppm	0.56
Iodine, ppm	1.5
Chromium (added), ppm	0.01
Selenium, ppm	0.33

Vitamins	
Carotene, ppm	Trace
Vitamin K (as menadione),ppm	3.1
Thiamin Hydrochloride, ppm	15
Riboflavin, ppm	8.0
Niacin, ppm	77
Pantothenic Acid, ppm	21
Choline Chloride, ppm	2200
Folic Acid, ppm	2.9
Pyridoxine, ppm	9.6
Biotin, ppm	0.30
B_{12}, mcg/kg	51
Vitamin A, IU/gm	15
Vitamin D_3 (added), IU/gm	3.4
Vitamin E, IU/kg	57
Ascorbic Acid, mg/gm	—

Calories provided by:	
Protein, %	23.209
Fat (ether extract), %	21.559
Carbohydrates, %	55.231

*Product Code

1. Formulation based on calculated values from the latest ingredient analysis information. Since nutrient composition of natural ingredients varies and some nutrient loss will occur due to manufacturing processes, analysis will differ accordingly.
2. Nutrients expressed as percent of ration except where otherwise indicated. Moisture content is assumed to be 10.0% for the purpose of calculations.
3. NDF = approximately cellulose, hemi-cellulose and lignin.
4. ADF = approximately cellulose and lignin.
5. Physiological Fuel Value (kcal/gm) = Sum of decimal fractions of protein, fat and carbohydrate (use Nitrogen Free Extract) x 4,9,4 kcal/gm respectively.

05/05/15

A.2 Standard Laboratory Diet (Lab Diet #5001) Formulation Sheet

Standard laboratory (Lab Diet #5001) use utilized for all non-breeding animals [291].

Laboratory Rodent Diet 5001*

DESCRIPTION

Laboratory Rodent Diet is recommended for rats, mice, hamsters and gerbils. This diet is a complete life cycle diet formulated using managed formulation, delivering Constant Nutrition®. This is paired with the selection of highest quality ingredients to assure minimal inherent biological variation in long-term studies. It is formulated for life-cycle nutrition; however, it is not designed for maximizing production in mouse breeding colonies. This product has been the standard of biomedical research for over 70 years.

Features and Benefits

- Managed Formulation delivers Constant Nutrition®
- High quality animal protein added to create a superior balance of amino acids for optimum performance
- Formulated for multiple species for single product inventory
- The rodent diet standard for biomedical research

Product Forms Available

- Oval pellet, 10 mm x 16 mm x 25 mm length (3/8"x5/8"x1")
- Meal (ground pellets)

Other Versions Available

- 5L0D PicoLab® Laboratory Rodent Diet (Minimum order required)

GUARANTEED ANALYSIS

Crude protein not less than	23.0%
Crude fat not less than	4.5%
Crude fiber not more than	6.0%
Ash not more than	8.0%
Moisture not more than	12.0%

INGREDIENTS

Dehulled soybean meal, ground corn, dried beet pulp, fish meal, ground oats, dehydrated alfalfa meal, cane molasses, brewers dried yeast, wheat germ, whey, porcine animal fat preserved with BHA and citric acid, wheat middlings, porcine meat and bone meal, salt, calcium carbonate, DL-methionine, choline chloride, cholecalciferol, folic acid, vitamin A acetate, menadione dimethylpyrimidinol bisulfite (source of vitamin K), pyridoxine hydrochloride, thiamine mononitrate, biotin, nicotinic acid, calcium pantothenate, dl-alpha tocopheryl acetate (form of vitamin E), vitamin B_{12} supplement, riboflavin supplement, ferrous sulfate, manganous oxide, zinc oxide, ferrous carbonate, copper sulfate, zinc sulfate, calcium iodate, cobalt carbonate, sodium selenite.

FEEDING DIRECTIONS

Feed ad libitum to rodents. Plenty of fresh, clean water should be available to the animals at all times.

Rats- All rats will eat varying amounts of feed depending on their genetic origin. Larger strains will eat up to 30 grams per day. Smaller strains will eat up to 15 grams per day. Feeders in rat cages should be designed to hold two to three days supply of feed at one time.

Mice-Adult mice will eat up to 5 grams of pelleted ration daily. Some of the larger strains may eat as much as 8 grams per day per animal. Feed should be available on a free choice basis in wire feeders above the floor of the cage.

Hamsters-Adults will eat up to 14 grams per day.

For information regarding shelf life please visit www.labdiet.com.

03/19/15

CHEMICAL COMPOSITION[1]

Nutrients[2]	
Protein, %	**25.0**
Arginine, %	1.57
Cystine, %	0.39
Glycine, %	1.28
Histidine, %	0.62
Isoleucine, %	1.06
Leucine, %	1.89
Lysine, %	1.48
Methionine, %	0.59
Phenylalanine, %	1.11
Tyrosine, %	0.77
Threonine, %	0.97
Tryptophan, %	0.28
Valine, %	1.16
Serine, %	1.18
Aspartic Acid, %	2.81
Glutamic Acid, %	4.74
Alanine, %	1.44
Proline, %	1.47
Taurine, %	0.03
Fat (ether extract), %	**5.0**
Fat (acid hydrolysis), %	**6.4**
Cholesterol, ppm	209
Linoleic Acid, %	1.05
Linolenic Acid, %	0.09
Arachidonic Acid, %	0.02
Omega-3 Fatty Acids, %	0.30
Total Saturated Fatty Acids, %	1.48
Total Monounsaturated Fatty Acids, %	1.62
Fiber (Crude), %	**5.3**
Neutral Detergent Fiber[3], %	16.7
Acid Detergent Fiber[4], %	6.9
Nitrogen-Free Extract (by difference), %	**47.5**
Starch, %	21.0
Glucose, %	0.19
Fructose, %	0.27
Sucrose, %	3.83
Lactose, %	2.01
Total Digestible Nutrients,%	**73.8**
Gross Energy, kcal/gm	**4.09**
Physiological Fuel Value[5], kcal/gm	**3.35**
Metabolizable Energy, kcal/gm	**2.91**

Minerals	
Ash, %	**7.0**
Calcium, %	0.95
Phosphorus, %	0.70
Phosphorus (non-phytate), %	0.42
Potassium, %	1.28
Magnesium, %	0.23
Sulfur, %	0.36
Sodium, %	0.39
Chloride, %	0.64
Fluorine, ppm	15
Iron, ppm	240
Zinc, ppm	85
Manganese, ppm	75
Copper, ppm	15
Cobalt, ppm	0.91
Iodine, ppm	0.99
Chromium (added), ppm	0.01
Selenium, ppm	0.41

Vitamins	
Carotene, ppm	2.3
Vitamin K,ppm	1.3
Thiamin Hydrochloride, ppm	16
Riboflavin, ppm	4.7
Niacin, ppm	120
Pantothenic Acid, ppm	24
Choline Chloride, ppm	2250
Folic Acid, ppm	7.1
Pyridoxine, ppm	6.0
Biotin, ppm	0.30
B_{12}, mcg/kg	51
Vitamin A, IU/gm	15
Vitamin D_3 (added), IU/gm	4.6
Vitamin E, IU/kg	42
Ascorbic Acid, mg/gm	—

Calories provided by:

Protein, %	29.829
Fat (ether extract), %	13.427
Carbohydrates, %	56.744

*Product Code

1. Formulation based on calculated values from the latest ingredient analysis information. Since nutrient composition of natural ingredients varies and some nutrient loss will occur due to manufacturing processes, analysis will differ accordingly.
2. Nutrients expressed as percent of ration except where otherwise indicated. Moisture content is assumed to be 10.0% for the purpose of calculations.
3. NDF = approximately cellulose, hemi-cellulose and lignin.
4. ADF = approximately cellulose and lignin.
5. Physiological Fuel Value (kcal/gm) = Sum of decimal fractions of protein, fat and carbohydrate (use Nitrogen Free Extract) x 4,9,4 kcal/gm respectively.

LabDiet
www.labdiet.com

Appendix B: NO-Release Using Losartan Metabolites

Losartan has two previously described metabolites: EXP3174 and EXP3179. These metabolites are generated upon oxidation by cytochrome P450 in the liver. Both ATR1 dependent and ATR1-independent functions have been attributed to the effects of these metabolites of losartan [219, 292-294]. However, how they effect the production of NO is unknown. Using the same experimental setup as previously described for analysis of acute ionophore-induced NO-release in BAECs (Chapter 3, section 3.4), EXP3174 and EXP3179 were tested for their ability to increase release of NO in ECs (Figure 35). Both metabolites were found to increase NO release similar to treatment with intact losartan. This is consistent with the conclusions of Watanabe *et al.* [219]; however, unlike Watanabe *et al.*, we did not observe a greater effect of EXP3179 relative to EXP3174 from this set of experiments.

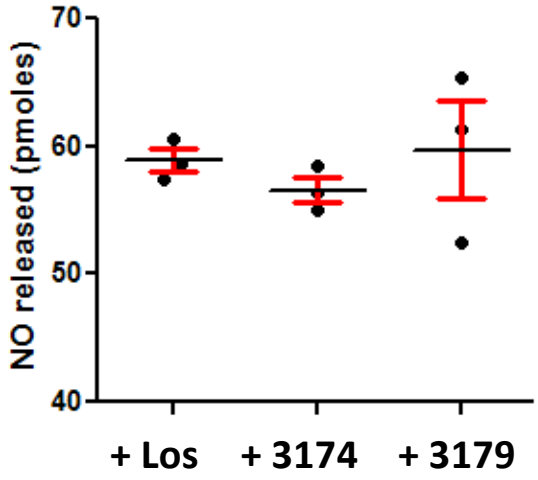

Figure 35: Evaluation of NO-release in BAECs treated with losartan or losartan metabolites EXP3174 or EXP3179.
Ionophore-induced NO-release in BAECs treated with intact losartan (+Los) or losartan metabolites EXP3174 (+3174) or EXP3179 (+3179) was measured as accumulation of nitrate in cell supernatant. Assays were completed in triplicate per treatment group. No significant difference was found between treatment groups.

Notably, as these experiments were completed in tandem with those presented previously on the impact of losartan treatment on levels of NO release, untreated cell controls are presented in Figure 23. Despite these interesting results, we chose to complete subsequent experiments using intact losartan rather than losartan metabolites. This choice was based on a number of factors including a greater translatability to whole animal experiments as the cost of treatment of MFS murine models with individual metabolites was found to be prohibitively expensive.

Appendix C: Endothelial Function in Patients Treated with Losartan

Previously, the collaborative MFS research groups in Vancouver studied the use of atenolol versus losartan on the biophysical properties of the aorta in MFS patients [130]. As part of this study, data on aortic root enlargement and flow mediated dilation (FMD) in patients treated with losartan was collected. However, analysis of how FMD dilation changed in respect to aortic root enlargement over the 1-year course of the study was not analyzed. Therefore, we performed a sub-analysis of this data to determine the effect of losartan on aortic root enlargement over the study period in relation to FMD. This revealed that of the patients treated with losartan, approximately half had improved FMD. Most interesting, all patients with improved FMD had a regression in aortic root enlargement. Conversely, those with declining FMD experienced a progression of aortic root diameter (Figure 36) ($p<0.02$ between groups).

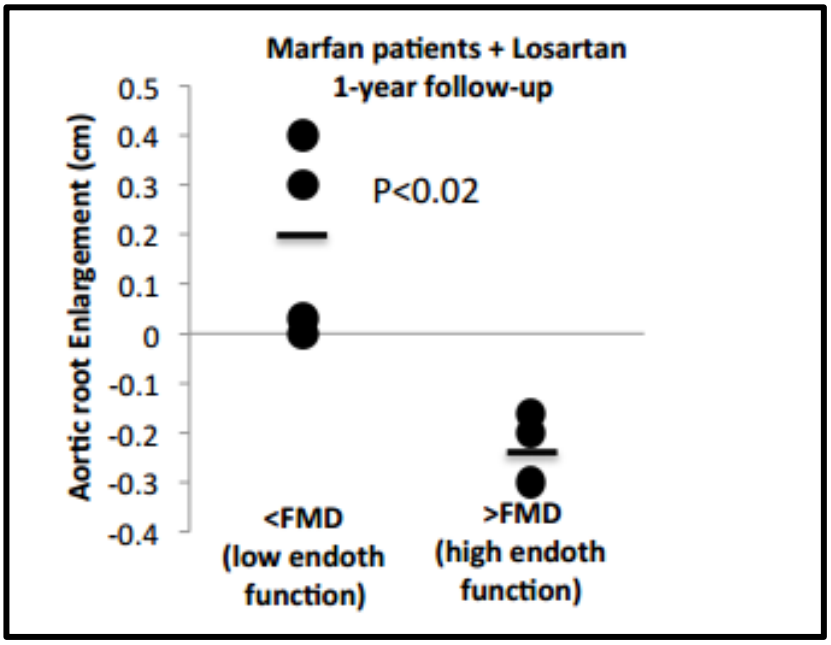

Figure 36: Changes in FMD and aortic root enlargement in MFS losartan treated patients. Analysis of aortic root enlargement at the level of the ST Junction via echocardiogram in patient treated with losartan revealed that those whom show increased endothelial function (>FMD, n=3) all exhibit reversal of aortic root enlargement, whereas patients who do not present increased endothelial function (<FMD, n=3) show expected aortic root enlargement. Black bar represents average.

Overall, these finding lend credence to the association of endothelial function in aortic root enlargement in MFS. Although the patient population seems to be split in their response to losartan (improved or declining FMD), a split in response has been noted in other MFS trials and may reflect the overall appreciated heterogeneity of MFS patients that is incurred by factors such as age, sex, and mutation type and speaks to the need to further investigate endothelial function in MFS patients with an eye to stratification of patients which may benefit most from the use of endothelial dysfunction targeted therapeutic approaches.

Appendix D: Assessment of MFS Pulmonary Pathology

Analysis of pulmonary artery pathology was completed using echocardiograms in which measurements were taken at the level of the pulmonary valve by a technician blinded to genotype and treatment group. This demonstrated significant aneurysm in C1039G$^{+/-}$ mice compared to WT control (Figure 37A, B). Furthermore, analysis of pulmonary artery aneurysm in the MFS eNOS^{S1776D} strain also showed significant aneurysm in C1039G$^{+/-}$ relative to WT control. However, C1039G S1176D mice were protected from aneurysm development (Figure 38C). This is akin with our findings of the benefit of the eNOS^{S1776D} expression in the aortic root and ascending aorta.

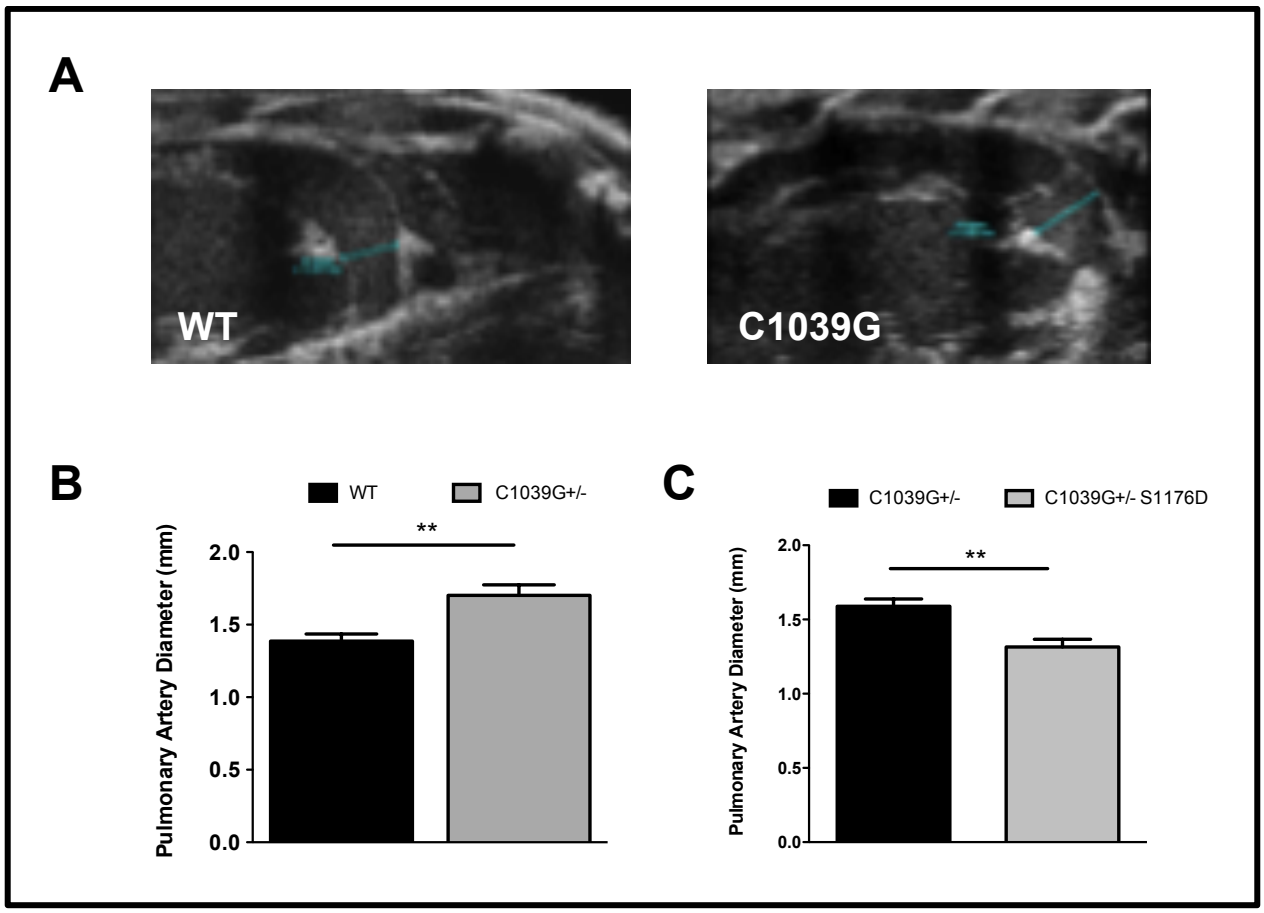

Figure 37: Pulmonary artery aneurysm in MFS mice.
Analysis of pulmonary artery aneurysm was completed using echocardiograms and demonstrates the presence of aneurysm at the level of the pulmonary valve in C1039G$^{+/-}$ mice (n=8), compared to WT controls (n=6) (**A**). Quantification of vessel diameter demonstrated that pulmonary artery diameter to be significantly enlarged in C1039G+/- mice relative to WT controls (**B**). However, eNOS^{S1776D} in MFS mice (C1039G$^{+/-}$ S1176D, n=6) significantly reduced pulmonary artery diameter compared to C1039G$^{+/-}$ mice (n=5) (**C**). Pulmonary artery diameters represent mean values ± SEM where values for each animal were determine using multiple measurements taken in B- and M-mode by a blinded technician and **$p<0.01$.

As our group and others have previously reported progressive airspace enlargement in models of MFS including the C1039G$^{+/-}$ model, this suggests a physiological defect that may alter lung function. However, lung function has never been studied in MFS mice. Therefore, in addition to analysis of pulmonary artery aneurysm, we expanded our study of MFS pulmonary

pathology to included evaluation of lung function. Analysis revealed a significant change in lung function in terms of increased compliance and decreased elastance in C1039G$^{+/-}$ mice versus control (Figure 38A, B). Interestingly, preliminary treatment with losartan did not result in a change in lung function (Figure 38A, B) and needs to be completed in future experiments.

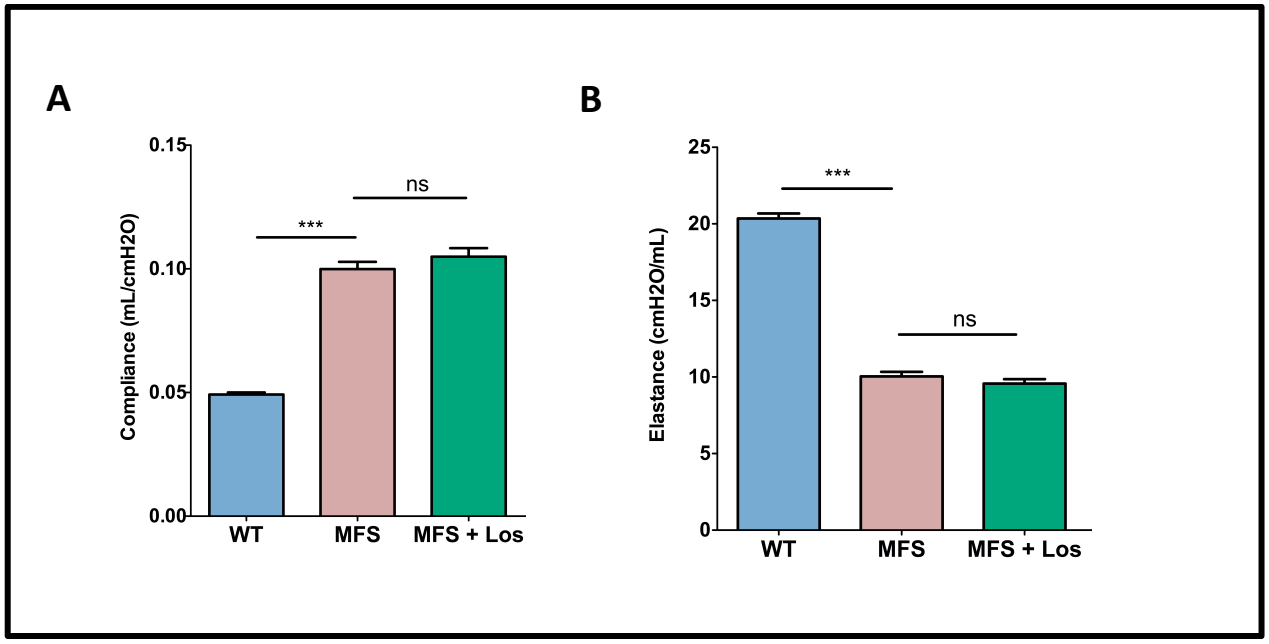

Figure 38: Analysis of lung function in MFS mice.
Analysis of lung function was completed on FlexiVent system on anesthetized WT and C1039G Marfan mice (MFS) or MFS mice treated with losartan (MFS + Los). Quantification of lung compliance shows a significant increased in MFS mice, which was unchanged with losartan treatment (**A**). Elastance was found to be significantly reduced in MFS mice and was unaltered with losartan treatment (**B**). N<5 in all groups.

In addition to analyzing lung function, airspace enlargement was studied. Previously, we analyzed airspace enlargement in groups of animals from our C1039G$^{+/-}$ S1176D and C1039G$^{+/-}$ eNOS transgenic lines. Interestingly, while we observed significant airspace enlargement in C1039G$^{+/-}$ mice compared to WT controls in both strains, we did not see improvement in distal

airspace enlargement with either the presence of the S1776D phospho-mutant (Figure 39A) or the eNOS transgene (Figure 39B). This suggests that a different signaling mechanism may regulate distal airspace enlargement in the lung than in the aorta where we observed a distinct benefit of the eNOS transgene and eNOS phospho-mutant. To analyze this further, lung tissue from WT and C1039G$^{+/-}$ is being analyzed by RNASeq to yield a comparison of changes in gene expression between the groups.

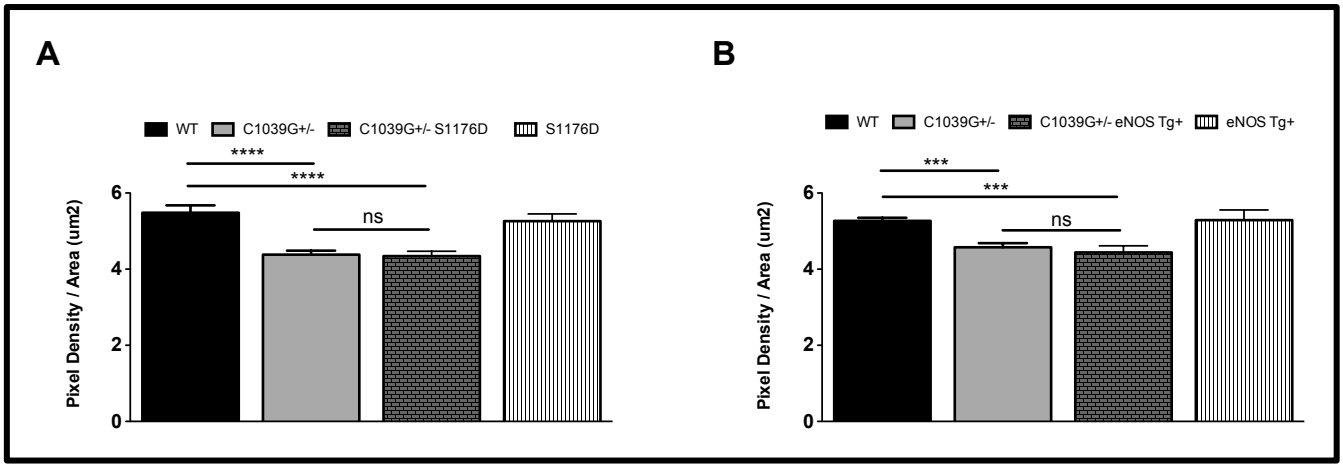

Figure 39: Analysis of airspace enlargement in C1039G$^{+/-}$ S1176D and C1039G$^{+/-}$ eNOS transgenic mice.
Analysis of airspace enlargement in distal lung parenchyma was completed using analysis of pixel density. C1039G$^{+/-}$ mice (n=18) were found to have a significant increase in airspace enlargement relative to WT control (n=8). However, C1039G$^{+/-}$ S1176D phospho-mutant mice (n=13) did not show improvement of airspace enlargement over C1039G$^{+/-}$ mice and showed decreased density relative to S1176 controls (n=10) (**A**). In the MFS eNOS transgenic line, C1039G$^{+/-}$ mice (n-12) were also found to have a significant increase in airspace enlargement relative to WT control (n=12). However, C1039G$^{+/-}$ eNOS Tg^{+} mice (n=7) did not show improvement of airspace enlargement over C1039G$^{+/-}$ mice (**B**) and had decreased density relative to eNOS Tg^{+} controls (n=6)

Subsequently, to further investigate of NO/NOS signaling in MFS in pulmonary system, we investigated the use of phosphodiesterase 5 (PDE5) inhibitor sildenafil. Essentially, PDE5

inhibitors such as sildenafil act to potentiate downstream NO signaling by blocking the conversion of cGMP to GMP and prolonging smooth muscle cell relaxation (Figure 40). Mice treated with sildenafil in drinking water (50mg/kg/day) were evaluated by echocardiogram. Preliminary data suggests that sildenafil may reduce pulmonary artery aneurysm (Figure 41B). Further, preliminary analysis of lung histology suggests that sildenafil may improve lung architecture (Figure 41A), but does not appear to correct lung function in MFS mice (Figure 41C, D). Unfortunately, blinded assignment of mice to treatment groups means that additional animals treated with sildenafil need to be evaluated in order to draw definitive conclusions and repetition of experiments to increase N-values is on-going.

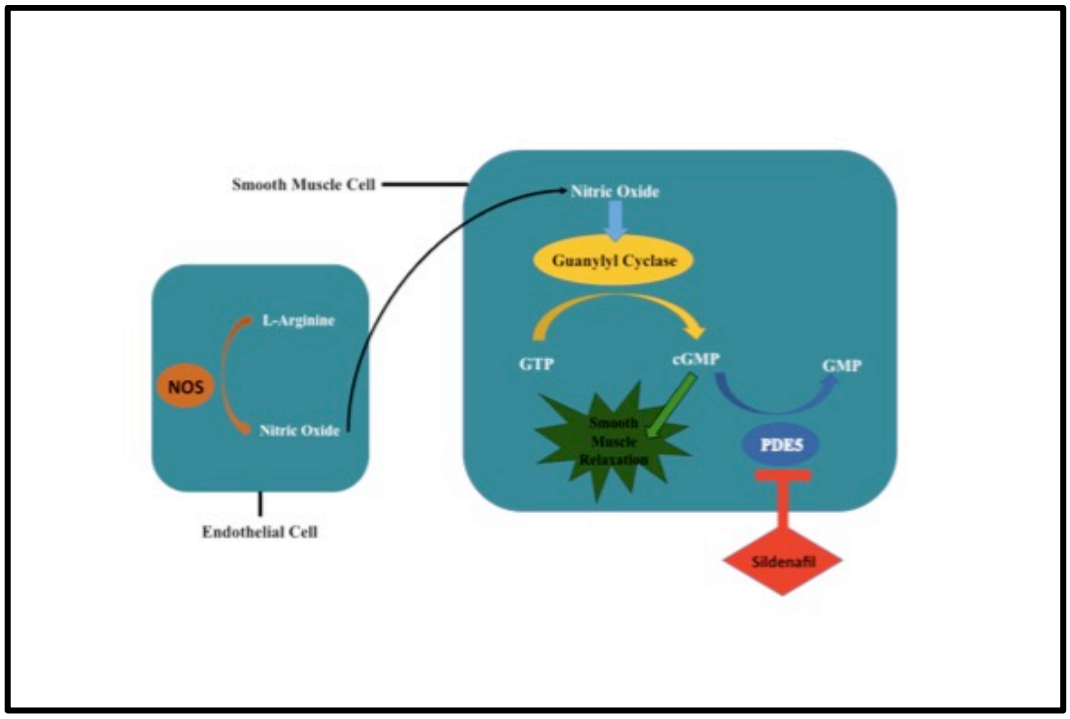

Figure 40: Mechanism of NO potentiation mediated by sildenafil.
Sildenafil blocks phosphodiesterase 5 (PDE5) and as such results in potentiation of NO signaling and vasodilation. Potentiation of NO signaling by sildenafil is mediated through inhibiting the conversion of cGMP to GMP which results from nitric oxide stimulation of the conversion of GTP to cGMP via guanylyl cyclase.

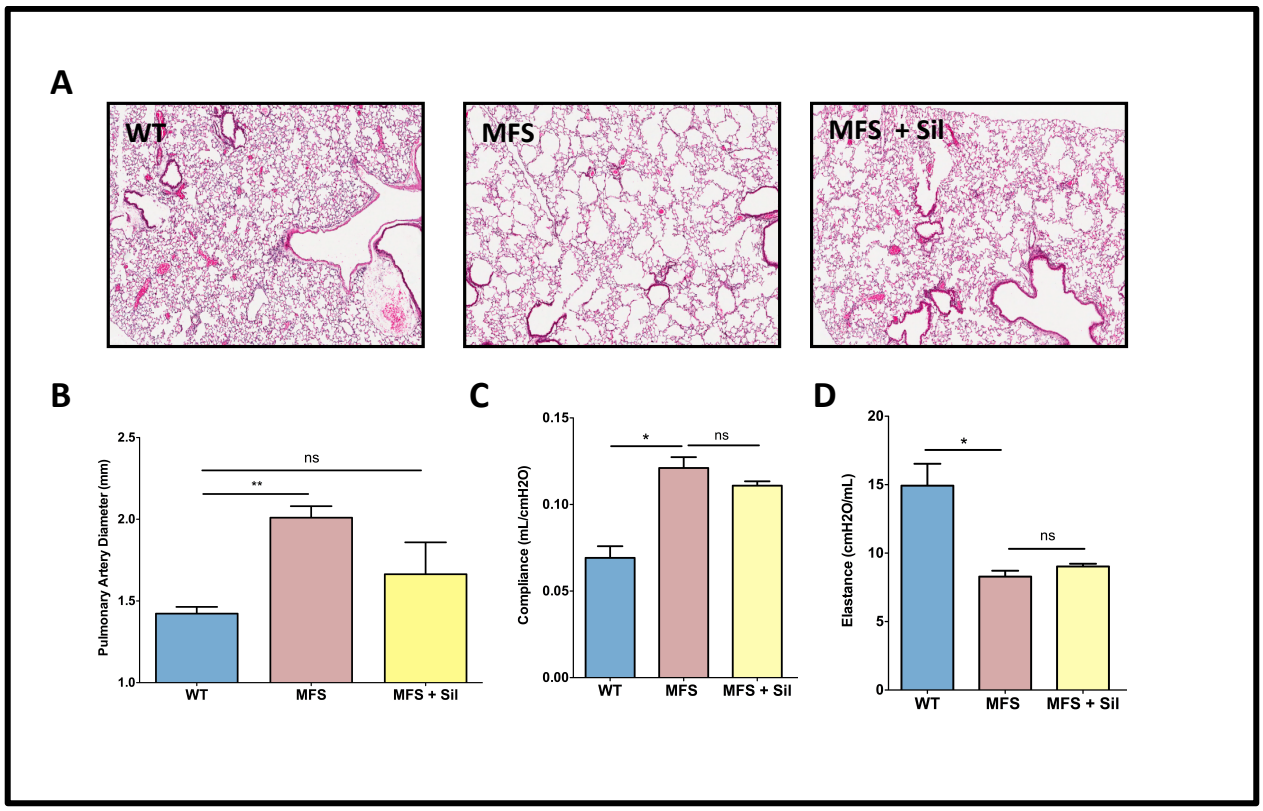

Figure 41: Analysis of sildenafil treatment in MFS mice.
Preliminary histological evaluation of MFS versus WT lungs show notable airspace enlargement that is partially corrected with sildenafil treatment (**A**). Analysis of the impact of sildenafil treatment in pulmonary artery aneurysm analyzed evaluated by echocardiogram (**B**) and study of the impact of sildenafil on lung function including compliance (**C**) and elastance (**D**). N<5 in all groups.

Collectively, these studies of MFS lung demonstrate pulmonary pathology to be a significant component of MFS. However, analysis of lung function is rarely reported in clinical studies and has not been included in the recently published clinical trials for new treatments

paradigms for MFS. The presented findings suggest that further analysis of MFS pathology is needed and is an important aspect of MFS pathology.

Appendix E: Evaluation of Coronary Artery Dissection

Dissection of the coronary artery has been noted in MFS case reports as well as those of related syndromes such as LDS [295-297]. However, coronary artery dissection is a rare phenotype of MFS and has not been reported in murine models. Yet, during dissection of hearts used in our MFS studies to determine elastic fiber fragmentations in the Sinus of Valsalva, areas of the coronary were evaluated at the level of the coronary ostia for evidence of coronary dissection. Slides stained with H&E and Movat's pentachrome were evaluated and dissection was scored by a cardiac pathologist blinded to genotype and treatment group. Scoring of disease severity was completed as described in Table 4 with examples given in Figure 42. Initial analysis suggests an increased frequency and severity of coronary artery dissection in $C1039G^{+/-}$ mice compared to $C1039G^{+/+}$ controls. Furthermore, similar to our findings of no benefit of ATR1 knockout in aortic aneurysm, $C1039G^{+/-}$ mice lacking ATR1 appear to show an increased severity and frequency of coronary dissection (Figure 43A, B) with frequency of dissection, regardless of severity, found to be 33% in WT controls, 80% in $C1039G^{+/-}$ mice, and 100% in $C1039G^{+/-}$ $ATR1^{-/-}$ mice.

Score	Description of Coronary Ostia Dissection
0	• No dissection
1	• Histological findings suggestive of dissection but not definitive o Focal granulation tissue and inflammation o Distorted ostia structure
2	• Definitive dissection o Granulation tissue, inflammation and/or o Blood within the vessel wall
3	• Significant / severe dissection o Presence of all dissection features (as described for a "2" in large portion of the ostia.

Table 4: Scoring system used for evaluation of dissection of the coronary ostia.
Dissection of the coronary arteries at the level of the coronary ostia was scored on a ordinate scale from 0 through 3 which reflects a range of no dissection (0), mild dissection (1), moderate dissection [150], and severe dissection (3) with phenotypic findings as described.

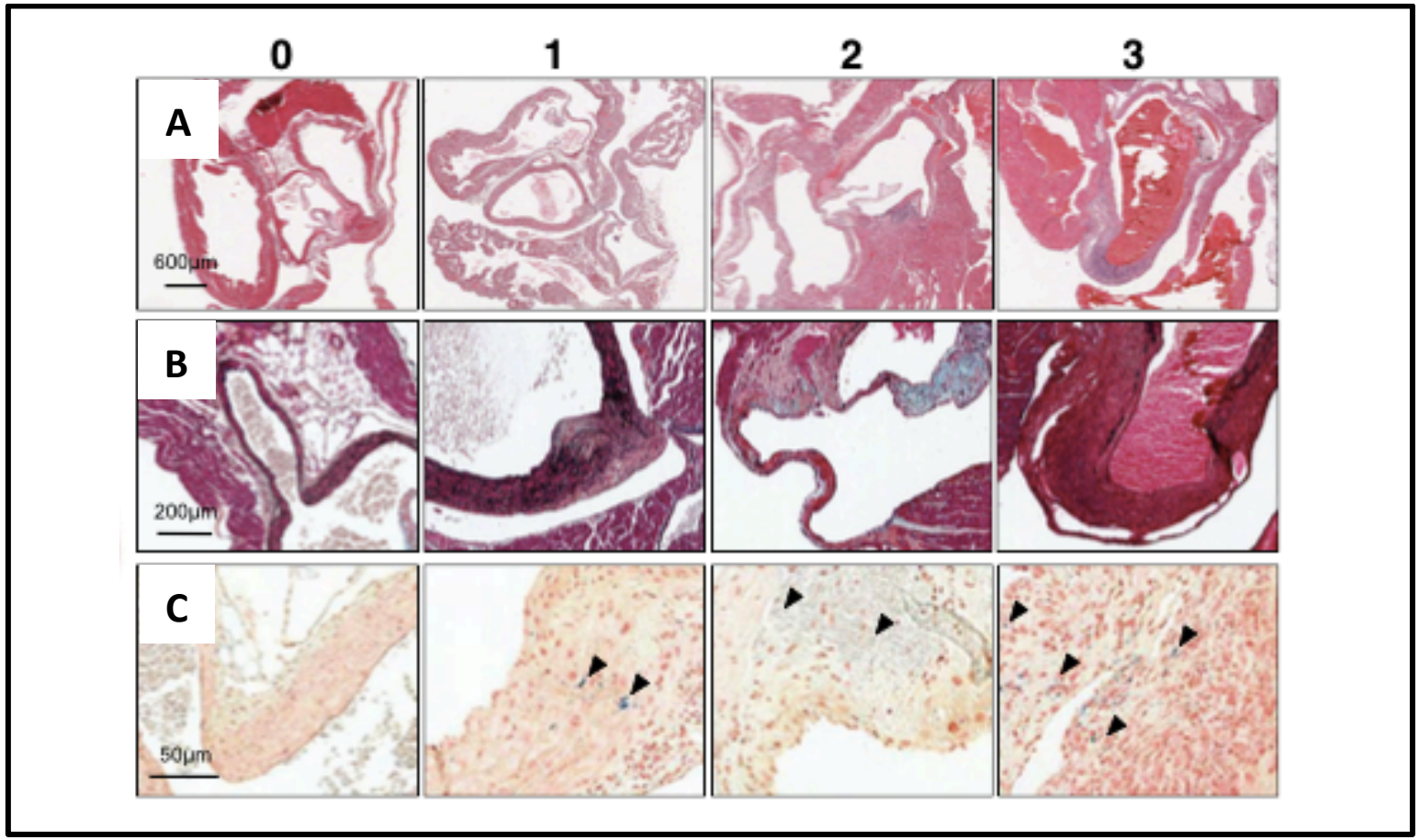

Figure 42: Staining and imaging of coronary artery dissection.
Representative images showing H&E staining (**A**), Movat's pentachrome (**B**), and Prussian blue staining (arrow heads indicate iron positive staining) (**C**) in coronary arteries given a severity scored of 0, 1, 2 or 3 by a cardiac pathologist blinded to genotype and treatment group.

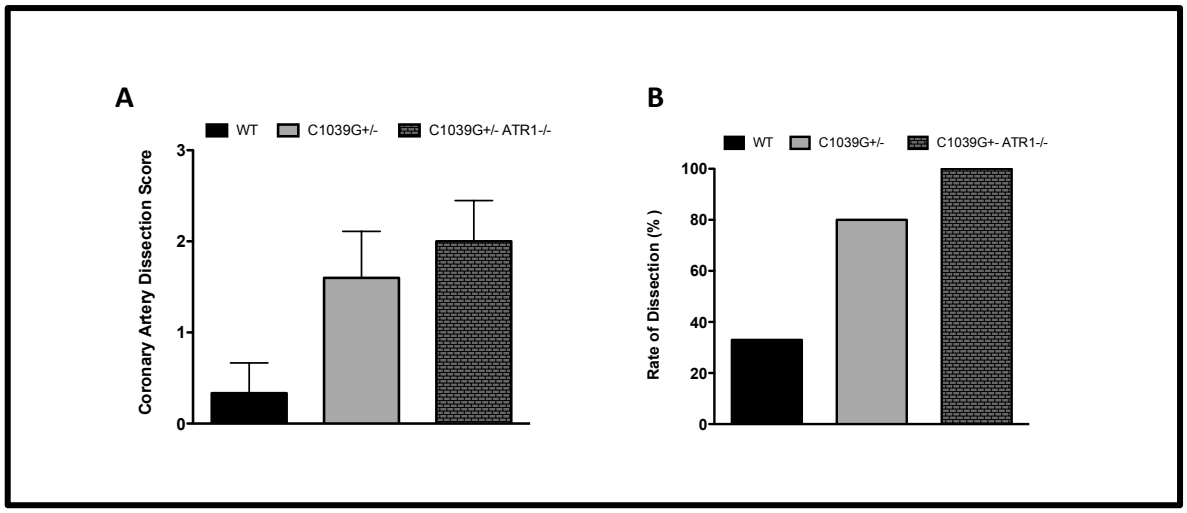

Figure 43: Analysis of severity and frequency of coronary artery dissection.
Dissection of the coronary arteries at the level of the coronary ostia was scored on a ordinate scale from 0 through 3 which reflects an increased severity of dissection in C1039G$^{+/-}$ and C1039G$^{+/-}$ ATR1$^{-/-}$ mice compared to none – mild dissection seen in WT controls (**A**). Analysis of frequency of dissection, irrespective of severity, demonstrated that while 33% of WT mice showed an indication of dissection (all mild), 80% of C1039G$^{+/-}$ and 100% of C1039G$^{+/-}$ ATR1$^{-/-}$ mice showed dissection (**B**) where in WT n=3, C1039G$^{+/-}$ n=5, and C1039G$^{+/-}$ ATR1$^{-/-}$ n=6 at 22 months of age.

Overall, these preliminary findings represent a novel model of coronary artery dissection as to our knowledge this represents the first reported genetic based murine model of cononary dissection. Moreover, these findings in the coronary artery further support our conclusion of the lack of benefit of ATR1 knockout in the C1039G$^{+/-}$ MFS model and leads us to conclude that despite hypotension resulting from ATR1 deletion, no improvement of coronary artery dissection is observed. This further suggests that hemodynamics and ATR1 signaling may not play as significant of a role as previously thought in MFS. Currently, analysis of histology is on-going to

evaluate mice at earlier time points of disease and well as in genetic models and treatment groups presented earlier including MFS mice treated with losartan as well as MFS mice expressing $eNOS^{S1176D}$ or $eNOS^{S1176A}$ or an eNOS transgene. Preliminary findings (not shown) suggest that losartan is able to reduce the rate of coronary artery dissection in $C1039G^{+/-}$ mice and is also able to prevent dissection in $C1039G^{+/-}$ $ATR1^{-/-}$ animals. If upon completion of this data set our preliminary findings of the effectiveness of losartan in $C1039G^{+/-}$ $ATR1^{-/-}$ to prevent coronary artery dissection were upheld, this would be consistent with our findings of the off-target effects of losartan in MFS and may be a novel model in which to study the off target effects of losartan in the pathology of vascular dissection. Moreover, this model may be an interesting counterpart to study the role of TGF-β in coronary dissection as TGF-β plays a controversial role in aneurysm including coronary artery aneurysm in Kawasaki disease. Therefore, utilization of a genetic model of increased TGF-β signaling, such as the $C1309G^{+/-}$ murine model, may provide a interesting counterpoint for researchers to delineate mechanism of TGF-β signaling in coronary dissection [298-300].

Appendix F: Candidate Highlights

I. PhD Awards:

Award	Institution/Organization	Effective	Value
Michael Smith Foreign Study Supplement	Canadian Institutes of Health Research (CIHR)	2015	6,000 (CAD)
Graduate Student Oral Presentation Award	UBC Anesthesiology, Pharmacology & Therapeutics Research Day	2016 2014 2013	300 (CAD) 300 (CAD) 300 (CAD)
Doctoral Research Award	Canadian Institutes of Health Research (CIHR)	2012 – 2015	105,000 (CAD)
Cardiovascular Research Award	Jean Francois Bowden Foundation / St. Paul's Hospital	2012	2,500
Experimental Biology Conference Travel Award	American Society for Pharmacology & Experimental Therapeutics (ASPET)	2016 2014	1500 [216] 1500 [216]
Best Poster Award	North American Vascular Biology (NAVBO): Cardiovascular Inflammation & Remodelling	2014	250 [216]
New Student of the Year Award	Centre for Heart Lung Innovation UBC & St. Paul's Hospital	2012	N/A
Doctoral Research Fellowship Award	University of British Columbia [164]	2011 – 2015	64,000 (CAD)
Graduate Tuition Scholarship	University of British Columbia [164]	2011 – 2015	17,000 (CAD)

Table 5: Awards received by the candidate during the time of study.

II. Publications:

- **Sellers, S.L.,** N. Milad, R. Chan, M. Mielnik, U. Jermilova, P.L. Huang, R. de Crom, J.A. Leipsic, J.A. Hirota, J.C. Hogg, C. Van Breeman, M. Esfrandiarei, M.A. Seidman, and P.N. Bernatchez. The Effects of Angiotensin II Receptor Blocker Losartan on Marfan Syndrome are Off-Target: Role of Nitric Oxide. *Nature Medicine*. Manuscript under review.
- Shen, Y., V. Russo, **S.L. Sellers**, M. Zeglinski, Z. Wu, C. Oram., S. Santacruz, Y. Merkulova, C. Turner, K. Tauh, H. Zhao, T. Bozin, L. Bohunek. H. Zeng, M.A. Seidman, B.M. McManus, C. Bleackley, E. Ruoslahti, T.A.H. Jarvinen, and D.J. Granville. Administration of Recombinant Decorin Fusion Protein, CAR-DCN, Reduces Severity of Abdominal Aortic Aneurysm in Mice. *Atherosclerosis, Thrombosis, and Vascular Biology.* Manuscript under review.
- Grover, R., J.A. Leipsic, J. Mooney, S. Kueh, M. Ohana, B. Norgaard, D. Murphy, C. Hague, M. Seidman, P. Blanke, T. Sedlak, and **S.L. Sellers**. Coronary Lumen Volume to Myocardial Ratio in Primary Microvascular Angina: A Novel Imaging Approach to a Challenging Clinical Dilemma. *Radiology.* Manuscript under review.
- Mooney J., **S.L. Sellers**, P. Blanke, P. Pibarot, R.T. Hahn, D. Dvir, P.S. Douglas, N.J. Weissman, S.K. Kodali, V.H Thourani, H. Jilaihawi, O. Khalique, C.R. Smith, S. Kueh, M. Ohana, R. Grover, C. Naoum, A. Crowley, W.A. Jaber, M.C. Alu, R. Parvataneni, M. Mack, J.G. Webb, M.B. Leon, and J.A. Leipsic. CT Defined Prosthesis-Patient Mismatch Downgrades Frequency and Severity, and Demonstrates No Association with Adverse Outcomes Following TAVR. *JACC Cardiovascular Interventions.* Manuscript under review.
- Leipsic J.A., **S. Sellers**, P. Blanke. 2017. Sex differences in the aortic root size: Implications for TAVR. *J Cardiovasc Comput Tomogr.* pii: S1934-5925(17)30027-8.
- Kueh, S.H., **S.L. Sellers**, and J.A. Leipsic. 2016. Developing a deeper understanding of sex differences in the diagnostic performance of computed tomographic perfusion imaging toward a more personalized approach. *Circulation: Cardiovascular Imaging.* 9(11): pii: e005718.
- Sharma, A, **S.L. Sellers,** N. Stefanovic, C. Leung, S.M. Tan, O. Huet, D. Granville, M. Cooper, J. de Haan, and P.N. Bernatchez. 2015. Direct Endothelial Nitric Oxizde Synthase Activation Provides Atheroprotection in Diabetes-Accelerated Atherosclerosis. *Diabetes.* 64(11):3937-50.

  Highlighted in: Jia, C., and J.R. Sowers. 2015. Caveolin-1 in Cardiovascular Disease: A Double-Edged Sword. *Diabetes.* 64(11):3645-3647
- **Sellers, S.L.**, A. Iwasaki, and G.W. Payne. 2013. Nitric oxide and TNF-alpha are critical regulators of reversible lymph node vascular remodeling and adaptive immune response. *PLoS One*. 8(4):e60741.
- **Sellers, S.L.**, A. Trane, and P.N. Bernatchez. 2012. Caveolin as a Potential Drug Target for Cardiovascular Protection. *Frontiers in Physiology*. 3:280.
- **Sellers, S.L**., and G.W. Payne. 2011. Intravital Microscopy of the Inguinal Lymph Node.

Journal of Visualized Experiments. 50: pii: 2551. doi: 10.3791/2551.

- Kumamoto, Y., L. Mattei, **S.L. Sellers**, G.W. Payne and A. Iwasaki. 2011. CD4+ T cells support CTL priming by controlling lymph node input. *Proc. Nat. Acad. Sci.*. 108(21): 8749-54.

  Highlighted in: Bordon, Y. 2011. CD4s work the doors. *Nat Rev Immunol.* 11:370-371.

II. Book Chapters:

- Mooney, J, Blanke P, Kueh SH, **Sellers S**, Leipsic JA. 2017. Chapter 41: CT for Minimally invasive Repair of the Mitral Valve and Other Structural Heart Disease. CT of the Heart (2nd ed.). New York, NY. Springer.
- Grover R, **Sellers SL**, Blanke P, Leipsic J. 2017. *'Computed Tomography Imaging for Mitral Valve Regurgitation'* Percutaneous Treatment of Left Side Cardiac Valves: *A Practical Guide for the Interventional Cardiologist – 3rd Edition (Springer)*

III. Manuscripts in Preparation

- Omid-Fard, N., A. Ahmadi, P. Blanke, **S.L. Sellers**, H. Gransar, D.S. Berman, T.Q. Callister, A. DeLago, M. Hadamitzky, J. Hausleiter, M.H. Al-Mallah, M.J. Budoff, P.A. Kaufmann, G. Raff, K. Chinnaiyan, F. Cademartiri, E. Maffei, T.C. Villines, Y. Kim, G. Feuchtner, G. Pontone, D. Andreini, H. Marques, R. Rubinshtein, S. Achenbach, L. J. Shaw, M. Gomez, N. Hindoyan, J.K. Min, and J.A. Leipsic. Smoking and its relationship with long term events: further insights from the CONFIRM (Coronary CT Angiography Evaluation for Clinical Outcomes: An International Multicenter) registry. Manuscript in Preparation.
- **Sellers, S.L**. R. Chan, J. Hirota, J.C. Hogg, C. Van Breeman and P.N. Bernatchez. Pulmonary Pathology of Marfan Syndrome: Role of Losartan and Nitric Oxide in Structural and Function Pathology. Manuscript in preparation.
- **Sellers, S.L.**, K.N. Hogh, A. Ayers, and G.W. Payne. Impact of gender on neurobiology of self-injury behaviour. Manuscript under review.
- **Sellers, S.L.,** N. Milad, M.A. Seidman and P.N. Bernatchez. Marfan Syndrome as a Novel Model of Coronary Artery Dissection. Manuscript in Preparation.
- **Sellers, S.L.,** N. Milad, C. Pascoe, Z. White, R. Chan, M. G. Grounds, C. Seow, G.W. Payne and P.N. Bernatchez. Hyperlipidemia via ApoE Deficiency Exacerbates Muscle Atrophy and Causes Loss of Locomotion in Dysferlinopathies. Manuscript in Preparation.
- Milad, N., **S.L. Sellers**, Z. White, P.N. Bernatchez. The role of Apolioprotein E in Duchenne Muscular Dystrophy. Manuscript in Preparation.
- **Sellers, S.L.,** Z. White, N. Milad, M. G. Grounds, G.W. Payne and P.N. Bernatchez. Use of statins and angiotensin receptor blockers in dysferlinopathies reduces muscle fibrosis, atrophy and necrosis. Manuscript in Preparation.

IV. Other Academic Work

- **Cardiovascular Tissue Registry Heart Explant Team**
  Centre for Heart Lung Innovation UBC & St. Paul's Hospital (2014-Present)
  - Heart explant recovery team member that is responsible for bio-banking of heart transplant explants into the cardiovascular registry.

- **Visiting Doctoral Student, University of Western Australia**
  Laboratory of Dr. Miranda Grounds (Feb – May 2015)
  - Work on the role of lipids in pathology of muscular dystrophy funded by the CIHR Michael Smith Foreign Study Supplement to a CIHR Doctoral Fellowship Award.

V. Invited Talks:

- The Role of Lipids and Diet in Pathology of Dysferinopathies. University of Western Australia. Perth, Australia, 2016.
- Are the Effects of Losartan on Aortic Aneurysm in Marfan Syndrome Off-Target? Canadian Cardiovascular Congress. CSATVB Symposium, Vancouver, 2014.
- Pulmonary Pathology in Marfan Syndrome. Pacific Northwest Epithelial Biology Meeting. Vancouver, Canada, 2013.

VI. Abstracts

- CT-derived Analysis of Coronary Blood Flow in Microvascular Angina. FEST Institute for Heart & Lung Health Fest. Vancouver, Canada, 2017.
- Prevalence and Impact of Scanxiety in Cardiac CT. Institute for Heart & Lung Health Fest. Vancouver, Canada, 2017.
- CT Defined Prosthesis-Patient Mismatch Downgrades Frequency and Severity, and Demonstrates No Association with Adverse Outcomes Following TAVR. Americana College of Cardiology (ACC). Washington D.C., USA, 2017.
- SMART1Map in Non-Ischemic Cardiomyopathy (NICM): Initial Single-Centre Experience. Society for Cardiovascular Magnetic Resonance Scientific Sessions. Washington D.C., USA, 2017.
- SMART1Map in Hypertrophic Cardiomyopathy (HCM): Initial Experience. Society for Cardiovascular Magnetic Resonance Scientific Sessions. Washington D.C., USA, 2017.
- Administration of Recombinant Decorin Fusion Protein, CAR-DCN, Reduces Severity of Abdominal Aortic Aneurysm in Mice. American Society of Matrix Biology. St. Petersburg, FL, USA, 2016.
- Losartan attenuates Marfan Syndrome aortic aneurysm through endothelial nitric oxide synthase. International Vascular Biology Meeting. Boston, MA, USA, 2016.
- ATR1 Independent Effects of Losartan in Marfan Syndrome. Experimental Biology. San Diego, CA, USA, 2016.

- The Off-Target Effects of Losartan in Marfan Syndrome: Role of Nitric Oxide. UBC Anesthesiology, Pharmacology & Therapeutics Research Day, Vancouver, Canada, 2016.
- Impact of Diet and Cardiovascular Disease in Dysferlinopathies. Jain Foundation Conference. Toronto, Canada, 2015.
- A New Use for Old Drugs: Are Statins the Future of Treating Muscular Dystrophy? UBC Anesthesiology, Pharmacology & Therapeutics Research Day, Vancouver, Canada, 2014.
- Nitric Oxide, TNF-alpha, and CD4+ T Cells are Critical Regulators of Lymph Node Vascular Remodeling During Infection. 2014 North American Vascular Biology Organization & Yale University Cardiovascular Inflammation & Remodeling Conference. New Haven, CT, USA.
- Characterizing and Treating Pulmonary Pathology in Marfan Syndrome. Experimental Biology. San Diego, CA, USA, 2014.
- Angiotensin Receptor Inhibition and Genetic Ablation in the Treatment of Marfan Syndrome. UBC Anesthesiology, Pharmacology & Therapeutics Research Day, Vancouver, Canada, 2013.
- Investigating the Role of ATR1-alpha in Marfan Syndrome. Institute for Heart & Lung Health Fest. Vancouver, Canada, 2013.
- The Role of Angiotensin Receptor Type I in Marfan Syndrome. UBC Anesthesiology, Pharmacology & Therapeutics Research Day, Vancouver, 2012.
- The Role of Angiotension Receptor Type I in Marfan Syndrome. Institute for Heart & Lung Health Fest. Vancouver, Canada, 2012.
- The Role of eNOS and TNF-alpha in Lymph Node Vascular Remodeling During Infection. Earl Davie Symposium. Vancouver, Canada, 2011.
- Lymph Node Vascular Remodeling During Infection. Gordon Research Conference, Endothelial Cell Phenotypes. Maine, USA, 2010.

VII. Committee and Society Membership

Institute for Heart & Lung Health FEST Organizing Committee
Centre for Heart Lung Innovation UBC & St. Paul's Hospital (August 2016 - Present)

- Organizing committee member for vascular biology, heart and lung focused conference involving local, national and international speakers including a large trainee focus.

Scientific Review and Space Committee
Centre for Heart Lung Innovation UBC & St. Paul's Hospital (Jan 2015 - Present)

- Committee trainee representative which facilitates internal grant review process and allocation and optimization of centre space use.

Training & Environment Committee
Centre for Heart Lung Innovation UBC & St. Paul's Hospital (Sept 2014 – August 2016)

- Committee trainee representative coordinating activities promoting workplace morale and

facilitating trainee events and learning opportunities.

Genetically Engineered Models [176] Users Committee
Centre for Heart Lung Innovation UBC & St. Paul's Hospital (Sept 2012 - Present)

- Committee student representative that guides use and policies of the GEM facility.

Co-Organizer, Annual Heart & Stroke Foundation Fundraiser
Centre for Heart Lung Innovation (2012 – 2014)

- Served as primary organizer of the annual fundraiser including event planning, sponsor recruitment, tickets sales, promotions and liaising with the Heart & Stroke Foundatio

Conference Chairs, Involvement and Organization

- Institute for Heart & Lung Health Symposium Heart Failure & Arrhythmias Session Chair, 2016
- Centre for Heart Lung Innovation Summer Student Research Day Judge 2014, 2015, 2016
- Canadian Cardiovascular Congress Canadian Society of Atherosclerosis, Thrombosis and Vascular Biology (CSATVB) Trainee and Social Events Coordination, 2014

Volunteer, Genome BC

- 2012-2013, community scientific outreach events

VIII. Supervisory Activity

- Co-supervisor, Una Jermilova, UBC undergraduate research studentship
  2014 - 2015

- Co-supervisor Rayleigh Chan, UBC Pharmacology Co-operative education student
  2013 - 2015

- Co-supervisor, Duncan Ferguson, UBC Pharmacology Co-operative education student
  (May – Aug 2013)

- Co-supervisor, Michael Mielnik, McMaster University Co-operative education student
  (Jan – Aug 2012)

- Co-supervisor, William Eisbrenner, University of Northern BC undergraduate student
  (2010 - 20110